Abstract

LI, LEI. Effects of Activated Carbon Surface Chemistry and Pore Structure on the Adsorption of Trace Organic Contaminants from Aqueous Solution. (Under the direction of Detlef R.U. Knappe)

The principal objectives of this research were (1) to identify activated pore structure and surface chemistry characteristics that assure the effective removal of trace organic contaminants from aqueous solution, and (2) to develop a procedure to predict the adsorption capacity of activated carbons from fundamental adsorbent and adsorbate properties.

To systematically evaluate pore structure and surface chemistry effects on the adsorption of organic micropollutants from aqueous solution, a matrix of activated carbon fibers (ACFs) with three activation levels and four surface chemistry levels was prepared and characterized. In addition, three commercially available granular activated carbons (GACs) were studied to verify whether correlations developed for the ACF matrix are valid for adsorbents that are typically used for water treatment. BET surface area, pore size distribution, elemental composition, point of zero charge and infrared spectroscopy data were obtained to characterize the adsorbents. The results showed that the ACF matrix prepared in this study permits a fairly independent evaluation of surface chemistry and pore structure effects on organic contaminant adsorption from aqueous solution. Methyl tertiary-butyl ether (MTBE), a relatively hydrophilic adsorbate, and

trichloroethene (TCE), a relatively hydrophobic adsorbate, served as adsorbate probes. To evaluate the effects of natural organic matter (NOM) on MTBE and TCE adsorption capacities, isotherm experiments were conducted in ultrapure water and Sacramento-San Joaquin Delta water.

With respect to surface chemistry, both single-solute isotherms and isotherms in the presence of NOM indicated that hydrophobic adsorbents more effectively removed TCE and MTBE from aqueous solution than hydrophilic adsorbents. Enhanced water adsorption on polar surface sites explained the poorer performance of the hydrophilic adsorbents. Based on the elemental composition of the low-ash carbons evaluated in this study, activated carbons should have oxygen and nitrogen contents that sum to no more than 2 to 3 mmol/g to assure sufficient hydrophobicity.

With respect to pore structure, both single-solute isotherms and isotherms in the presence of NOM indicated that adsorbents should exhibit a large pore volume in micropores with widths that are about 1.5 times larger than the kinetic diameter of the target adsorbate. Furthermore, micropollutant isotherm data obtained in the presence of NOM showed that an effective adsorbent should possess a micropore size distribution that extends to widths that are approximately twice the kinetic diameter of the target adsorbate to prevent pore blockage or restriction as a result of NOM adsorption.

A procedure based on the Polanyi Potential Theory (PPT) was developed to predict the adsorption capacities of activated carbons from fundamental adsorbent and

adsorbate properties. It was assumed that trace organic compound adsorption from aqueous solution is primarily controlled by non-specific dispersive forces while water molecules interact with the oxygen-containing functional groups on carbon surfaces. A correlation between the coalescing factor for water adsorption and adsorbent oxygen content was developed. Based on this correlation, the PPT yielded reasonable estimates of aqueous phase adsorption capacities for both relatively polar and non-polar adsorbates on both relatively hydrophobic and hydrophilic activated carbons. With the developed procedure, the adsorption capacities of organic compounds that are partially miscible in water can be predicted from (1) N_2 and CO_2 adsorption isotherms of a given adsorbent, (2) the adsorbent oxygen content, and (3) the molar volume and parachor of the target adsorbate.

EFFECTS OF ACTIVATED CARBON SURFACE CHEMISTRY AND PORE STRUCTURE ON THE ADSORPTION OF TRACE ORGANIC CONTAMINANTS FROM AQUEOUS SOLUTION

By

LEI LI

A dissertation submitted to the Graduate Faculty of
North Carolina State University
in partial fulfillment of the
requirements for the
Degree of Doctor of Philosophy

DEPARTMENT OF CIVIL ENGINEERING

Raleigh

2002

APPROVED BY:

Advisory Committee Chair

Advisory Committee Co-chair

Dedication

To my parents

谁言寸草心
报得三春晖

Biography

Lei Li, was born in Shanxi, China. She received her B.S. and M.S. in Chemical Engineering from Taiyuan University of Technology in 1993 and 1996. In 1998, she came to the United States and began her doctoral studies at North Carolina State University. She received her doctoral degree in May 2002.

Acknowledgements

First, I would like to thank my advisor, Dr. Detlef Knappe, for his insight, guidance and support during my graduate study. I am also thankful for my committee members, Drs. Morton Barlaz, Joel Ducoste and Stefan Franzen for contributing their expertise and time to this work.

I also appreciate the help that I received from Phillip Calvert and David Black throughout my research. Furthermore I would like to credit my friends inside and outside the lab, from whom I not only enriched my knowledge but also felt the personal growth.

Finally, I am indebted to my parents and sisters for their unconditional love, encouragement and support throughout my study overseas. I am also grateful to my husband for his patience, love and encouragement.

Table of Contents

List of Tables

List of Figures

Chapter 1. Introduction and Objectives

1.1. Introduction

Activated carbon adsorption is the best available technology to remove many trace organic contaminants from drinking water sources. Adsorption of organic compounds onto activated carbon is mainly influenced by (1) adsorbate characteristics (e.g., size, shape, charge, polarity, aromaticity) and (2) the activated carbon pore structure and surface chemistry (e.g., surface area, pore volume, pore size distribution, surface charge, surface hydrophobicity/hydrophilicity).

The surface chemistry and pore structure of commercially available activated carbons varies greatly depending on the base material and activation conditions. For example, a chemically activated wood-based activated carbon may have a wide distribution of pore sizes and an acidic surface, whereas a thermally activated coconut shell based activated carbon may have a narrow distribution of pore sizes and a basic surface [Newcombe and Drikas 1997]. To date, water treatment professionals lack information on how to choose an activated carbon with suitable pore structure and surface chemistry.

While a number of researchers have evaluated the effect of adsorbent pore structure on the adsorption of micropollutants and natural organic matter (NOM) [Kasaoka et al. 1989, Pelekani and Snoeyink 1999 and 2000, Ebie et al. 1995 and 2001, Lee et al. 1981], only a few studies have been conducted to evaluate the effect of adsorbent surface chemistry on the adsorption of organic micropollutants from organic-free water [Franz et al. 2000, Kaneko and Abe 1989, Mangun et al. 1999 and Pendleton

1997]. The effects of adsorbent surface chemistry on the adsorption of organic micropollutants from natural waters remain largely unexplored to date.

Proper design of an activated carbon adsorber requires that the adsorption capacity of a given activated carbon for a target organic compound is known. Unfortunately, relatively few adsorption isotherms are available for the about 70 000 organic compounds currently in use and the wide array of activated carbons that are marketed by numerous manufacturers. Therefore, it is desirable to predict adsorption capacities using an isotherm model with parameters that can be determined from the physical and chemical properties of adsorbents and adsorbates.

1.2. Objectives

The principal objective of this research was to aid drinking water treatment professionals in selecting the best possible activated carbon for a given application. Specifically, the research program was designed to:

1. Prepare and characterize an activated carbon fiber (ACF) matrix that permits the systematic study of surface chemistry and pore structure effects on the activated carbon adsorption of trace organic contaminants from aqueous solution.
2. Evaluate the effects of activated carbon surface chemistry and pore structure on the adsorption of MTBE and TCE.
3. Evaluate the effects of activated carbon surface chemistry and pore structure on the adsorption of MTBE and TCE in the presence of co-adsorbing natural organic matter (NOM).

4. Use the information obtained in phases 1 to 3 to develop activated carbon selection criteria that are based on adsorbent pore structure and surface chemistry.
5. Develop a tool to predict the adsorption capacity of activated carbons from fundamental adsorbent and adsorbate properties.

1.3. References

Ebie K, Li F, and Hagishita T. Effect of pore size distribution of activated carbon on the adsorption of humic substances and trace organic compounds. Water Supply 1995; 13(3/4): 65-70.

Ebie K, Li F, Azuma Y, Yuasa A, and Hagishita T. Pore distribution effect of activated carbon in adsorbing organic micropollutants from natural water. Water Research 2001; 35(1): 167-179.

Franz M, Arafat HA, and Pinto NG. Effect of chemical surface heterogeneity on the adsorption mechanism of dissolved aromatics on activated carbon. Carbon 2000; 38(13): 1807-1819.

Kaneko Y, Abe M, and Ogino K. Adsorption characteristics of organic compounds dissolved in water on surface-improved activated carbon fibers. Colloids and Surfaces 1989; 37: 211-222.

Kasaoka S, Sakata Y, Tanaka E, and Naitoh R. Design of molecular-sieve carbon-Studies on the adsorption of various dyes in the liquid phase. International Chemical Engineering 1989; 29(4): 734-742.

Lee MC, Snoeyink VL, and Crittenden JC. Activated carbon adsorption of humic substances. Journal of the American Water Works Association 1981; 73(8): 440-446.

Mangun CL, Benak KR, Daley MA, and Economy J. Oxidation of activated carbon fibers: effect on pore size, surface chemistry, and adsorption properties. Chem. Mater. 1999; 11: 3476-3483.

Newcombe G, and Drikas M. Adsorption of NOM onto activated carbon: Electrostatic and non-electrostatic effects. Carbon 1997; 35(9): 1239-1250.

Pelekani C, and Snoeyink VL. Competitive adsorption in natural water: role of activated carbon pore size. Water Research. 1999; 33(5): 1209-1219.

Pelekani C, and Snoeyink VL. Competitive adsorption between atrazine and methylene blue on activated carbon: the importance of pore size distribution. Carbon 2000; 38: 1423-1436.

Pendleton, P. Properties of activated carbon controlling 2-Methylisoborneol adsorption. Carbon 1997; 35(8): 1141-1149.

Chapter 2. Activated Carbon Surface Chemistry and Characterization

2.1. Objectives

The objectives were (1) to create an activated carbon fiber (ACF) matrix including ACFs with different surface chemistry, and (2) to determine their surface chemistry characteristics.

2.2. Background

2.2.1. Activated Carbon Surface Chemistry

It is well known that activated carbons are characterized by a certain degree of surface chemical heterogeneity, which is related to the presence of heteroatoms such as oxygen, nitrogen, hydrogen and phosphorus. The content of these elements varies, depending on the nature of an organic precursor and the method of activation. The heteroatoms are important in determining the acidity/basicity of activated carbon surfaces in aqueous dispersion.

Acidic Surfaces. The acidic character of activated carbon surfaces is related to the surface oxygen contents. Oxygen-containing functional groups, such as carboxyl, phenolic, lactone, lactol and quinone groups are primarily located at the edges of graphene layers that contribute the building blocks of activated carbons [Puri 1970, Boehm 1994]. Oxygen-containing functionalities such as carboxylic acid or carboxylic anhydride, lactone or lactol, and phenolic hydroxy have been postulated as the sources of surface acidity. Activated carbons can acquire an acidic character when exposed to

oxygen between 473-973K or to oxidants such as air, water vapor, nitric acid, a mixture of nitric and sulfuric acids, and hydrogen peroxide [Puri 1970].

Basic Surfaces. Carbon surfaces acquire a basic character upon high-temperature (> 973K) heat treatment, provided that any subsequent exposure to air falls outside the 473-973K temperature range [Menendez et al. 1996]. The basic properties of the activated carbon surface are not well understood. Garten and Weiss [1957] ascribed the basic properties of activated carbons to chromene-like and pyrone-type structures. But it has not been clearly established that oxide structures are responsible for the basic character exhibited by some carbon surfaces [Boehm et al. 1964]. Fabish and Schleifer [1984] advanced the opinion that no surface oxides are responsible for basic sites in aqueous solution. Leon y Leon et al. [1992] studied the surface basicity of two series carbons and provided direct evidence that oxygen-free carbon sites (C_π) can adsorb protons from solution. The C_π sites are located in π-electron rich regions on the basal plane of carbon crystallites, i.e. away from the crystallite edges. Therefore, basic sites are Lewis type basic sites associated with the carbon structure itself [Boehm, 1994]

Several methods have been developed to obtain a carbon surface with basic properties. One method involves heat treatment in an inert atmosphere. Carbons can acquire a basic character upon high-temperature (>973K) treatment in an inert atmosphere and subsequent exposure to air below 473K [Puri and Bansal 1966]. Heat treatment will create unsaturated surfaces as a result of thermal desorption of acidic functional groups in the form of CO_2, and these surfaces are prone to oxygen readsorption when the sample is exposed to air. Another method to create basic carbon surfaces involves heat treatment in an ammonia-atmosphere. Treatment with ammonia at

673-1173K effectively removes acidic oxygen-containing functional groups and introduces basic nitrogen containing groups (see details in section 2.3). A third method involves heat treatment in a hydrogen- atmosphere. Activated carbons treated in hydrogen at high temperature (1173K or higher) or at a lower temperature (773K) in the presence of platinum, were found to be basic and stable in ambient laboratory conditions (see details in section 2.3)

2.2.2. Characterization of Activated Carbon Surface Chemistry

The chemistry of activated carbon has been studied by using both classical wet chemical methods and modern spectroscopic methods. A summary of the applications and limitations of these methods is given below.

Elemental Analysis. Because it is convenient, easy and inexpensive, elemental analysis is employed in most studies as a quantitative and qualitative measurement for changes in carbon chemistry as a result of chemical modifications. Elemental analysis is a destructive test that gives the composition of the bulk material instead of information about the carbon surface. Therefore, results from elemental analysis should not simply be treated as a reflection of surface chemistry. Nonetheless, changes in the surface chemistry for a series of carbons as a result of chemical modifications should be detected relative to a reference adsorbent.

Surface Titrations. (1) *Boehm Titration.* The acidity constants of carboxyl groups, lactones, and phenols differ over several orders of magnitude, and it was established that the different groups can be distinguished by their neutralization behavior [Boehm et al. 1964, Noh and Schwarz 1989]. The concentrations of acidic sites of various types are

calculated under the assumption that NaOH neutralizes carboxylic, phenolic and lactonic groups; Na_2CO_3 neutralizes carboxylic and lactonic groups; and $NaHCO_3$ neutralizes only carboxylic groups. The concentrations of basic sites can be calculated from the amount of HCl that is consumed by the carbon. Surface titration methods are not practical when dealing with small samples. In addition, they fail to account for a large proportion (as high as 50%) of the total oxygen content of carbon materials [Noh and Schwarz 1989]. (2) *pH Drift and Mass Titration.* These two methods are usually used to measure the pH at which the carbon surface carries no charge (i.e., the point of zero charge or PZC). For pH drift tests, a plot of initial pH vs. equilibrium pH following carbon addition is constructed, and the PZC is determined as the point at which no change in solution pH occurs. In mass titration tests, a plot of equilibrium pH vs. adsorbent mass fraction in suspension yields a curve where the pH corresponding to the plateau of the curve corresponds to the PZC (see experimental details in next section). A practical limitation of mass titration tests is that the solid/water ratio should be below 20%, because the suspension becomes too dense for proper pH measurement [Noh and Schwarz 1989].

Temperature-programmed Desorption (TPD). TPD has become rather popular for the characterization of the solid surfaces. Surface oxygen groups on carbon materials decompose upon heating by releasing CO and CO_2 at different temperatures. Some general trends are (1) a CO_2 peak results from carboxylic acid at low temperatures, or lactones at higher temperatures, (2) carboxylic anhydrides produce both a CO and a CO_2 peak, and (3) phenol, ethers and carbonyls (and quinones) produce a CO peak [Polovina et al. 1997]. However, the TPD spectra showing CO and CO_2 peaks must be deconvoluted (separated) before the surface composition can be estimated.

Infrared Spectroscopy (IR). IR has played an important part in the investigation of activated carbon surface chemistry [Vicete GS 1999, Hu and Vansant 1995, Castilla 2000, Sellitti et al. 1990, Zawadzki 1988, Mattson and Mark 1971]. Direct information on the presence of surface functional groups can be obtained from IR studies. However, carbon materials often present difficulties in IR studies, because of their unique physicochemical properties (such as difficulties in sample preparation, poor transmission and uneven light scattering). Some success has been reported with attenuated total reflection (ATR) - Fourier Transform IR (FTIR). ATR-FTIR spectroscopy is a versatile and powerful technique for infrared sampling that requires minimal or no sample preparation for rapid analysis. Also, ATR is ideal for those materials that are strong absorbers of infrared light, such as activated carbon. When light travels across the boundary between two materials, the change in refractive index between the two materials causes reflection of some of the light. The proportion of reflected light is a function of the angle of incidence, θi, at which the light encounters the boundary. When the refractive index of the first material (n_1) is higher than the refractive index of the second material (n_2), the amount of reflected light increases with θi, until it reaches 100% at the critical angle, θc. Beyond θc, all of the incident radiation is reflected. This is the region of total internal reflection. If the second material absorbs the incident radiation appreciably, the amount of reflected light will be reduced by the amount absorbed. This results in attenuated total reflection (ATR). By measuring the attenuated total reflection as a function of wavelength, an absorption spectrum of the absorbing medium is obtained. This is the principle behind ATR Fourier transform infrared spectroscopy [Lambert 1998, Zawadzki 1998]. IR spectra of activated carbons indicate the possible

presence of oxygen containing groups, such as carbocylic, quinone, ether, phenolic, and lactone, C=C of aromatic rings, and nitrogen containing groups like pyridine, nitrile, cyclic amide [Sellitti et al. 1990, Zawadzki 1998, Mangun et al. 2001]. However, in general, the interpretation of the spectra is complicated by the fact that each group originates several bands at different wave numbers, therefore each band may include contributions from various groups. Furthermore, IR does not provide quantitative information about the presence of individual functional groups on the activated carbon surface. It should also be noted that because of the very limited depth of penetration of the internal reflectance evanescent wave, the internal surface of an activated carbon is largely not accessible to IR spectroscopic techniques [Mattson and Mark 1971].

X-ray Photoelectron Spectroscopy (XPS). XPS is based on the photoelectric effect outlined by Einstein in 1905, where the concept of photons impinging a surface was used to describe the resulting ejection of electrons from that surface. The XPS technique is highly surface specific due to the short range of the photoelectrons that are excited from the solid. The energies of the photoelectrons leaving the sample, which is determined using a Concentric Hemispherical Analyser (CHA), gives a spectrum with a series of photoelectron peaks. The binding energies of the peaks are characteristic of each element. The peak areas can be used (with appropriate sensitivity factors) to determine the chemical composition of the surface. The shape of each peak and the binding energy can be slightly altered by the chemical state of the emitting atom [Macdonald et al. 1996]. Hence XPS can provide chemical bonding information as well. XPS is not sensitive to hydrogen or helium, but can detect all other elements. XPS is a non-destructive (or weak)

surface technique that provides the information of the few uppermost layers of the material. XPS can provide valuable information from the C1s region for carbon materials. Substantial changes in the nature of the carbon due to changes in surface chemistry such as oxidation can be identified through an examination of the C1s core region [Proctor and Sherwood 1982]. Kaneko [1995] showed that the surface oxidation increased the intensity of the XPS C1s tail in the high-energy region. In the C1s core region, surface oxides were identified as –C–O groups, –C=O groups, and carboxylic acid or ester groupings, which correspond to chemical shifts of 1.6, 3.0 and 4.5eV (in C1s), respectively [Proctor and Sherwood 1982]. The interpretation of XPS spectra is complex because the chemically shifted carbon must first be distinguished from the primary carbon and then associated with specific surface groups. One can also examine the chemical shifts in the N1s region. XPS is the most successful method for studying nitrogen-containing functionalities in solid materials. Pels [1995] concluded that two major constituents of nitrogen functional groups in chars and coals are pyrrolic and pyridinic groups with XPS N1s peaks at binding energies of 400.3 and 398.7 eV, respectively. Mangun [1997 and 2001] reported that pyridine with a binding energy of 398.4 eV was the dominant nitrogen-containing functional group when activated carbon fibers were heat-treated in ammonia at high temperature.

2.3. Materials and Methods

2.3.1. Surface Chemistry Modification

As-received Activated Carbon Fibers (ACF). ACF samples with three activation levels (ACF-10, ACF-15, and ACF-20) were donated towards this research project by

Nippon Kynol. The base material for these ACFs was a phenolic resin. Following carbonization, the fibers were oxidized with steam and CO_2 to different levels of activation. The surface chemistry of as-received ACFs was modified as described below to prepare a matrix of adsorbents with 3 activation levels and 4 surface chemistry levels.

Acid Washing. As-received ACF samples were acid-washed by soaking the ACF overnight in 2N HCl and subsequently boiling the ACF for 1 hour in 2N HCl. The samples were then rinsed with organic-free water until no more chloride could be detected by $AgNO_3$ in the rinse water. Acid-washed ACF was dried at room temperature in a vacuum desiccator.

Oxidation. Acid-washed activated carbon fiber samples were oxidized by contacting 5g of ACF with 200mL of 30% H_2O_2 for 16 hours at room temperature. Following oxidation, the ACF was dried in an oven at 110°C.

Hydrogen Treatment. Heat treatment of activated carbons in a hydrogen atmosphere will create a stable basic activated carbon surface by removing acidic oxygen-containing functional groups in the form of CO and CO_2. Furthermore, H_2 treatment stabilizes the resulting basic activated carbon surface by producing relatively stable carbon atoms at the edges of the graphitic platelets that no longer contain unpaired electrons [Menendez et al. 1996]. To minimize impacts on pore structure, a recently developed method by Menendez et al [Menendez et al. 1996] was used to create stable basic surfaces by exposing adsorbents to hydrogen at 773 K in the presence of a platinum catalyst. A 1.5 g sample of acid-washed ACF was mixed with 1 g of commercially available granular carbon containing 1% platinum by weight in highly dispersed form (Alfa Aesar, Ward Hill, MA), and the mixture was placed into an alumina sample boat,

which was placed into a tube furnace. The furnace temperature was raised to 1173 K with a nitrogen flow rate of 200mL/min. The sample was held at 1173 K for 2 hours in flowing nitrogen, then cooled to 773K and held at that temperature for 3 hours with a hydrogen (research grade) flow rate of 200mL/min. Upon cooling to room temperature in the tube furnace under nitrogen, the hydrogen- treated ACF samples were stored in a vacuum desiccator.

Ammonia Treatment. Heat treatment in an ammonia atmosphere is also capable of creating basic ACF surfaces. To obtain ammonia-treated ACF samples, 1.5g acid-washed ACF was placed into an alumina sample boat, which was placed into the tube furnace. The furnace temperature was raised to 1173K with a nitrogen flowrate of 200mL/min. The sample was held at 1173 K for 2 hours and then cooled to 973 K while maintaining a flowrate of 200mL/min nitrogen. Subsequently, nitrogen was replaced with 200mL/min UHP-grade ammonia, and the sample was exposed to ammonia at 973 K for 1 hour. Upon cooling to room temperature in the tube furnace under nitrogen, the ammonia-treated ACF samples were stored in a vacuum desiccator. To facilitate comparisons among modified ACFs, the abbreviations shown in Table 2.1 will be used throughout this thesis.

For hydrogen and ammonia treatments, a 3-zone tube furnace (Lindberg/Blue M, Asheville, NC) was used. The furnace was equipped with PID temperature controllers and was capable of reaching a maximum temperature of 1373K. The reaction tube was an inert 3-inch O.D. alumina (Al_2O_3) tube (Vesuvius McDanel, Beaver Falls, PA). The reaction tube was sealed using Gore-Tex insertable gaskets (McMASTER-CARR Inc., Atlanta, GA) and a LOX 8 PTFE lubricant (FLUORAMICS Inc., Mahwah, NJ) To

determine the temperature inside of the reaction tube, an additional thermocouple was installed. The furnace set up is depicted in Figure 2.1.

As-received GACs. To verify whether correlations developed for the ACF matrix are also valid for commercially available granular activated carbons (GACs), tests were conducted with as received bituminous coal-based F-600 GAC (Calgon Carbon Corporation, Pittsburgh, PA), coconut shell-based G-219 GAC (PicaUSA, Columbus, OH), and chemically activated wood-based Picazine GAC (PicaUSA, Columbus, OH).

2.3.2. Characterization of ACFs and GACs

Point of Zero Charge (PZC). The point of zero charge for activated carbon surfaces was assessed by (1) mass titration as described by Noh and Schwarz [1989] and Barton et al. [1997], and (2) pH drift experiments as described by Karanfil [1995].

Mass Titration. Using carbon doses up to 5% (wt/wt), mass titrations were performed in 25-mL crimp-cap culture tubes containing 20 mL of 0.1N NaCl solution. To eliminate interference from dissolved and atmospheric CO_2, the NaCl solution was sparged with N_2 for four hours and culture tubes were filled and capped in an anaerobic hood (N_2/H_2 atmosphere). Changes in solution pH as a result of the activated carbon additions were measured in an anaerobic hood after tumbling suspensions for 48 hours. The pH_{PZC} was taken as the average plateau value that was obtained for the largest carbon doses.

pH Drift. Solution preparation and pH measurements were performed in an anaerobic hood at constant temperature. ACF and GAC samples (100 mg) were contacted with 100 mL of 0.01 M NaCl solution in 100 ml serum bottles. The pH of each solution

was adjusted using NaOH and HCl such that initial pH values ranged from approximately 3 to 11 (or 2 to 10 for the most acidic carbons) for each carbon sample. Blank samples without activated carbon were also prepared at the same initial pH values. The bottles were sealed with teflon-faced grey butyl rubber stoppers, placed on a rotary tumbler, and allowed to equilibrate for 48 hours. Following equilibration, a second pH reading was taken. A plot showing the initial pH versus the final pH was prepared for each tested activated carbon. The pH_{pzc} was determined as the point at which no change in solution pH occurred during the equilibration period.

Infrared Spectroscopy. For the IR analysis of ACF samples, the attenuated total reflectance (ATR) technique was used. Surface functional groups of ACF samples were analyzed by FTIR using an FTS 6000 Spectrometer (Bio-Rad Laboratories, Cambridge, MA) equipped with an MCD detector. Spectra were obtained using a multi-point reflection ATR attachment (Spectra-Tech, Shelton, CT) with a germanium internal reflection element (IRE) crystal. Germanium was selected because it has the highest refractive index (n = 4.0) which ensured the total reflection of the incident light for carbon (n = 3.3). Samples were placed on the IRE crystal in the sample chamber, which was purged with dry air. Each spectrum was obtained with 4 cm^{-1} resolution and 128 coadditions.

Elemental Analysis. To obtain information about the elemental compositions of the adsorbents, the C, H, N, and O contents of each ACF and GAC were measured. The percentages of carbon, hydrogen, and nitrogen were determined using a Perkin-Elmer CHN Elemental Analyzer (Perkin-Elmer Corp., Norwach, CT) in the Soil Science

Department at North Carolina State University. The oxygen content was being determined by Huffman Laboratories (Golden, CO) according to ASTM D5622.

2.4. Results and Discussion

2.4.1. pHpzc

The point of zero charge of ACF surfaces was assessed as by both pH drift and mass titration methods. Table 2.2 summarizes the pH_{PZC} results for the ACF matrix. In general, the two titration methods provided similar results. The data for the acid-washed ACF samples illustrate that their surfaces exhibited a slightly acidic character. Oxidation by H_2O_2 clearly lowered the pH_{PZC}, a result that suggests that the chosen oxidation technique introduced acidic functional groups such as carboxylic acid groups on the ACF surfaces. Hydrogen treatment created ACFs that were more basic than the AW samples; however, the carbons still exhibited a slightly acidic character. When ACF samples were treated in an ammonia atmosphere, the ACFs assumed a strong basic character with pH_{PZC} values of about 10.5. To assess the stability of the ACF surface chemistry following hydrogen-treatment and ammonia-treatment, pH drift experiments were repeated after storage of HAW and AAW samples for several months. As shown in Table 2.2, the ammonia-treated carbons appeared to lose some of their basicity, while the pH_{PZC} of hydrogen-treated carbons did not change. The latter result is consistent with those of Menendez et al. [21] who showed that activated carbons treated in H_2 adsorb very little oxygen at room temperature. It was postulated that treatment in H_2 not only removes oxygen (as CO and CO_2) but also stabilizes some of the very reactive residual carbon atoms. Table 2.3 shows pH_{PZC} data for GACs in both granular and pulverized forms.

Pulverized GACs were used in this study to reach adsorption equilibrium more rapidly. As indicated in Table 2.3, pulverization had little effect on the surface acidity of the GACs, as expected.

2.4.2. Elemental analysis

Table 2.4 shows the element analysis results for ACFs and GACs. The C, H, N, and O contents of the ACF samples represented approximately 94-98% of the total adsorbent mass, confirming that the ash content of the phenolic resin-based ACF samples is small. The oxygen contents for the HAW and AAW samples were over 50% less than those for the corresponding AW samples, a result that suggests that outgassing and the subsequent hydrogen- or ammonia-treatments resulted in more hydrophobic ACFs. The oxidation of acid-washed ACFs increased the oxygen content to about 10%. The results of the elemental analysis are consistent with the pH_{PZC} data because the surface acidity increases with the increase of oxygen content [Barton et al. 1997]. Furthermore, incorporation of nitrogen functional groups tends to give a basic character for the AAW samples. Table 2.4 also showed that the low-ash GACs exhibited a wide range of oxygen contents. F600 and G219, the GACs with the lower oxygen contents exhibited a basic character while Picazine with an oxygen content of nearly 16% was strongly acidic. Because Picazine is chemically activated using phosphoric acid, one could argue that a fraction of the measured oxygen content was associated with phosphates instead of the carbon surface. A phosphorous content of approximately 1% (wt/wt) was measured for Picazine, suggesting that no more than approximately 2% (wt/wt) oxygen was associated with phosphates. Consequently, the largest fraction of the measured oxygen content of

Picazine (Table 2.4) was associated with the carbon surface, which explains its acidic character.

2.4.3. IR

To further evaluate the effects of chemical modifications on ACF surface chemistry, IR spectra were collected for all members of the ACF matrix (Figures 2.2 to 2.4). In addition, Figure 2.5 depicts IR spectra for the three GAC samples evaluated in this study. Functional group assignments are summarized in Table 2.5.

In the range of 3600-3000 cm^{-1}, a broad O-H stretching vibration was observed for all ACF samples (Figures 2.2 to 2.4). The width and asymmetry of this band indicates the presence of strong hydrogen bonds. These hydrogen bonds could be a result of interactions between N, H, and O containing moieties on the ACF surface or a result of strongly adsorbed water on hydrophilic functional groups on the ACF surfaces. In contrast, the broad O-H stretching vibration in the range of 3600-3000 cm^{-1} was not observed for GACs (Figure 2.5). Given that the ACFs were prepared from a phenolic resin, it is therefore likely that the broad O-H stretching vibration in the range of 3600-3000 cm^{-1} resulted from the presence of phenolic O-H groups. A comparison between ammonia-treated and other ACFs shows the same band shapes in the 3600-3000 cm^{-1} range, suggesting that N-H groups, which also absorb in this range [Lambert 1998], were not formed during ammonia-treatment or their presence was overshadowed by the presence of O-H stretching vibrations.

For the ACF samples, dominant peaks in the 2000-1500cm^{-1} range are observed at the 1720-1750, 1650, and 1550-1570 cm^{-1} bands, which can be attributed to C=O

moieties in carboxylic acids, esters, and lactones (at 1720-1750 cm^{-1}); quinone structures (at 1650 cm^{-1}); and conjugated systems such as diketone, ketoester, and keto-enol structures (at 1570 cm^{-1}) [Sellitti et al. 1990, Meldrum and Rochester 1990, Nakahara and Sanada 1995]. Compared to other ACFs, the intensities of 1750 cm^{-1} peaks of OAW ACFs increased. ACFs Peaks in this range may also be related to vibrations of the condensed aromatic ring system. The 1750 cm^{-1} peak of HAW20 is split into two peaks (1778 and 1734 cm^{-1}), which may be attributable to the presence of acid anhydrides. IR spectra for ammonia-treated samples did not exhibit a peak around 1610 cm^{-1}, which would be characteristic for pyridine-type functional groups [Mangun 1997]. Although the pH_{PZC} data clearly indicated that ammonia-treatments led to the incorporation of basic surface functionalities, the employed IR technique was not able to prove the presence of nitrogen-containing functional groups in ammonia-treated ACFs. IR spectra for pulverized F600 and G219 GACs exhibited peaks at the 1550-1570 cm^{-1} bands (Figure 2.5), which may again be attributable to the presence of diketone, ketoester, and keto-enol structures. In addition, F600 exhibited a peak at the 1650 cm^{-1} band, indicating the possible presence of quinone and /or ion-radical structures. The dominant peak in the 2000-1500cm^{-1} range for Picazine, a strongly acidic carbon, was observed at the 1600 cm^{-1} band, which may indicate the presence of COO^- salts [Starsinic et al. 1983]. COO^- salts may have formed from COOH groups during the pulverization process, in which pulverized GAC was washed through a 45-μm sieve. Although deionized water was used for this purpose, metals may have eluted from the acidic Picazine carbon. Because the carbon was subsequently dried in the wash water, the formation of COO^- salts may have occurred during the drying process.

A number of ACF samples exhibited smaller bands in the 1450-1300 cm^{-1} range. These bands consist of a series of overlapping absorption bands that can be attributed to C-O stretching in O-C=O structures, the deformation vibration of surface hydyoxyl groups, in-plane C-H vibrations and C-N vibrations in heterocyclic structures. For both ACFs and GACs, the overlapping peaks that form a broad absorption band in the 1300-1000 cm^{-1} range can be assigned to ether, epi-oxide and phenolic structures (Figures 2.2 to 2.5).

Compared to all other ACFs, oxidized ACFs exhibited an increase in the intensities of bands at 1720-1750 cm^{-1} and 1300-1000 cm^{-1}. Stronger signals in these two regions suggest an increase in carboxylic acid functionalities, a result that is consistent with the larger oxygen content and the greater acidity of the oxidized ACFs (Tables 2.2 and 2.4). The intensity of the band in the 1300-1000 cm^{-1} region decreased in both hydrogen-treated and ammonia-treated ACF samples. This result suggests that oxygen-containing functional groups were lost during hydrogen- and ammonia-treatments, which again is consistent with the results of the elemental analysis data and the loss of acidic functional groups.

2.5. Conclusions

An ACF matrix containing twelve ACFs (3 activation levels, 4 surface chemistry levels) was prepared. Elemental composition, pHpzc and IR data were used to characterize the ACFs and 3 commercially available GACs. The results showed that:

(1) Oxidation treatment increased the acidity of ACFs; while heat treatment in H_2 and NH_3 yielded ACFs more basic. Compared to the NH_3 treated ACFs, H_2 treated ACFs which maintained their basicity were more stable.

(2) A given chemical treatment yielded ACFs with similar heteroatom content and surface acidity/basicity, which permitted the study of pore structure effects on micropollutant adsorption with little interference from surface chemistry effects.

2.6. References

Barton SS, Evans MJB, Halliop E, MacDonald JAF. Acidic and basic sites on the surface of porous carbon. Carbon 1997; 35(9): 1361-1366.

Boehm HP, Diehl E, Heck W, Sappok R. Surface oxides of carbon. Angew. Chem. Internat. Edit. 1964; 3: 669-677.

Boehm, HP. Some Aspects of the surface chemistry of carbon blacks and other carbon. Carbon 1994, 32(5), 759-769.

Biniak S, Szymanski G, Siedlewski J and Swiatkowski A. The characterization of activated carbons with oxygen and nitrogen surface groups. Carbon 1997; 35(12):1799-1810

Castilla CM. Changes in surface chemistry of activated carbons by wet oxidation. Carbon 2000, 38: 1995-2001.

Fabish TJ and Schleifer DE. Surface-chemistry and the carbon-black work function. Carbon 1984; 22(1): 19-38.

Garten, VA, Weiss DE. A new interpretation of the acidic and basic structures in carbons. II. The chromene-carbonium couple in carbon. Austr. J. Chem.1957; 10: 309-328.

Hu, ZH and Vansant EF. Chemical activation of elutrilithe producing carbon-aluminosilicate composite adsorbent. Carbon 1995; 33(9), 1293-1300.

Kaneko, Y. Evaluation of low concentrated hydrophilic sites on microporous carbon surfaces with an XPS ratio method. Langmuir 1995; 11(3): 708.

Karanfil, T. Oxygen sensitivity of natural and synthetic organic maromolecule sorption by activated carbon. Ph.D. Dissertation, 1995; The University of Michigan, Ann Arbor, MI.

Karanfil T and Kilduff JE. Role of granular activated carbon surface chemistry on the adsorption of organic compounds. 1. Priority pollutants. Environ. Sci. Technol. 1999; 33(18): 3217-3224.

Lambert, JB. Organic Structural Spectroscopy. Prentice Hall, 1998; Upper Saddle River, NJ.

Leon y Leon CA, Solar JM, Calemma V and Radovic LR. Evidence for the protonation of basal plane sites on carbon. Carbon 1992; 30(5): 797-811.

MacDonald RJ, Taglauer EC, and Wandelt KR. Surface science: principles and current applications. 1996; Berlin, New York: Springer.

Mangun CL. Synthesis and characterization of chemically treated activated carbons for adsorption of trace contaminants. Ph.D. Dissertation, 1997; University of Illinois, Urbana, IL.

Mangun CL, Benak KR, Economy J and Foster KL Surface chemistry, pore sizes and adsorption properties of activated carbon fibers and precursors treated with ammonia. Carbon 2001; 39 (12): 1809-1820

Mattson JS and Mark HB Jr. Activated carbon-surface chemistry and adsorption from solution. New York: Marcel Dekker. 1971.

Meldrum BJ and Rochester CH. In situ infrared study of the surface oxidation of Activated Carbon Dispersed in Potassium Bromide. J. Chem. Soc. Faraday Trans. 1990; 89(11): 2997-3002.

Menendez JA, Radovic LR, Xia B and Phillips J. Low-temperature generation of basic carbon surfaces by hydrogen spillover. J. Phys. Chem. 1996; 100(43): 17243-17248.

Nakahara M and Sanada Y. FT-IR ATR Spectroscopy of the edge surface of pyrolytic graphite and its surface / PVC interface. J. Mater. Sci. 1995; 30: 4363-4368.

Noh JS and Schwarz JA. Estimation of the point of zero charge of simple oxides by mass titration. J. Coll. Interf. Sci. 1989; 130(1): 157-164.

Pels JR. Evelution of nitrogen functionalities in carbonaceous materials during pyrolysis. Carbon 1995; 33 (11): 1641-1653.

Polovina M, Babic B, Kaluderovic B and Dekanski A. Surface characterization of oxidized activated carbon cloth. Carbon 1997; 35(8): 1047-1052.

Proctor A and Sherwood P. XPS Studies of carbon fiber surface. Surface and Interface Analysis 1982; 4(5): 213.

Puri BR and Bansal RC. Studies in surface chemistry of carbon blacks Part 3. Interaction of carbon black and aqueous bromine. Carbon 1966; 3: 53-539.

Puri BR. Surface complexes on carbons. In Walker PL Jr., editor. Chemistry and Physics of Carbon, 1970; New York, Marcel Dekker Inc., 6: 191-282.

Sellitti C, Koenig JK and Ishida H. Surface characterization of graphitized carbon fibers by Attenuated Total Reflection Fourier Transform Infrared Spectroscopy. Carbon 1990; 28: 221-228.

Starsinic M, Taylor RL, Walker PL Jr and Painter PC. FTIR studies of saran chars. Carbon 1983: 21(1): 69-74.

Vicete GS. Formation of oxygen structures by air activation. A study by FT-IR spectroscopy. Carbon 1999; 37: 1517-1528.

Zawadzki J. Infrared spectroscopy in surface chemistry of carbons in “Chemistry and physics of carbons”. Editor,Thrower PA. 1988; Marcel Dekker Inc, New York and Basel.

2.7. Tables

Table 2.1. Nomenclature for ACF matrix

Treatment	Abbreviation		
	ACF-10	**ACF-15**	**ACF-20**
Acid-washed	AW10	AW15	AW20
Oxidized after acid-washing	OAW10	OAW15	OAW20
Hydrogen-treated after acid-washing	HAW10	HAW 15	HAW 20
Ammonia-treated after acid-washing	AAW10	AAW15	AAW20

Table 2.2. pH_{pzc} values of ACFs from pH drift and mass titration experiments

Treatment		ACF10		ACF15		ACF20	
		pH drift	**Mass titration**	**pH drift**	**Mass titration**	**pH drift**	**Mass titration**
AW		5.6	4.8	5.7	5.4	5.4	4.4
OAW		2.4	3.0	2.4	2.9	2.4	3.2
HAW	Fresh	6.4	6.4	6.8	6.5	6.4	6.7
	Aged	6.4	6.4	6.2	6.5	6.4	6.7
AAW	Fresh	10.5	N/A	10.3	N/A	10.6	N/A
	Aged	9.4	8.7	9.6	8.7	9.2	8.7

Table 2.3. pH_{pzc} values of GACs from pH drift and mass titration experiments

	F600		G219		Picazine	
	pH drift	**Mass titration**	**pH drift**	**Mass titration**	**pH drift**	**Mass titration**
GAC	7.08	8.3	10.25	9.7	2.92	2.1
GAC (pulverized)	7.85	N/A	10.34	N/A	2.88	N/A

Table 2.4. Elemental analysis results for ACFs and GACs*

ACF	C (Wt. %)	H (Wt. %)	N (Wt. %)	O (Wt. %)	Ash (Wt. %)	Total (%)
AW10	90.18 ± 0.31	0.34 ± 0.02	0.17 ± 0.02	4.57	N/A	95.26
AW15	92.73 ± 0.29	0.40 ± 0.17	0.18 ± 0.01	3.62	N/A	96.93
AW20	92.33 ± 0.15	0.27 ± 0.01	0.15 ± 0.01	3.58	N/A	96.33
OAW10	82.21 ± 1.17	0.54 ± 0.04	0.14 ± 0.01	10.78	N/A	93.68
OAW15	82.37 ± 0.84	0.36 ± 0.02	0.19 ± 0.02	11.34 ± 0.54	N/A	94.25
OAW20	86.30 ± 0.48	< 0.04	<0.04	9.58 ± 0.06	N/A	97.63
HAW10	93.14 ± 0.92	0.36 ± 0.17	0.11 ± 0.03	2.32 ± 0.19	N/A	95.92
HAW15	96.00 ± 0.60	0.27 ± 0.03	0.09 ± 0.01	1.39	N/A	97.74
HAW20	95.68 ± 0.23	0.24 ± 0.02	0.09 ± 0.02	1.66	N/A	97.68
AAW10	92.22 ± 0.81	0.38 ± 0.08	1.80 ± 0.63	2.08 ± 0.17	N/A	96.47
AAW15	95.26 ± 0.55	0.73 ± 0.06	1.89 ± 0.23	1.45 ± 0.16	N/A	99.33
AAW20	93.50 ± 0.53	0.29 ± 0.04	1.52 ± 0.66	1.23 ± 0.45	N/A	96.54
F600	92.50 ± 1.68	< 0.04	0.33 ± 0.04	2.60	1.84±0.01	97.27
G219	90.61 ± 0.45	< 0.04	0.05 ± 0.04	4.90	2.82±0.04	98.37
Picazine	76.92 ± 0.53	0.40 ± 0.03	0.03 ± 0.03	15.88	3.37±0.11	96.59

*Values represent means ± one standard deviation of replicate analyses (n = 2-3).

Table 2.5. Peak assignments for IR spectra

Moiety	Peak	Reference
CO_2	3730, 3710 cm^{-1}	Lambert 1998
Bonded O-H	3100~3600 cm^{-1}	Lambert 1998
Germanium crystal Aliphatic CH_3, CH_2 stretching	2930, 2860 cm^{-1}	Spectra-Tech[a] Biniak et al. 1997 Lambert 1998
Carboxylic acids, ester, lactone	1750 cm^{-1}	Meldrum and Rochester 1990, Nakahara and Sanada 1995 Sellitti et al. 1990
Quinones, ion radical structures C=O stretching	1650 cm^{-1}	Meldrum and Rochester 1990, Nakahara and Sanada 1995 Sellitti et al. 1990 Biniak et al. 1997
Ketones, esters, keto-enol C=O stretching	1570 cm^{-1}	Biniak et al. 1997
Deformation vibrations of surface – OH groups, in-plane C-H vibrations in C=C-H structure	1450-1300 cm^{-1}	Biniak et al. 1997
Carboxylic acids, esters, C-O-C stretching	1300-1000 cm^{-1}	Biniak et al. 1997 Lambert 1998

[a] Information provided with germanium crystal.

2.8. Figures

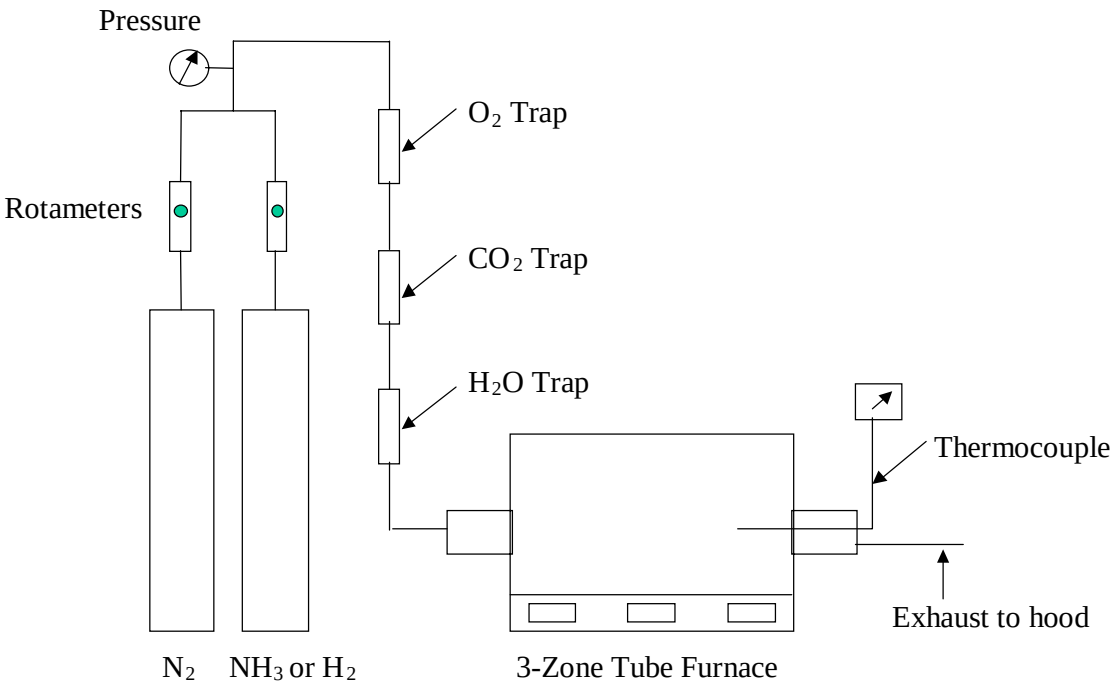

Figure 2.1. Tube furnace setup

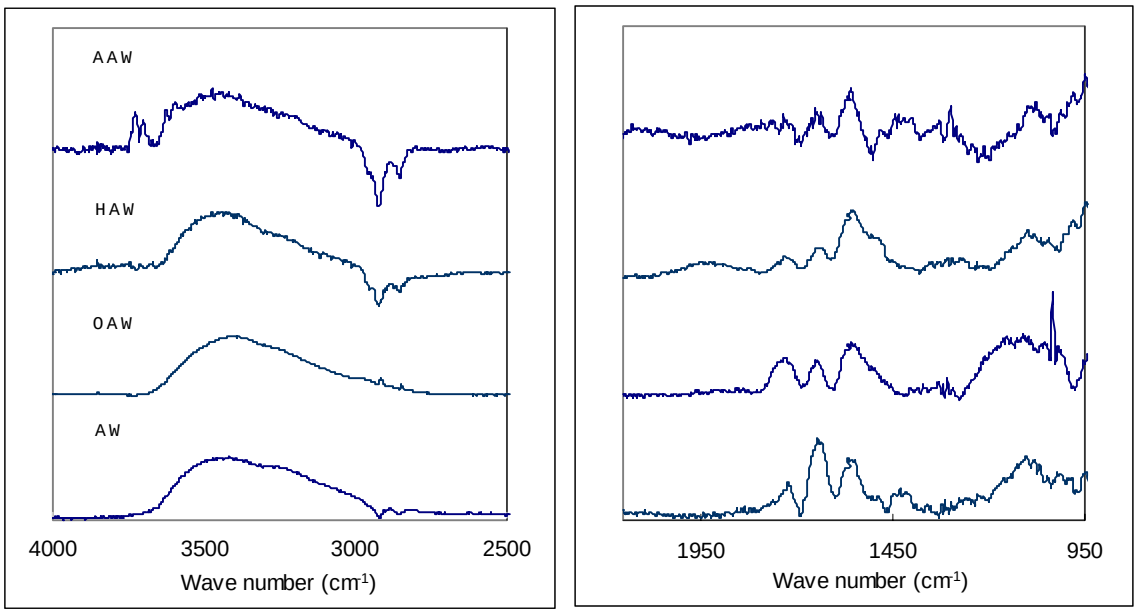

Figure 2.2. IR spectra of ACF10s

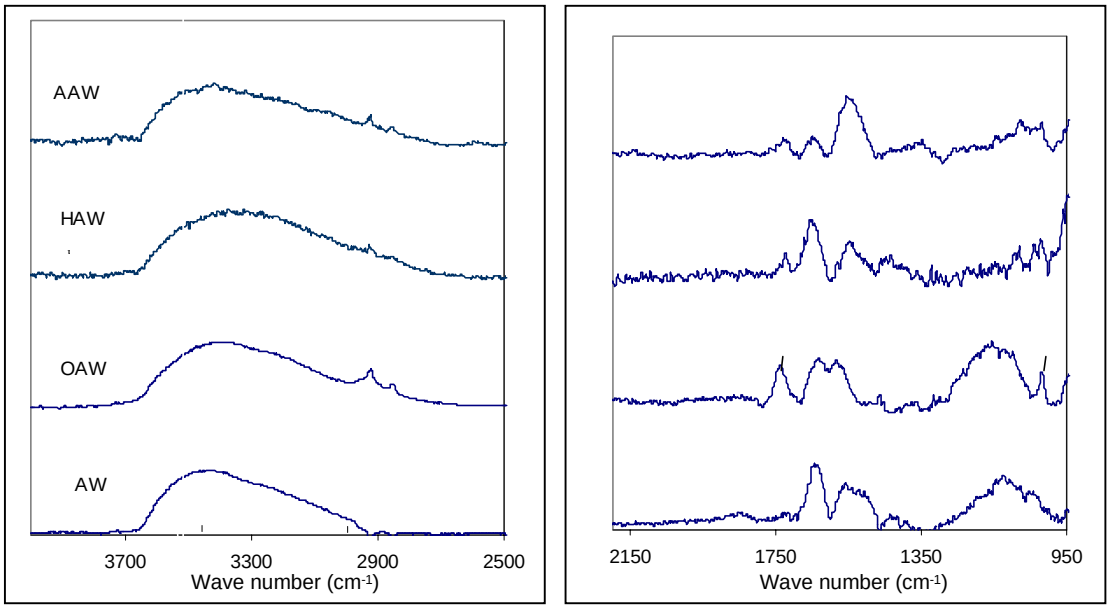

Figure 2.3. IR spectra of ACF15s

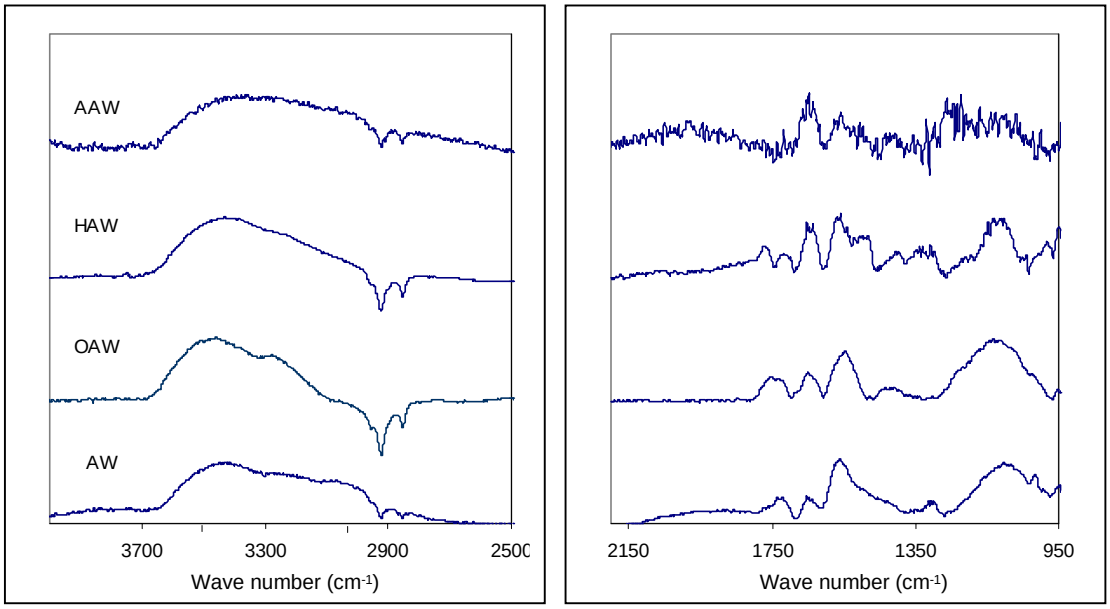

Figure 2.4. IR spectra of ACF20s

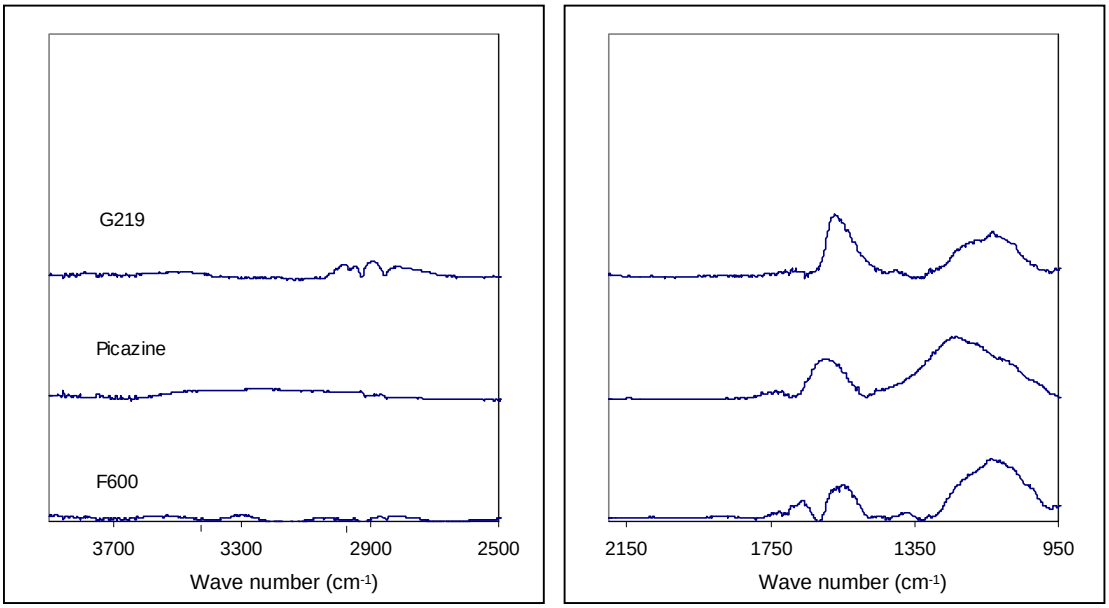

Figure 2.5. IR spectra of GACs

Chapter 3. Characterization of Activated Carbon Pore Structure

3.1. Objectives

The objectives were (1) to determine adsorbent physical properties such as the Brunauer, Emmett and Teller (BET) surface area, pore volume and pore size distribution, and (2) to compare different methods for the estimation of pore size distributions.

3.2. Background

3.2.1. Activated Carbon Pore Structure

Pore shape. The shape of activated carbon pores is mainly unknown, but is typically approximated by a) cylindrical pores having a circular cross section, b) ink-bottle pores having a narrow neck and wide body, or c) slit-shaped pores between parallel plates. For ACFs employed in this study, direct observation suggests that pores exhibit an ellipsoidal cross section [Daley et al. 1996]

Pore size and pore size distribution (PSD). Activated carbon pores can be divided into (1) micropores (< 20 Å width) (2) mesopores (20-500 Å width), and (3) macropores (> 500 Å width) as defined by the International Union of Pure and Applied Chemistry (IUPAC) [Sing et al. 1985]. Micropores can be further subdivided into primary (< 8 Å width) and secondary micropores (8-20 Å width). The macropores represent the entrance to the internal activated carbon pore structure, the mesopores facilitate diffusive transport of adsorbates to adsorption sites and the micropores represent the region where the majority of trace organic micropollutants adsorb. Powdered activated carbon and granular activated carbon traditional employed in drinking water treatment plants contain

macropores close to the external particle surface that branch into mesopores and finally micropores. In contrast, ACFs have narrowly defined pore size distributions and micropores that are distributed throughout the entire fiber [Daley et al. 1995]. The PSD of the micropore region is difficult to obtain [Manes 1998, Ishizaki 1998, Patrick 1995, Fraissard 1997], but it is often the most useful for determining the adsorption capacity of a given adsorbent for an adsorbate of a given size.

3.2.2. Characterization of Pore Structure and Pore Size Distribution

Indirect observation

Porous media are generally characterized indirectly by gas adsorption methods that provide information about adsorbent porosity, surface area, mean pore size and pore size distributions.

Surface area. Surface areas are most commonly obtained through the analysis of adsorption isotherm data of nitrogen or other gaseous adsorbents. In the Brunauer-Emmett-Teller (BET) method, the experimental isotherm is fitted by a multi-layer adsorption model, from which a monolayer capacity of the material is extracted. To convert the monolayer capacity to a surface area, the monolayer (adsorbate) density needs to be known. Its value is obtained experimentally using a reference system of known surface area. The accuracy of this method requires that the monolayer density be transferable; i.e., that it is not dependent on the surface curvature or pore structure, and not strongly dependent on the chemistry of the underlying surface [Ishizaki 1998].

Pore size distribution (PSD). The determination of PSD of a given adsorbent usually involves the approximate solution of the generalized adsorption isotherm (*GAI*)

$$V(P) = \int f(w)v(w,P)dw \qquad (1)$$

where V(P) is the experimentally determined adsorption volume at pressure P, f (w) is the PSD, and ν (w, P) is the *kernel* function (or the local isotherm) which describes the adsorption isotherm inside a pore of width w [Olivier 1998]. The solution to equation (1) requires that the kernel function, ν(w, P), is known. Density functional theory (DFT) [Fraissard 1997] and the Stoeckli [2000 and 2002] method are two approaches to construct ν (w, P).

The density functional theory (DFT) is one of the most widely applied methods for the characterization of microporous carbons [Dombroski et al. 2000]. DFT is a thermodynamic approach which assumes that pores are slit-shaped and adsorbate molar density (ρ) varies as a function of pore size (w). The procedure employed in the DFT includes (1) defininining the grand potential functional Ω which varies with the average density of the adsorbate in the pore, and (2) minimizing Ω to obtain the local density profile and the net quantity adsorbed at each pressure. The DFT method bridges the gap between micropore, mesopore, and macropore distribution calculations by a combination of innovative mathematical, statistical, and numerical techniques for interpreting data [Patrick 1995]. In other words, the entire pore size distribution of an adsorbent can be obtained from a single data reduction technique. Simpler methods predate the DFT, such as the Kelvin equation and the Horvath and Kawazoe (HK) equation can only predict PSD in a certain pore size range [Sweatman 2001]. The DFT method has been incorporated in the computational software supplied with commercially available adsorption instruments. While the DFT is a major achievement in the estimation of PSD, it is still under development and some aspects require improvement. For example, the

effects of surface heterogeneity is neglected in the slit pore model and PSDs obtained from adsorption isotherms of different gases at different temperatures frequently do not match [Ravikovitch 2000].

The Stoeckli method [Stoeckli 2000 and 2002, Carrott 1999] represents a simpler alternative approach to estimate the local isotherm ν(w, P). This approach is based on the empirical Dubinin–Astakhov (DA) equation which was developed from Dubinin's theory of volume filling of micropores (TVFM). The DA method has been used to describe adsorption in micropores and is extensively used in the calculations of pore size distributions due to its convenient mathematical form [Carrott 1999]

$$\ln V_a = \ln V_{0,1} - (\varepsilon/\beta E_0)^n \quad (2)$$

and

$$\varepsilon = RT \ln (P_s/P) \quad (3)$$

where V_a (cm^3/g) is the experimentally determined adsorbate volume in a condensed state; $V_{0,1}$ (cm^3/g) is the apparent micropore volume; ε is the adsorption potential; β is an affinity coefficient; E_0 (KJ/mol) is the characteristic energy; R is the ideal gas constant; and P_s and P are the saturation pressure and equilibrium pressure of an adsorbate, respectively. Parameters $V_{0,1}$, E_0 and n can be determined from regression analysis of gas adsorption isotherm data plotted in the form $\ln V_a$ vs. ε/β. Based on the DA equation, Stoeckli developed the following expression from the GAI

$$\ln V_a = \ln V_{0,2} + 3m \ln (M) - m \ln (M^3 + \varepsilon^3) \quad (4)$$

$$M = \beta K_0^3 \sqrt[3]{a} \quad (5)$$

$$K_0 = 10.8 + 123.1/(E_0 - 11.4) \quad (6)$$

where the parameters $V_{0,2}$ (apparent micropore volume), a and m can be obtained from regression analysis. The PSD is then obtained from the following expression, which assumes a gamma (Γ) type distribution of pore width (w)

$$\frac{dV}{dw} = \frac{3V_{0,2}a^m w^{3m-1}\exp(-aw^3)}{\Gamma(m)} \qquad (7)$$

Compared to the DFT, the Stoeckli method is more easily to implement. However, the limitation of this method is that it is not recommended to isolated samples, but only to series of related samples [Carrott 1999]. Also, one has to choose the range of data to be used for the calculation for each sample [Carrott 1999].

Direct observation

The direct observation of carbon pores started with the development of scanning and transmission electron microscopy (SEM/TEM) [Bota etal 1997, Brasquet 2000]. In recent years, the development of scanning tunneling microscopy (STM) and atomic force microscope (AFM) opened up further possibilities to directly image the structure of surfaces at the atomic scale in most cases. Daley et al. [1995] found that phenolic based ACFs contain elongated mesopores and ellipsoidally-shaped micropores, with porosity parallel to the fiber axis. The STM observations indicated that ACFs have a uniform pore sizes which makes ACFs ideal candidates for exploring pore size effects on adsorption. The authors concluded that PSDs obtained from STM are close to those derived from the Dubinin-Radushkevich-Stoeckli (DRS) method from nitrogen adsorption isotherms.

3.3. Material and Methods

Surface areas and pore size distributions of ACFs and GACs were determined from N_2 adsorption isotherms at 77K. Prior to analysis, samples were outgassed overnight at 473 K. BET surface areas were determined from 11-point adsorption isotherms that were completed with a 0.1-g sample in the 0.01-0.1 relative pressure range. Subsequently, N_2 isotherms were obtained over a relative pressure range from 10^{-6} to 1 with 0.01-g sample sizes. The low starting relative pressure (10^{-6}) permits the characterization of small micropores in activated carbon. The ACF sample mass for the latter isotherm was adjusted such that the BET surface area matched the value obtained with the larger sample mass. These adsorption isotherms included approximately 100 data points, and more data points were collected at lower relative pressures in order to obtain micropore size distributions from the DFT. The micropore volume and pore size distribution of each adsorbent were subsequently calculated from the adsorption data using the DFT (Vulcan kernel, PC software version 1.19. Quantachrome, Boynton Beach, FL). In addition, CO_2 iotherm data were obtained for AW10 and AW15 at 273K over a relative pressure range of 10^{-6}-10^{-2}.

3.4. Results and Discussion

3.4.1. Isotherms

Figure 3.1 depicts N_2 isotherms that were obtained for AW15 and Picazine. The iostherm shape of both adsorbents is characteristic of type I isotherms which are observed for microporous solids with a relatively small external surface. For Picazine, the steeper

slope of the isotherm at relative pressure above 0.1 and the hysteresis between the adsorption and desorption isotherms is related to the greater presence of mesopore.

3.4.2. Surface Area

Table 3.1 summarizes the BET surface area results for the ACF matrix. The results show that BET surface areas of the acid-washed ACFs increased from 760 m^2/g for AW10 to 1670 m^2/g for AW20, which is consistent with the increasing level of activation. A comparison between BET surface areas of acid-washed and oxidized ACF samples shows that the oxidation procedure had little effect on the BET surface area of ACF10 while the oxidation treatment led to a 9% decrease in BET surface for ACF15s and ACF20s. Hydrogen-treatment increased surface areas by 2 to 9% compared to the acid-washed ACF samples, and ammonia-treatment changed BET surface areas by 2 to 5%. Overall, the employed chemical modification altered the BET surface area by less than 10%. The coefficient of variation (CV) for acid-washed, hydrogen-treated and ammonia-treated ACFs are shown in Table 3.1 (no CV data are available for OAW ACFs and AW15 because no replicates were tested). The two tailed t-test indicated that the BET surface areas of hydrogen- and ammonia- treated ACF10 and ACF20 were significant different from the corresponding acid washed samples (α =0.05).

In addition, BET surface areas were determined for granular and pulverized forms of Calgon F600, Pica G219 and Picazine. Table 3.2 shows that pulverization with a mortar and pestle altered the BET surface areas by less than 5% with the exception of Picazine, for which a 16% increase in BET surface area resulted upon pulverization.

3.4.3. Comparison of Different PSD Models

The PSDs of AW10 and AW15 calculated from different DFT kernels (PC software, Quantachrome, Boynton Beach, FL) and the Stoeckli method were compared to STM [Daley 1995] results. PSDs of ACF10 and ACF15 that resulted from STM are presented in Figures 3.2 and 3.3, respectively [Daley et al. 1995]. Based on these results, average pore sizes of ACF10 and ACF15 are 9.4 Å and 16.1 Å, respectively, which agrees with the increasing level of activation. Furthermore, the PSD of the more highly activated ACF15 was broader than that of ACF10. Pores with sizes less than 5 Å were observed for both ACF10 and ACF15. Mesopores (20-500 Å width) were nearly absent in ACF10 while mesopores constituted about 27% of the pore volume in ACF15.

The PSDs of AW10 and AW15 calculated from the different DFT kernels are shown in Figures 3.4 and 3.5, respectively. For N_2 adsorption data, the DFT kernels Vulcan (version 1.19) and N_2_Carb (version 1.20) were used, while CO_2 adsorption data were analyzed with the CO_2_nldf (version 1.20) and CO_2_gcmc (version 1.20) DFT kernels. Figures 3.4 and 3.5 show that PSDs differed when (1) different probe gases were used and, (2) when different kernels were used for the same adsorbate. Furthermore, only the Vulcan kernel showed the trend that PSDs shifted to larger pores as the activation level increased. The inconsistency of PSDs derived from N_2 and CO_2 was also observed in previous studies [e.g., Ravikovitch et al. 2000, Scaife et al. 2000]. Figures 3.4 and 3.5 also indicated that the PSDs derived from the Vulcan 1.19 kernel gave results that most closely resembled those measured by STM. Therefore, all PSD data reported in this study were calculated with the Vulcan kernel (version 1.19).

The PSDs of AW10 and AW15 calculated from the Stoeckli method are

presented in Figure 3.6. Similar to the DFT method that employed the Vulcan kernel, the Stoeckli method indicated that PSDs shifted to larger pores as the activation level increased. For AW10, the Stoeckli method overestimated the small pores (< 5 Å width), while the DFT (Vulcan kernel) underestimated their presence (Figures 3.2, 3.4 and 3.6). Because the sensitivity limit of N_2 is about 6 Å (base on a minimum relative pressure of 10^{-7}) [Raviovitch et al. 2000], both DFT and Stoeckli methods derived from nitrogen adsorption isotherms are not suitable for analyzing activated carbons with a relatively large volume of pores with widths less than 6 Å. Fortunately, direct observations suggest that such pores were present only to a limited extent in the adsorbents used in this study. For AW15, the PSD derived from the Stoeckli method closely matched the one derived from the DFT (Vulcan kernel) method. Figures 3.5 and 3.6 also indicated that PSDs of AW15 are concentrated in the secondary micropore range, which agrees with the STM results (Figure 3.3).

Pressure ranges used for the DFT and Stoeckli methods are presented in Table 3.3 along with pore volume and pore size results. Stoeckli method parameters were determined using Matlab (Version 5.2, Mathworks Inc.) non-linear functionality. In the DFT method, a relative pressure range of 10^{-6} to 10^{-1} was used, while a more limited pressure range of 10^{-5} (or 10^{-4}) to 10^{-2} is typical for the Stoeckli method. Average pore widths calculated from the DFT (Vulcan kernel) method were 8.9 Å for ACF10 and 11.6 Å for ACF15. Average pore widths of ACF10 and ACF15 calculated from the Stoeckli method were 6.2 Å and 10.1 Å, respectively. The micropore volumes calculated from the DFT method are higher than the micropore volumes calculated from the Stoeckli method. The Stoeckli parameters a and m are also the indications of activation level; as the

activation level increased, a values decreased and m values increased. The results indicate that PSDs derived from the DFT and Stoeckli methods are reasonably consistent if the micropores of the adsorbent are located primarily in the secondary micropore region.

3.4.4. Pore Structure and Pore Size Distribution

Table 3.4 summarizes micropore and mesopore volumes as well as adsorption energies of nitrogen on ACFs. Micropore volumes were calculated by the DFT method (Vulcan kernel, version 1.19) while mesopore volumes were calculated from both DFT (Vulcan kernel, version 1.19) and Barrett, Joyner and Halenda (BJH) methods. Adsorption energies were calculated by the Dubinin-Radushkevich (DR) method. In conjunction with Table 3.1, the results presented in Table 3.4 illustrate that increases in BET surface area were primarily attributable to increases in micropore volume although the mesopore volumes of the ACFs also increased somewhat with increasing activation level. Adsorption energies, which are related to pore sizes, decreased from ACF10s to ACF20s.

Mesopore volumes calculated from DFT and BJH methods differed, but they were linearly related, as shown in Figure 3.7. Therefore, BJH and DFT methods provide the same trends but different absolute values. A similar phenomenon was also observed for DR micropore volume (Table 3.4) and DFT micropore volume. This observation has important practical meaning since reported pore volumes in the literature are frequently calculated by different methods. It is therefore more important to compare relative values of pore volumes among different adsorbents rather than placing a lot of emphasis on the absolute values. DFT mesopore volumes were used in this study because their magnitude

agreed more closely with direct observations that showed the presence of only few mesopores.

Figures 3.8 to 3.10 depict the micropore size distributions for chemically modified ACFs. Micropores of ACF10s were concentrated in the 7 to 11Å width range while those of ACF15 and ACF20s were concentrated in the 9 to 13Å width range. The micropore size distributions obtained in the current study are in close agreement with prior results for as-received ACFs with the same designations [Pelekani and Snoeyink 1999]. As shown in Figures 3.8 to 3.10 and Table 3.4, oxidative treatments reduced the micropore volumes of the activated carbons by about 12 to 23% while heat treatments in H_2 or NH_3 atmospheres had little effect on micropore volumes (4% decrease to 7% increase). With the exception of OAW15, mesopore volume changes were in the ±20% range and were relatively small (in terms of cm^3/g) given the microporous nature of the ACFs. Although surface chemistry modifications had small effects on BET surface areas and pore volumes, they had no noticeable effects on pore size distributions. PSDs calculated from the DFT were very reproducible as illustrated in Figure 3.9 (OAW15(1) and OAW15(2)).

Table 3.5 and Figure 3.11 present the pore volumes and pore size distributions of the commercially available GACs. Both F600 and G219 exhibited pore size distributions that were broader and less uniform than those of the ACFs. Micropores of F600 were concentrated in the 7 to 12Å width range while those of G219 were concentrated in the 7 to 13Å width range. The micropores of Picazine were largest among the commercially available GACs and were concentrated in the 9 to 15Å width range. Table 3.5 also indicates that pulverization had little effect on micropore volumes except for Picazine.

Again, PSDs calculated from the DFT were very reproducible as illustrated in Figure 3.11 (F600(1) and F600(2)).

3.5. Conclusions

The BET surface area, pore volume and pore size distribution of ACFs and GACs were determined. In addition, a comparative analysis of different methods for the assessment of pore size distributions was performed. The results showed that:

(1) The chemical modifications employed in this research did not change the pore size distributions of ACFs. Therefore, the developed ACF matrix permitted the evaluation of surface chemistry effects on micropollutant adsorption in the absence of pore size effects.

(2) A standard method for the determination of micropore size distributions is still lacking. The density functional theory (DFT) is a promising tool; however, questions remain with respect to which adsorbate (e.g., N_2, CO_2 or Ar) is most suitable for the determination of micropore size distributions. Perhaps even more importantly, DFT kernels need to be developed that produce congruent PSDs for activated carbons.

3.6. References

Brasquet C. Observation of activated carbon fibers with SEM and AFM correlation with adsorption data in aqueous solution. Carbon 2000; 38: 407-422.

Bota A, Laszlo K, Nagy LG, and Copitzky T. Comparative study of active carbons from different precursors. Langmuir 1997; 13 (24): 6502-6509.

Carrott PJM and Ribeiro-Carrott MML Evaluation of the Stoeckli method for the estimation of micropore size distributions of activated charcoal cloths. Carbon 1999; 37: 647-656.

Daley MA, Tandon D, Economy J and Hippo EJ. Elucidating the porous structure of activated carbon fibers using direct and indirect methods. Carbon 1996; 34(10): 1191-1200.

Dombroski RJ, Hyduke DR and Lastoskie CM. Pore size analysis of activated carbons from argon and nitrogen porosimetry using density functional theory. Langmuir 2000; 16(11): 5041-5050.

Fraissard J. Physical adsorption: experiment, theory and applications. Kluwer Academic Publishers, 1997; Dordrecht, Boston and London.

Ishizaki K. Porous materials, process technology and applications. 1998. Kluwer Academic Publishers. Boston.

Manes M. Activated carbon adsorption fundamentals. In Encyclopedia of environmental analysis and remediation. 1998; Editor: Meyers, RA. John Wiley & Sons Inc. NY.

Olivier J. Improving the models used for calculating the size distribution of micropore volume of activated carbons from adsorption data. Carbon 1998; 36(10): 1469-1472.

Patrick JW. Porosity in carbons. 1995. John Wiley & Sons, Inc. NY

Pelekani C, Snoeyink VL. Competitive adsorption in natural water: role of activated carbon pore size. Water Research 1999; 33(5): 1209-1219.

Ravikovitch PI, Vishnyakov A, Russo R and Neimark A. Unified approach to pore size characterization of microporous carbonaceous materials from N_2, Ar, and CO_2 adsorption isotherms. Langmuir 2000; 16: 2311-2320.

Scaife S, Kluson P and Quirke N. Characterization of porous materials by gas adsorption: do different molecular probes give different structures? Journal of Physical Chemistry B 2000; 104: 313-318.

Sing KSW, Everett DH, Haul RAW, Moscou L, Pierotti RA, Rouquerol J, and Siemieniewska T. Reporting physisorption data for gas solid systems with special reference to the determination of surface-area and porosity (recommendations 1984). Pure and Applied Chemistry 1985; 57(4):603-619.

Stoeckli F, Guillot A, Hugi-Cleary D and Slasli AM. Pore size distributions of activated carbons assessed by different techniques. Carbon 2000; 38: 929-941.

Stoeckli F, Guillot A, Hugi-Cleary D and Slasli AM. The comparison of experimental and calculated pore size distributions of activated carbons. Carbon 2002; 40: 383-388.

Sweatman MB and Quirke N. Characterization of porous materials by gas adsorption at ambient temperatures and high pressure. Journal of Physical Chemistry B 2001; 105: 1403-1411.

3.7. Tables

Table 3.1. BET surface areas of ACF samples

Treatment	BET Surface Area (m^2/g)		
	ACF-10	**ACF-15**	**ACF-20**
Acid-washed (AW)	760 (μ=755, σ=5.9, CV=0.78%)*	1480	1670 (μ=1671, σ=11.3, CV=0.67%)*
Oxidized (OAW)	750 (-0.9 %)+	1350 (-9.0 %)+	1530 (-9.1%)
Hydrogen-treated (HAW)	830 (μ=827, σ=3.5, CV=0.42%)§ (+9.2 %)+	1530 (μ=1532, σ=15.0, CV=0.98%) § (+4.6 %)+	1710 (μ=1714, σ=30.4, CV=1.78%) § (+2.4 %)+
Ammonia-treated (AAW)	720 (μ=715, σ=28.3, CV=3.96%) § (-5.3%)+	1510 (μ=1508, σ=42.1, CV=2.79%) § (+2.0%)+	1700 (μ=1696, σ=16.3, CV=0.96%) § (+1.8%)+

* μ ,σ and CV for AW represent the mean, standard deviation and coefficient variation of replicate analyses

§ μ ,σ and CV for HAW and AAW represent the mean, standard deviation and coefficient variation of different batches

+ Percent change from BET surface area for corresponding acid-washed ACF sample is shown in parentheses for chemically modified adsorbents

Table 3.2. BET surface areas of GAC samples

GAC		Surface Area(m^2/g)
F600	Granular	860
	Pulverized	820 (-4.7 %)+
G219	Granular	1290
	Pulverized	1270 (-1.6 %)+
Picazine	Granular	1450
	Pulverized	1680 (+15.9 %)+

+ Percent change from BET surface area for corresponding GAC sample is shown in parentheses for pulverized adsorbents

Table 3.3. PSD parameters in DFT (Vulcan 1.19) and Stoeckli methods

Sample	Relative Pressure Limit in Calculation		Micropore Volume (cm^3/g)	Mesopore Volume (cm^3/g)	Average Pore Width (Å)
	Upper	Lower			
AW10 (DFT)	6.5090E-01	3.1059E-06	0.387	0.075	8.93
AW10* (Stoeckli)	6.1823E-03	6.099E-05	0.270	N/A	6.21
AW15 (DFT)	6.5060E-01	3.0119E-06	0.567	0.099	11.61
AW15+ (Stoeckli)	8.1398E-03	8.059E-05	0.492	N/A	10.10

***** a=2.5397 and m= 0.8923

+ a=1.2973 and m= 1.6902

Table 3.4. Micropore and mesopore volumes of ACFs

Sample	DFT Micropore Volume (cm^3/g)	DR Micropore Volume (cm^3/g)	DFT Mesopore Volume (cm^3/g)	BJH Mesopore Volume (cm^3/g)	Adsorption Energy E_{N2} (KJ/mol)
AW10	0.387	0.287	0.075	0.254	15.7
OAW10	0.340	0.278	0.089	0.320	14.9
HAW10	0.414	0.313	0.074	0.257	15.4
AAW10	0.371	0.276	0.061	0.215	15.4
AW15	0.567	0.541	0.099	0.295	11.8
OAW15	0.439	0.472	0.154	0.439	11.0
HAW15	0.593	0.569	0.085	0.248	11.6
AAW15	0.573	0.533	0.098	0.295	11.7
AW20	0.594	0.596	0.120	0.342	11.3
OAW20	0.504	0.536	0.144	0.394	11.1
HAW20	0.622	0.617	0.096	0.247	11.3
AAW20	0.599	0.607	0.130	0.355	11.2

Table 3.5. Micropore and mesopore volumes of GACs

Sample	DFT Micropore Volume (cm^3/g)	DFT Mesopore Volume (cm^3/g)
Picazine (pulverized)	0.377	0.252
Picazine (granular)	0.303	0.233
G219 (pulverized)	0.438	0.118
G219 (granular)	0.467	0.100
F600 (pulverized)	0.353	0.0847
F600 (granular)	0.375	0.0747

3.8. Figures

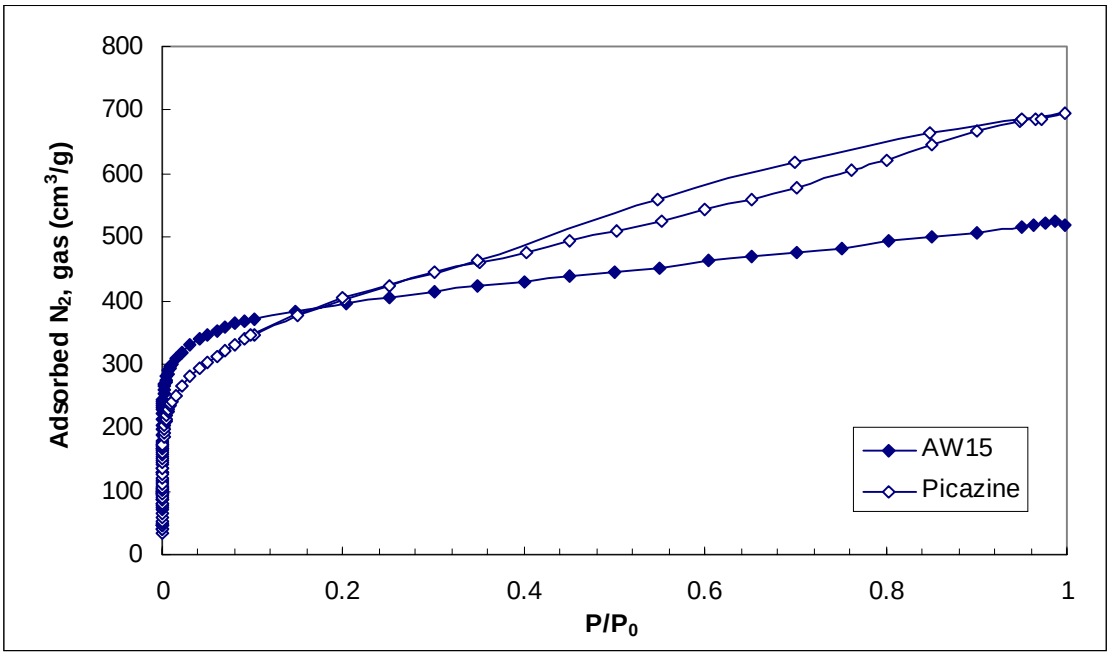

Figure 3.1. N_2 isotherms of AW15 and Picazine

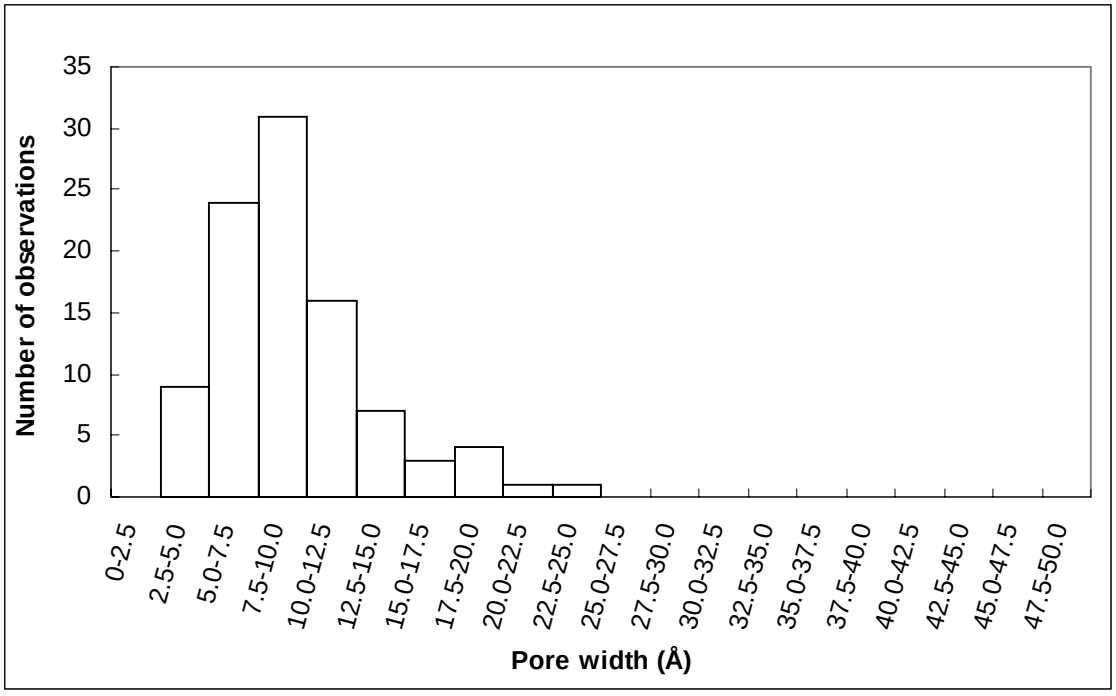

Figure 3.2. STM of ACF10*

*Replotted from Daley et al. [1995]

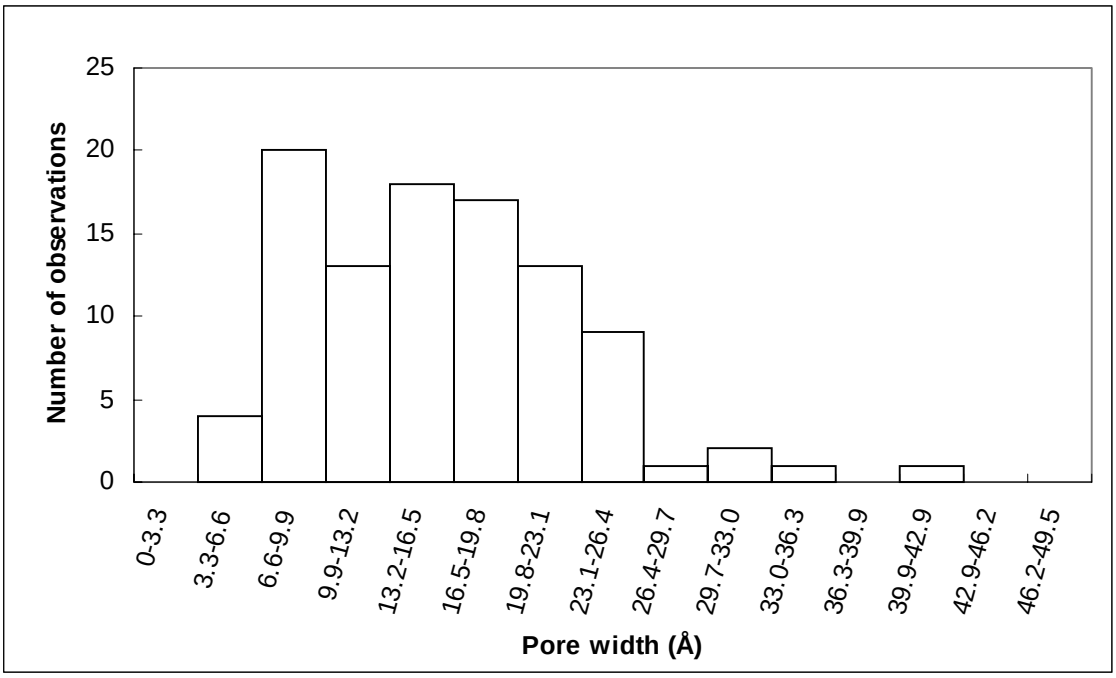

Figure 3.3. STM of ACF15*

*Replotted from Daley et al. [1995]

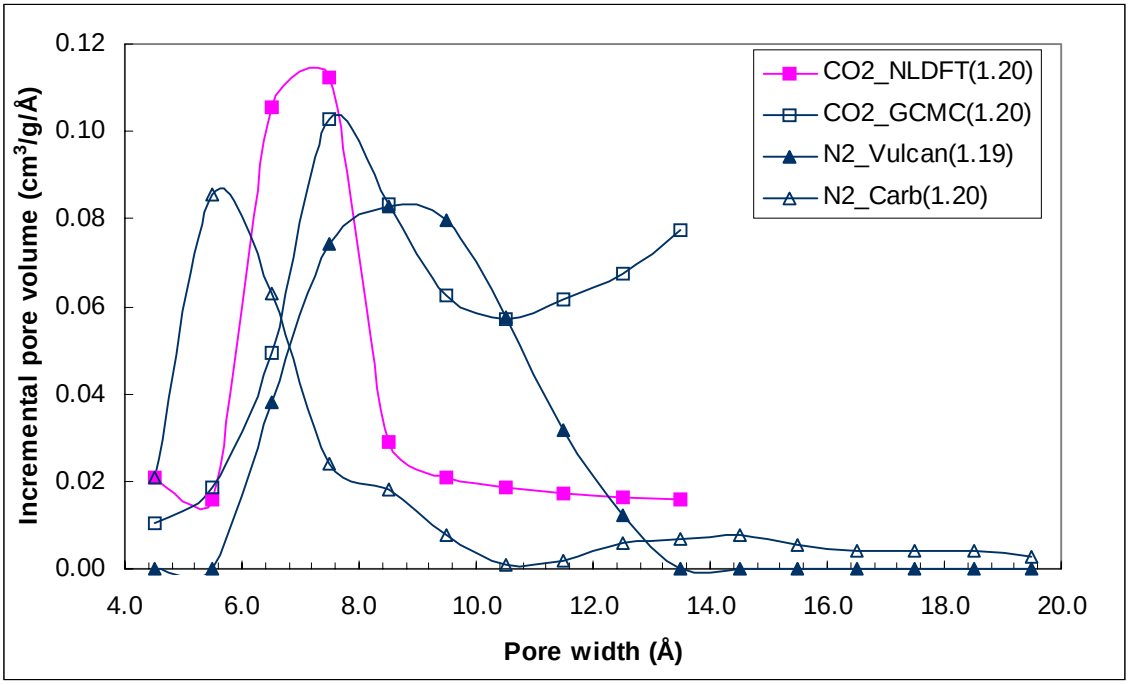

Figure 3.4. PSDs of AW10 calculated from the different DFT kernels*

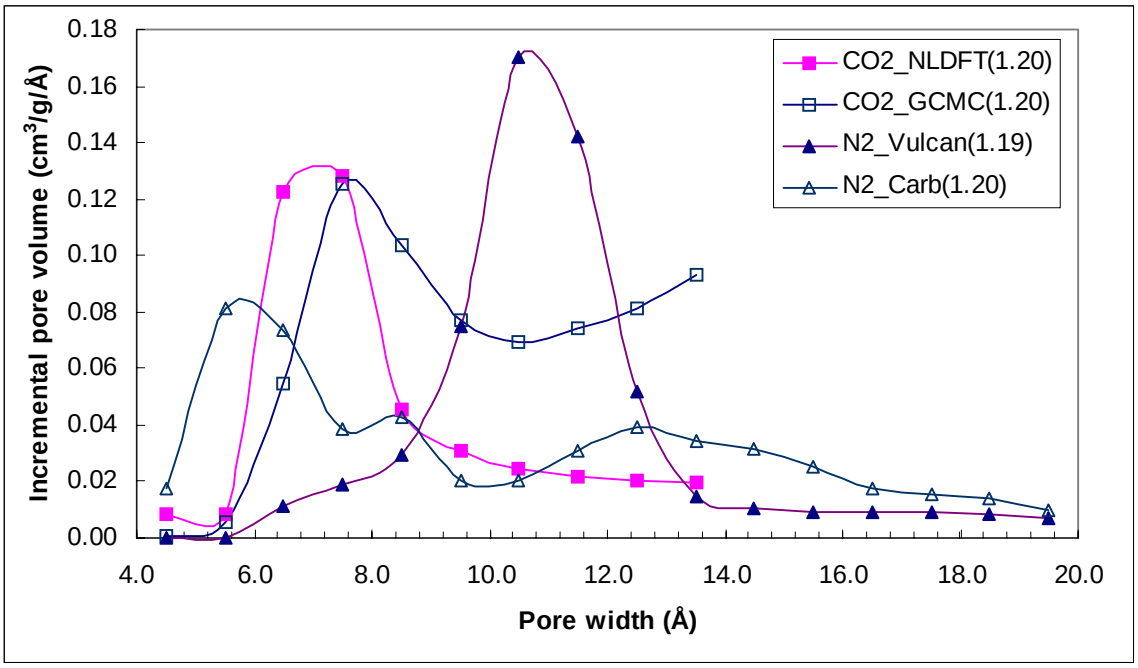

Figure 3.5. PSDs of AW15 calculated from the different DFT kernels*

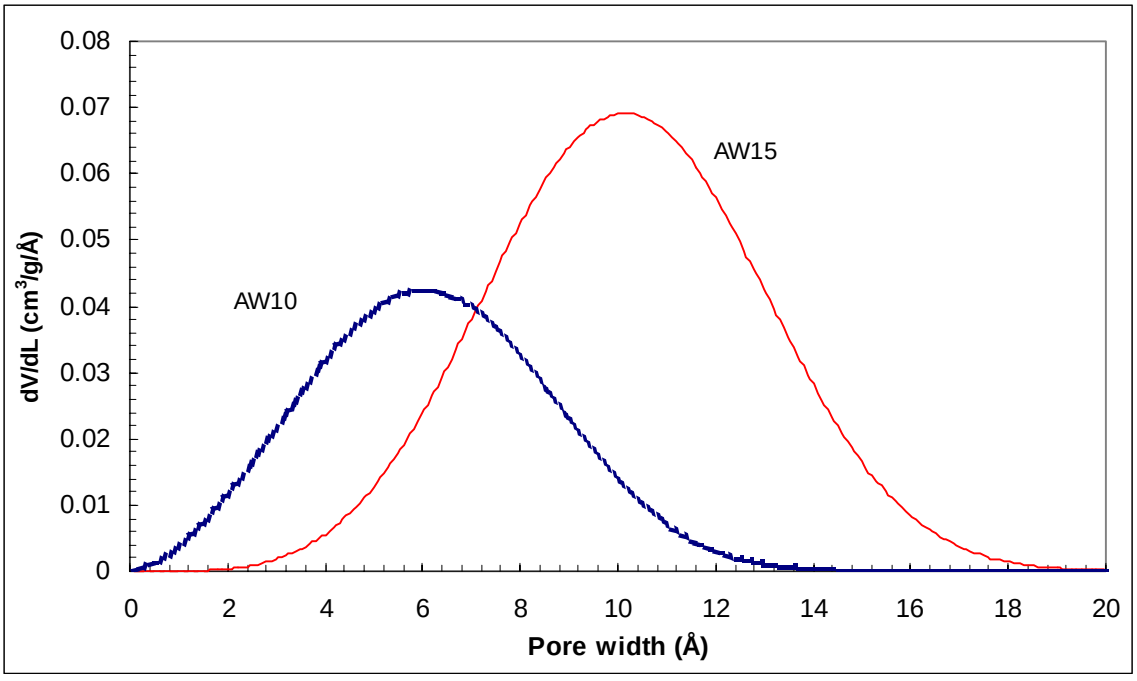

Figure 3.6. PSDs of AW10 and AW15 calculated from the Stoeckli method

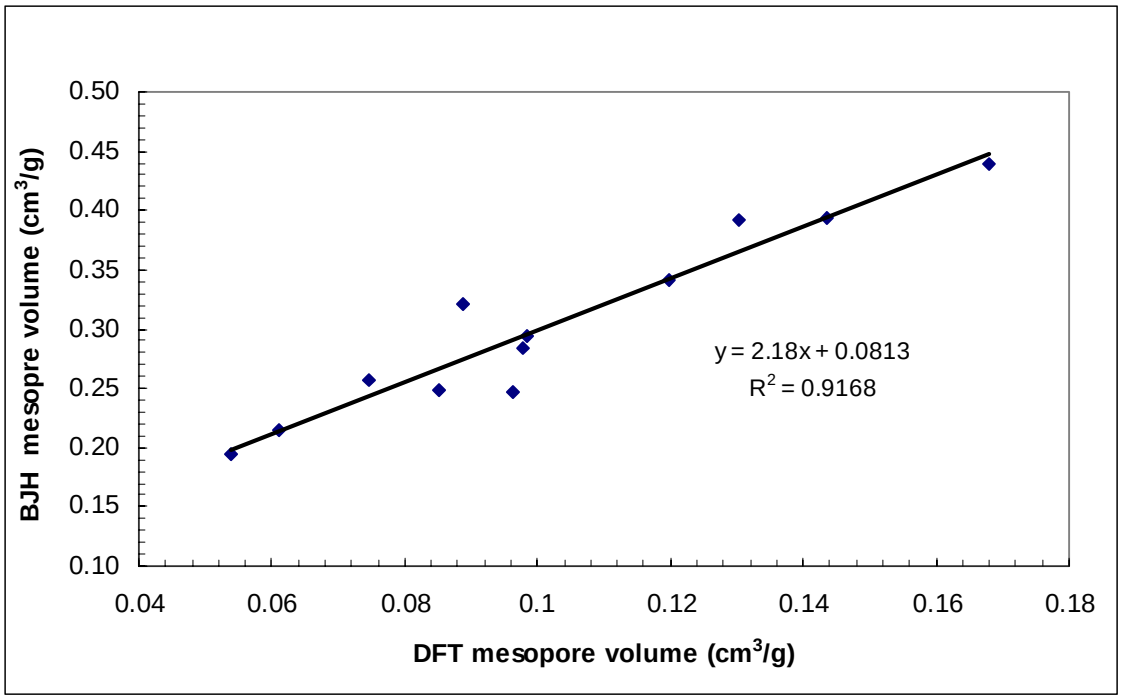

Figure 3.7. Correlation of DFT mesopore volume and BJH mesopore volume

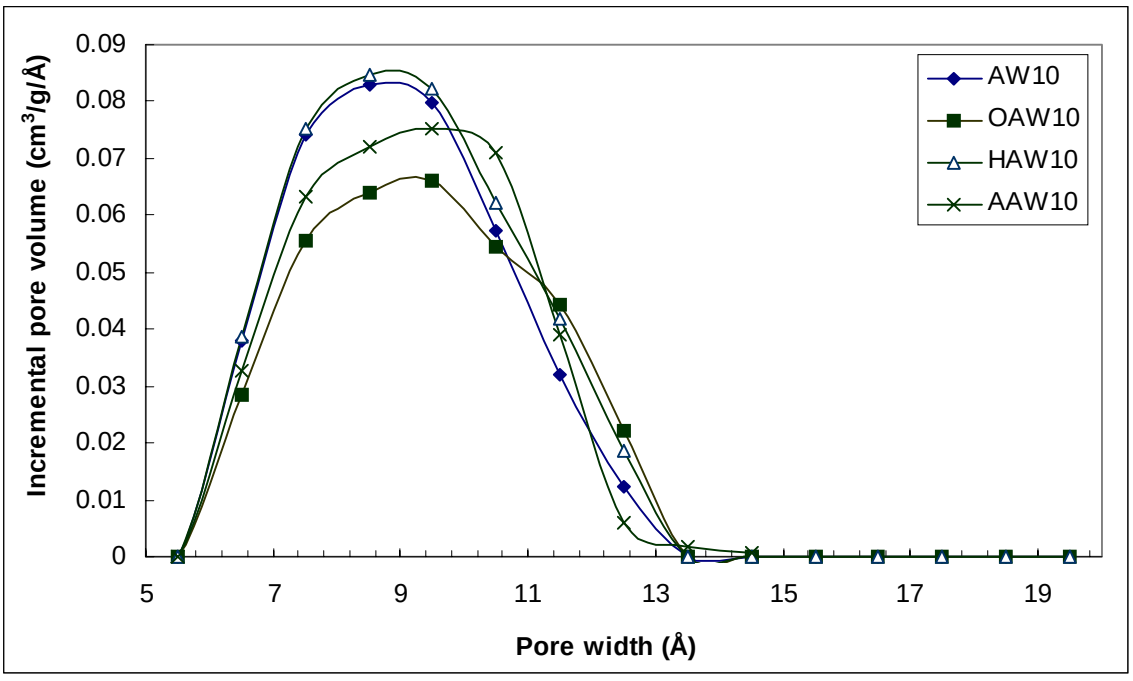

Figure 3.8. Effects of surface chemistry modifications on micropore size distributions of ACF10s

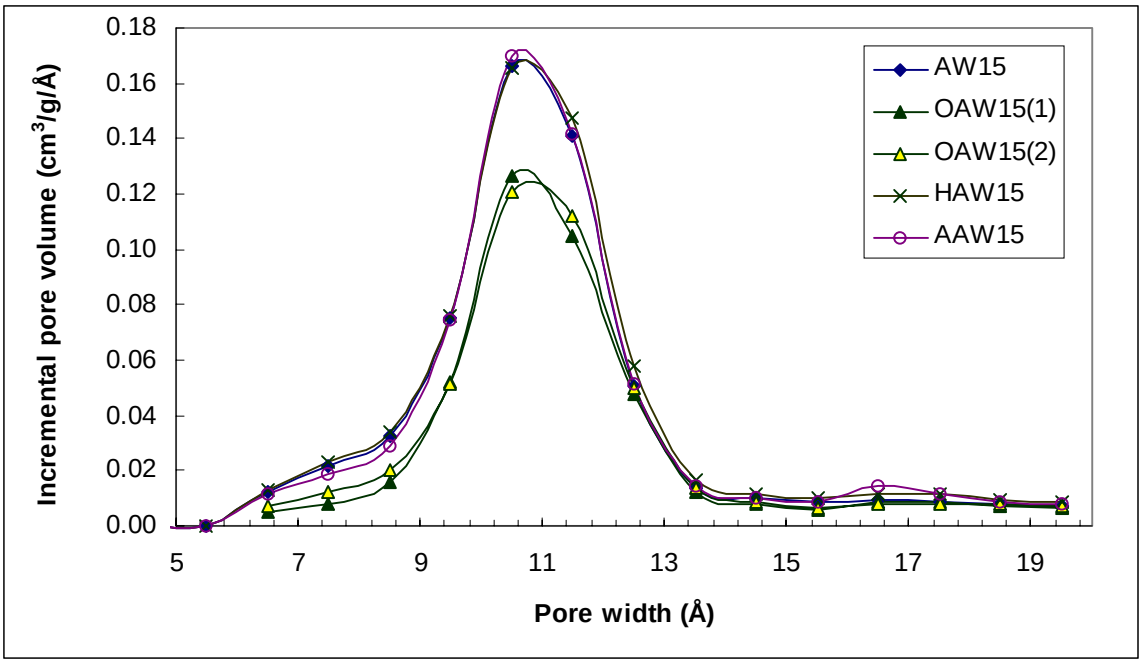

Figure 3.9. Effects of surface chemistry modifications on micropore size distributions of ACF15s

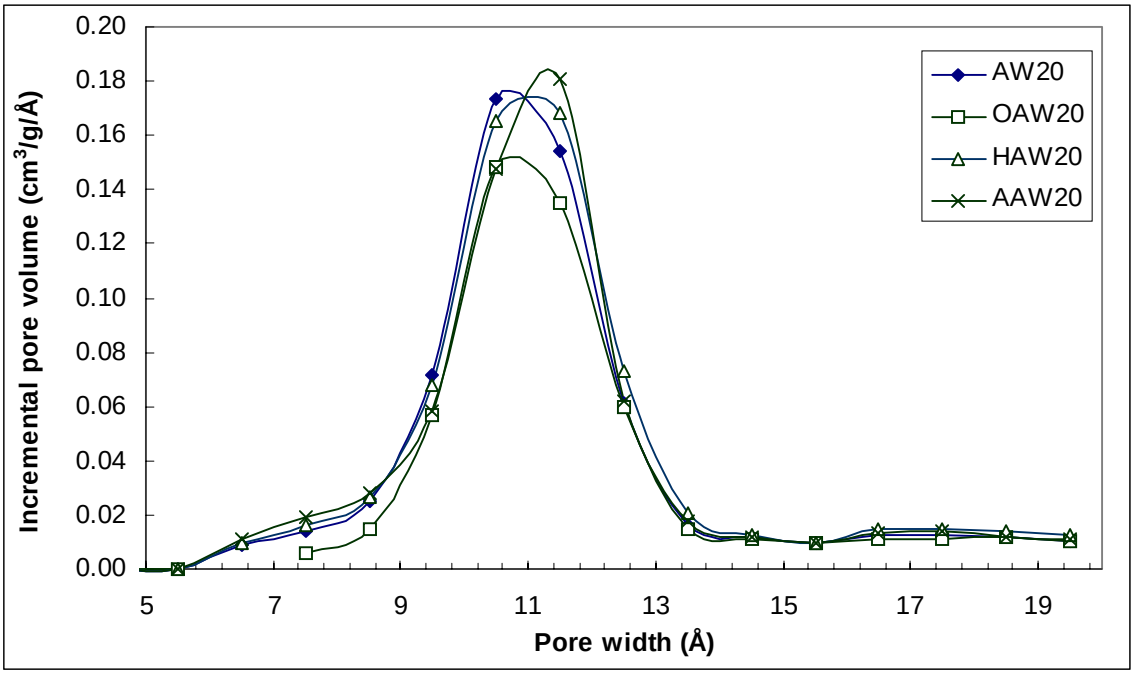

Figure 3.10. Effects of surface chemistry modifications on micropore size distributions of ACF20s

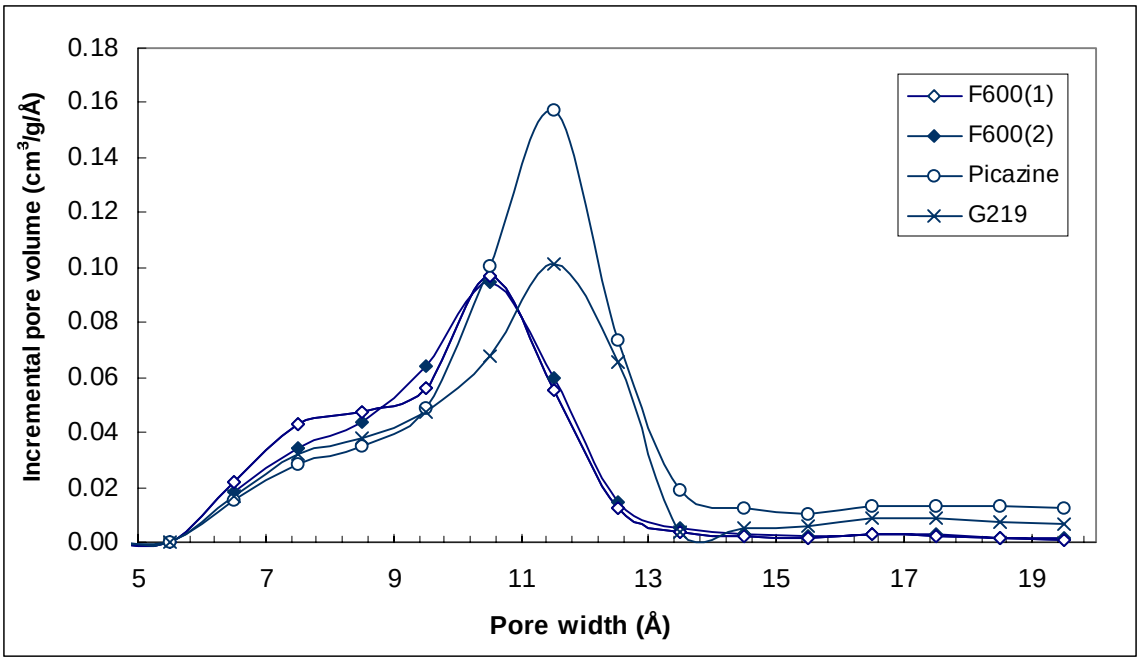

Figure 3.11. Micropore size distributions of pulverized GAC samples

Chapter 4. Effects of Activated Carbon Surface Chemistry and Pore Structure on the Adsorption of MTBE and TCE from Aqueous Solution

4.1. Objectives

The objectives were (1) to systematically evaluate the effects of activated carbon pore structure and surface chemistry on the adsorption of two common drinking water contaminants: the relatively polar fuel oxygenate methyl tertiary-butyl ether (MTBE) and the relatively nonpolar solvent trichloroethene (TCE), and (2) to develop simple descriptors of activated carbon characteristics that facilitate the selection of suitable adsorbents for the removal of organic contaminants from aqueous solution.

4.2. Background

4.2.1. Effects of Activated Carbon Pore Structure

The size of adsorbent pores affects the adsorption of organic contaminants in two ways. First, adsorption strength increases with decreasing pore size because (1) contact points between the adsorbate and the adsorbent surface increase [Newcombe et al. 1997] and (2) adsorption potentials between opposing pore walls begin to overlap once the micropore width is less than about twice the adsorbate diameter [Sing 1995]. Second, size exclusion limits the adsorption of contaminants of a given size and shape if pores are too small. In aqueous systems, size exclusion is observed when the pore width is smaller than about 1.7 times the second largest dimension of the adsorbate [Kasaoka et al. 1989]. Given that many organic contaminants are small (i.e. total surface areas of about 100-300 $Å^2$ [Okouchi et al. 1992], which corresponds to spherical diameters of about 5.5-10 Å),

the above observations suggest that the presence of small micropores is important for their removal from aqueous solution.

4.2.2. Effects of Activated Carbon Surface Chemistry

Studies have shown that increases in the oxygen or acidic functional group contents of activated carbons impair the adsorption of organic compounds from aqueous solution [Kaneko et al. 1989, Pendleton et al. 1997, Karanfil and Kilduff 1999, Franz et al. 2000, Considine et al. 2001]. Although oxidation of activated carbons enhanced the removal of polar organic compounds from the gaseous phase [Mangun et al. 1999, Dimotakis et al. 1995, Kaneko et al. 1989] showed that the *removal* of acidic functional groups enhanced the adsorption of both relatively polar and relatively nonpolar organic compounds from aqueous solution. This observation was explained by the preferential adsorption of water on carbon surfaces containing oxygen groups [Kaneko et al. 1989]. Water can adsorb by means of hydrogen bonds on oxygen-containing functional groups, and clustering of additional water molecules occurs around water molecules adsorbed at these sites [Puri 1970, Dubinin et al. 1955, Barton et al. 1984, Pan and Jaroniec 1984, Müller et al. 1996, Müller and Gubbins 1998, McCallum et al. 1999, Müller et al. 2000]. Such water clusters can prevent pollutant access to hydrophobic regions on the activated carbon surface, reduce the interaction energy between the pollutant and the adsorbent surface, and/or effectively block pollutant access to micropores [Kaneko et al. 1989, Pendleton et al. 1997, Franz et al. 2000, Coughlin and Ezra 1968, Müller et al. 2000, Mahajan et al. 1980]. Pendleton et al. [1997] also remarked that organic contaminant adsorption from aqueous solution necessitates the displacement of water from the

activated carbon surface. Enthalpy measurements showed that water displacement by MIB became increasingly difficult with an increase in the hydrophilic site concentration on the activated carbon surface. Consequently, water adsorption explains why polar activated carbons exhibit a smaller adsorption capacity for trace organic compounds than less polar activated carbons with similar micropore volumes [Pendleton et al. 1997, Newcombe et al. 1997]. Overall, the detrimental effects of water adsorption illustrate that adsorbents with stable hydrophobic surfaces bear the greatest promise for the removal of trace organic contaminants from drinking water sources. Nonetheless, adsorbents need to be sufficiently hydrophilic so that they are wetted by water to be useful for water treatment applications [Davis and Powers 2000].

4.3. Materials and Methods

Solvents

Single solute isotherm experiments were conducted in ultrapure laboratory water (tap water treated by reverse osmosis, ion exchange, and granular activated carbon adsorption, resistance ≥ 14.85 MΩ/cm). Ultrapure water was amended with a 1 mM phosphate buffer (0.5 mM $Na_2HPO_4 \bullet H_2O$ and 0.5 mM NaH_2PO_4) to maintain a pH of 7.2. Furthermore, 100 mg/L sodium azide were added to eliminate aerobic biological activity.

Adsorbates

TCE and MTBE, two common drinking water contaminants, served as probe molecules for the assessment of adsorbate polarity effects. TCE is a relatively hydrophobic adsorbate while MTBE is relatively hydrophilic. TCE and MTBE differ in

molecular size and shape (Figure 4.1); TCE is a planar molecule while MTBE approximates a tetrahedron. Kinetic diameters for TCE and MTBE are 5.6 Å [Chintawar and Greene 1997] and 6.2 Å [Sano et al. 1995], respectively.

Isotherms

For isotherms in ultrapure water, adsorbent doses between 10 and 7500 mg/L were utilized. Adsorbents were placed into brown glass bottles that were subsequently filled to the neck with the amended ultrapure water. Micropollutant stock solutions were added with a constant rate syringe (CR-700, Hamilton, Reno, NV) to yield an initial concentration of about 1000 μg/L. Once the micropollutant was added to a bottle, it was topped off immediately with ultrapure water to create headspace-free conditions and capped using PTFE-faced silicon septa and open-top closures. A mixing time of 2 weeks in a rotary tumbler was sufficient to reach adsorption equilibrium. Upon equilibration, adsorbents were separated from the liquid by sedimentation (ACFs) or filtration through 0.45 μm filters (pulverized GACs). Remaining liquid-phase TCE and MTBE concentrations were measured by purge and trap concentrator followed by gas chromatographic (Shimadzu 14a, Columbia, MD) and flame ionization detector (FID). The micropollutant concentrations were quantified using external standards.

4.4. Results and Discussion

4.4.1. TCE and MTBE Single-Solute Isotherms

To elucidate the effects of adsorbent surface chemistry and pore structure on the adsorption of organic pollutants from aqueous solution, single-solute TCE and MTBE isotherms experiments were conducted with each member of the ACF matrix. To

compare single-solute isotherm results in a quantitative manner, isotherms were described by the Freundlich model [$q_e = K (C_e)^{1/n}$], where q_e and C_e are the equilibrium solid-phase and liquid-phase concentrations, respectively, and K and 1/n are fitting parameters. A larger K value represents a larger adsorption capacity while a larger 1/n value represents a more homogeneous adsorbent with a narrower site energy distribution [Derylo-Marczewska et al. 1984, Carter et al. 1995]. Figure 4.2 summarizes TCE and MTBE isotherm data along with Freundlich isotherm model fits for hydrogen-treated ACFs, and Table 4.1 summarizes TCE and MTBE Freundlich isotherm parameters for all studied adsorbents. As indicated in Figure 4.2 and by the K values in Table 4.1, TCE adsorbed to a greater extent on activated carbon surfaces than MTBE. Given the greater aqueous solubility of MTBE, primarily because its ether oxygen can serve as a hydrogen bond acceptor in water, MTBE adsorption on activated carbon surfaces requires the disruption of relatively strong solute/solvent interactions. Consequently, adsorption of MTBE is energetically less favored than adsorption of TCE, for which solute/solvent interactions are weaker. These results are consistent with adsorbate solubility or polarity effects on adsorption that have been well established in the literature [e.g. Lundelius 1920, Weber 1972, McGuire et al. 1978, Belfort 1979, Crittenden 1999].

4.4.2. Effects of Activated Carbon Surface Chemistries and Pore Structures

With respect to pore structure, the results in Figure 4.2 show that the ranking of the ACFs in terms of adsorption capacity differed for the two solutes. For TCE, HAW10 exhibited the largest adsorption capacity even though it had the smallest BET surface area of the hydrogen-treated ACFs. The same trend was observed for all other surface

chemistry modifications as indicated by the Freundlich K-values in Table 4.1. In comparison, MTBE adsorption capacities were relatively similar at all three ACF activation levels (Figure 4.2). The TCE isotherm data therefore suggest that ACF10 had a larger pore volume in a size range suitable for TCE adsorption than ACFs 15 and 20. Similarly, the MTBE isotherm data suggest that ACFs at all three activation levels had similar pore volumes in a size range suitable for MTBE adsorption. Both TCE and MTBE isotherm data clearly illustrate that adsorption capacities cannot be predicted from the BET surface areas or total micropore volumes.

To assess in which pore sizes TCE and MTBE adsorb preferentially, adsorption capacities at an equilibrium liquid-phase concentration of 50 µg/L ($q_{e,\,50}$) were correlated with ACF pore volumes in a given size range for each surface chemistry modification. Following a trial-and-error approach similar to that described by Ebie et al. [1995], the results showed that TCE adsorption was controlled by pores in the 7-10 Å width range while MTBE adsorption was controlled by pores in the 8-11 Å width range. These results suggest that both TCE and MTBE adsorb primarily in pores with widths that are 1.3 to 1.8 times larger than their kinetic diameters. Considering that the second-largest dimension of both adsorbates is similar (Figure 4.1), the results of the current study do not fully substantiate that adsorption of organic compounds from aqueous solutions is controlled by the second-largest adsorbate dimension as suggested by Kasaoka et al. [1989]. Given that pores of the studied ACFs are elliptical [Daley et al. 1996], it appears reasonable that the flat TCE molecule is able to access pores with a smaller dimension along the minor axis than the MTBE molecule, which approximates a tetrahedron. Thus,

pores accessible to TCE corresponded to pores with smaller widths, as calculated by the DFT, which assumes slit-shaped pores.

For TCE, Figure 4.3 illustrates that the available pore volume in the 7-10 Å diameter range primarily controlled TCE adsorption on the more hydrophobic ACFs (AW, HAW, AAW) even though the oxygen contents of these carbons varied by a factor of about three (~1.5 - 4.5%). A comparison among Freundlich K-values (Table 4.1), representing TCE adsorption capacities at an equilibrium liquid-phase concentration of 1 µg/L, substantiated that pore structure effects dominated over surface chemistry effects for the more hydrophobic ACFs; i.e., 95% confidence intervals generally overlapped for AW, HAW, and AAW at a given activation level while ACF 10 always exhibited the largest K-value for a given surface chemistry modification. Figure 4.3 also shows that the correlation established by the more hydrophobic ACFs predicted the adsorption capacity of the relatively hydrophobic F600 and G219 GACs reasonably well. For the oxidized ACFs, a separate correlation indicated that surface chemistry effects in addition to the availability of a suitable pore volume controlled TCE adsorption for ACFs with larger oxygen contents (~10%). The correlation established by the oxidized ACFs appropriately predicted the adsorption capacity of Picazine GAC with an oxygen content of about 16%. A plot of MTBE adsorption capacity versus micropore volume in the 8-11 Å diameter range (Figure 4.4) showed a trend similar to that depicted in Figure 4.3 for TCE. However, surface chemistry effects were of some importance even among the more hydrophobic ACFs. A comparison of the Freundlich K-values in Table 4.1 also shows that the hydrogen-treated ACFs, i.e. the most hydrophobic ACFs of the matrix, exhibited the largest MTBE adsorption capacities at a given activation level. Nonetheless,

differences among the more hydrophobic ACFs at a given activation level were small compared to the decrease in MTBE adsorption capacity that was observed upon oxidation (Table 4.1).

Overall, the isotherm data showed that the adsorption of both relatively hydrophobic (TCE) and relatively hydrophilic (MTBE) organic pollutants from aqueous solution is adversely affected by the introduction of surface oxygen groups (see Freundlich K-values in Table 4.1). Prior studies have shown that the adsorption of polar organics such as acetone [Dimotakis et al. 1995, Mangun et al. 1999] or acetaldehyde [Dimotakis et al. 1995] from the gas-phase is enhanced upon surface oxidation because of dipole-dipole interactions [Mangun et al. 1999] or hydrogen bonding, and a similar result may be anticipated for MTBE vapor. However, in aqueous solution, MTBE has to compete with water for polar adsorption sites. Given that the concentration of MTBE is small compared to that of water, water adsorption should be favored over MTBE adsorption at polar surface sites.

To verify the importance of solvent/adsorbent interactions, MTBE and TCE adsorption was also studied from cyclohexane, a nonpolar solvent. In contrast to the results obtained in aqueous solution, Figure 4.5 shows that the oxidized ACF exhibited the largest MTBE adsorption capacity (by a factor of about 5 to 6) when the solvent was cyclohexane, and the observation was reproducible for the two tested adsorbent doses. The improved performance of the oxidized ACF in cyclohexane can be explained by the preferential adsorption of MTBE on oxygen-containing functional groups such as carboxylic acid and phenolic hydroxyl groups. In that case, hydrogen bonds can form between the hydrogen atoms of these surface groups and the ether-oxygen of MTBE.

However, in the presence of water, hydrogen bonds will preferentially form between water and these surface groups. Consequently, the availability of specific adsorption sites, i.e., hydrogen-bond donor sites, for MTBE will decrease greatly in aqueous solution. However, the loss of such sites to water adsorption alone cannot explain why the MTBE adsorption capacity of oxidized ACFs in aqueous solution is lower than that of more hydrophobic ACFs with a smaller surface concentration of hydrogen-bond donor sites. It is plausible that hydrogen-bond donor sites become essentially unavailable to MTBE in aqueous solution and that MTBE adsorption therefore shifts from a site-specific hydrogen-bonding mechanism in cyclohexane to a non-specific dispersive mechanism in aqueous solution, where MTBE adsorbs instead on the graphitic basal planes of the adsorbent. Hence, the lower MTBE adsorption capacity of oxidized adsorbents with a larger concentration of surface-oxygen groups results from the increased formation of water clusters that reduce access to the graphitic basal planes, reduce the interaction energy between MTBE and the adsorbent surface, and/or block pore entrances [Coughlin and Ezra 1968, Mahajan et al. 1980, Kaneko et al. 1989, Pendleton et al. 1997, Franz et al. 2000, Müller et al. 2000].

Results for TCE adsorption from cyclohexane showed that surface chemistry effects were negligible (Figure 4.6), a result that suggests that TCE adsorption occurs by a non-specific dispersive mechanism. In aqueous solution, however, the TCE adsorption capacity of oxidized adsorbents was compromised because of the enhanced formation of water clusters as explained above for MTBE. The results and interpretations of the current study are consistent with those of a recent study by Franz et al. [2000] who investigated the adsorption of phenol, aniline, nitrobenzene, and benzoic acid from both

water and cyclohexane. Overall, the above results as well as those by Franz et al. [2000] show that enhanced water adsorption on polar adsorbents negates the benefits of providing specific adsorption sites capable of forming hydrogen-bonds with a targeted adsorbate such as MTBE (this study), phenol, aniline, or benzoic acid [Franz et al. 2000].

To determine the effects of adsorbent polarity on TCE and MTBE adsorption, micropollutant adsorption capacities were plotted against the sum of the oxygen and nitrogen contents (mmol/g) of each adsorbent as shown in Figures 4.7 and 4.8 for TCE and MTBE, respectively. To eliminate pore structure effects, equilibrium solid-phase concentrations at an equilibrium liquid-phase concentration of 50 µg/L were normalized by the pore volume in the pore width range that controlled the adsorption of the targeted micropollutant (i.e. 7-10 Å for TCE, 8-11 Å for MTBE). Figure 4.7 illustrates that the TCE adsorption capacity decreased with increasing adsorbent polarity, and a similar trend was observed for MTBE (Figure 4.8). These results reiterate that hydrophobic adsorbents, i.e. activated carbons with a low oxygen and nitrogen content (< 2 to 3 mmol/g), are most effective for the removal of both hydrophobic and hydrophilic adsorbates from aqueous solution. Figures 4.7 and 4.8 further illustrate that the trends established by the ACF matrix successfully predicted the adsorption behavior of the commercially available GACs.

4.5. Conclusions

From the relationships observed between the adsorbent characteristics and the micropollutant TCE and MTBE adsorption isotherm data in ultrapure water, the following conclusions were drawn:

(1) Regardless of the pore structure or surface chemistry, adsorbents always exhibited a larger adsorptive capacity for TCE than for MTBE, a result that is consistent with the greater aqueous solubility of MTBE.

(2) For carbons with similar surface chemistry, the pore volume of micropores with widths corresponding to about 1.3 to 1.8 times the kinetic diameter of the targeted adsorbate controlled the adsorption capacity. Consequently, relatively small changes in the micropore size distribution of an adsorbent (e.g. 7-11 Å widths in ACF 10 versus 9-13 Å widths in ACFs 15 and 20) alter the effectiveness of an adsorbent for a given micropollutant. Similarly, small differences in the kinetic diameters among individual target adsorbates (e.g. 5.6 Å for TCE versus 6.2 Å for MTBE) affect the choice of the most effective adsorbent.

(3) Adsorbent polarity, as expressed by the sum of the oxygen and nitrogen (O+N) contents, has the potential to serve as a useful activated carbon selection criterion. As the polarity of a carbon increased, or the O+N content increased, the micropollutant adsorption capacity decreased. To assure that activated carbons are sufficiently hydrophobic to effectively remove organic contaminants from aqueous solution, the results of this research suggest that the O+N content of the adsorbent should be less than about 2 to 3 mmol/g.

4.6. References

Barton SS, Evans MJB, Holland J, Koresh JE. Water and cyclohexane vapour adsorption on oxidized porous carbon. Carbon 1984; 22(3): 265-272.

Belfort G. Selective adsorption of organic homologues onto activated carbon from dilute aqueous solutions. Solvophobic interaction approach and correlations of molar adsorptivity with physicochemical parameters. Environ. Sci. Technol. 1979; 13(8): 939-946.

Cambridge Structural Database. CSD Version 5.20. Cambridge UK: Cambridge Crystallographic Data Center.

Carter MC, Kilduff JE, Weber WJ Jr. Site energy distribution analysis of preloaded adsorbents. Environ. Sci. Technol. 1995; 29(7): 1773-1780.

Chintawar PS, Greene HL. Adsorption and catalytic destruction of trichloroethylene in hydrophobic zeolites. Applied Catalysis B: Environmental 1997; 14: 37-47.

Considine R, Denoyel R, Pendleton P, Schumann R, Wong SH. The influence of surface chemistry on activated carbon adsorption of 2-methylisoborneol from aqueous solution. Colloid and Surfaces A: Physicochemical and Engineering Aspects 2001; 179: 271-280.

Coughlin RW, Ezra FS. Role of surface acidity in the adsorption of organic pollutants on the surface of carbon. Environ. Sci. Technol. 1968; 2(4): 291-297.

Coulson CA. The electronic structure of the boundary atoms of a graphite layer. Proc. of the fourth conf. on carbon, Oxford: Pergamon Press, 1960: 215-219.

Crittenden JC, Sanongraj S, Bulloch JL, Hand DW, Rogers TN, Speth, TF, Ulmer M. Correlation of aqueous-phase adsorption isotherms. Environ. Sci. Technol. 1999; 33(17): 2926-2933.

Daley MA, Tandon D, Economy J, Hippo EJ. Elucidating the porous structure of activated carbon fibers using direct and indirect methods. Carbon 1996; 34(10): 1191-1200.

Davis SW, Powers SE. Alternative sorbents for removing MTBE from gasoline-contaminated ground water. J. Environ. Engrg. 2000; 126(4): 354-360.

Derbyshire F, Jagtoyen M, Andrews R, Rao A, Martin-Gullon I, Grulke EA. Carbon materials in environmental applications. In Radovic LR, editor. Chemistry and Physics of Carbon, Vol. 27, New York: Marcel Dekker, 2001: 1-66.

Derylo-Marczewska A, Jaroniec M, Gelbin D, Seidel A. Heterogeneity effects in single-solute adsorption from dilute solutions on solids. Chemica Scripta 1984; 24: 239-246.

Dimotakis ED, Cal MP, Economy J, Rood MJ, Larson SM. Chemically treated activated carbon cloths for removal of volatile organic carbons from gas streams: evidence for enhanced physical adsorption. Environ. Sci. Tech. 1995; 29(7): 1876-1880.

Dubinin MM, Zaverina ED, Serpinsky VV. The sorption of water vapor by active carbon. J. Am. Chem. Soc. 1955; 77: 1760-1766.

Ebie K, Li F, Hagishita, T. Effect of pore size distribution of activated carbon on the adsorption of humic substances and trace organic compounds. Water Supply 1995; 13(3/4): 65-70.

Franz M, Arafat HA, Pinto NG. Effect of chemical surface heterogeneity on the adsorption mechanism of dissolved aromatics on activated carbon. Carbon 2000; 38(13): 1807-1819.

Kaneko Y, Abe M, Ogino K. Adsorption characteristics of organic compounds dissolved in water on surface-improved activated carbon fibers. Colloids and Surfaces 1989; 37: 211-222.

Karanfil T, Kilduff JE. Role of granular activated carbon surface chemistry on the adsorption of organic compounds. 1. Priority pollutants. Environ. Sci. Technol. 1999; 33(18): 3217-3224.

Kasaoka S, Sakata Y, Tanaka E, Naitoh R. Preparation of activated fibrous carbon from phenolic fabric and its molecular-sieve properties. International Chemical Engineering 1989; 29(1): 101-114.

Kasaoka S, Sakata Y, Tanaka E, Naitoh R. Design of molecular-sieve carbon. Studies on the adsorption of various dyes in the liquid phase. International Chemical Engineering 1989; 29(4): 734-742.

Lundelius EF. Adsorption und Löslichkeit. Koll. Zeitschr. 1920; 26(4): 145-151.

Mahajan OP, Moreno-Castilla C, Walker PL Jr. Surface-treated activated carbon for removal of phenol from water. Sep. Sci. and Technol. 1980; 15(10): 1733-1752.

Mangun CL, Benak KR, Daley MA, Economy J. Oxidation of activated carbon fibers: effect on pore size, surface chemistry, and adsorption properties. Chem. Mater. 1999; 11: 3476-3483.

McCallum CL, Bandosz TJ, McGrother SC, Müller EA, Gubbins KE. A molecular model for adsorption of water on activated carbon: comparison of simulation and experiment. Langmuir 1999; 15: 533-544.

McGuire MJ, Suffet IH, Radziul JV. Assessment of unit processes for the removal of trace organic compounds from drinking water. J. AWWA 1978; 70(10): 565-572.

Menendez JA, Phillips J, Xia B, Radovic LR. On the modification and characterization of chemical surface properties of activated carbon: in the search of carbons with stable basic properties. Langmuir 1996; 12(18): 4404-4410.

Menendez JA, Radovic LR, Xia B, Phillips J. Low-temperature generation of basic carbon surfaces by hydrogen spillover.” J. Phys. Chem. 1996; 100(43): 17243-17248.

Müller EA, Rull LF, Vega LF, Gubbins KE. Adsorption of water on activated carbons: a molecular simulation study. J. Phys. Chem. 1996; 100: 1189-1196.

Müller EA, Gubbins KE. Molecular simulation study of hydrophilic and hydrophobic behavior of activated carbon surfaces. Carbon 1998; 36(10): 1433-1438.

Müller EA, Hung, FR, Gubbins KE. Adsorption of water vapor-methane mixtures on activated carbons. Langmuir 2000, 16: 5418-5424.

Newcombe G, Drikas M, Hayes R. Influence of characterised natural organic matter on activated carbon adsorption: II. Effect on pore volume distribution and adsorption of 2-methylisoborneol. Water Research 1997; 31(5): 1065-1073.

Okouchi S, Saegusa H, Nojima O. Prediction of environmental parameters by adsorbability index: water solubilities of hydrophobic organic pollutants. Environment International 1992; 18: 249-261.

Pan D, Jaroniec M. Adsorption and thermogravimetruc studies of unmodified and oxidized active carbons. Langmuir 1996; 12: 3657-3665.

Pauling L. The nature of the chemical bond, and the structure of molecules and crystals: an introduction to modern structural chemistry; 3rd edition. Ithaca NY: Cornell University Press. 1960.

Pendleton P, Wong SH, Schumann R, Levay G, Denoyel R, Rouquerol J. Properties of activated carbon controlling 2-methylisoborneol adsorption. Carbon 1997; 35(8): 1141-1149.

Puri BR. Surface complexes on carbons. In Walker PL Jr., editor. Chemistry and Physics of Carbon, Vol. 6, New York: Marcel Dekker, 1970: 191-282.

Sano T, Hasegawa M, Kawakami K, Yanagishita H. Separation of methanol/methyl tert-butyl ether mixture by pervaporation using silicalite membrane. J. Membrane Science 1995; 107: 193-196.

Schwarzenbach RP, Gschwend PM, Imboden DM. Environmental Organic Chemistry. New York: John Wiley and Sons, Inc. 1993.

Sing KSW. Physisorption of nitrogen by porous materials. Journal of Porous Materials 1995; 2: 5-8.

Weber WJ Jr. Physicochemical processes for water quality control. New York: John Wiley and Sons, 1972, pp 199-259.

4.7. Tables

Table 4.1. Freundlich parameters for single-solute TCE and MTBE isotherms (The 95% confidence intervals for each parameter are shown in parentheses)

Carbon	TCE		MTBE	
	K* Average (Lower; Upper)	1/n Average (Lower; Upper)	K* Average (Lower; Upper)	1/n Average (Lower; Upper)
AW10	5.23 (3.95; 6.92)	0.487 (0.403; 0.570)	0.0886 (0.0785; 0.1000)	0.603 (0.572; 0.633)
AW15	2.11 (1.82; 2.43)	0.554 (0.511; 0.596)	0.141 (0.128; 0.155)	0.634 (0.608; 0.660)
AW20	1.56 (1.35; 1.81)	0.593 (0.545; 0.641)	0.103 (0.0947; 0.112)	0.672 (0.646; 0.697)
OAW10	1.19 (1.04; 1.35)	0.604 (0.572; 0.637)	0.0451 (0.0413; 0.0493)	0.589 (0.571; 0.606)
OAW15	0.627 (0.494; 0.798)	0.591 (0.534; 0.649)	0.0376 (0.0342; 0.0412)	0.630 (0.611; 0.648)
OAW20	0.677 (0.584; 0.786)	0.595 (0.559; 0.632)	0.0301 (0.0241; 0.0375)	0.664 (0.610; 0.718)
HAW10	6.75 (5.67; 8.05)	0.426 (0.374; 0.479)	0.190 (0.152; 0.238)	0.532 (0.471; 0.594)
HAW15	2.85 (2.10; 3.86)	0.482 (0.393; 0.570)	0.206 (0.183; 0.232)	0.597 (0.566; 0.627)
HAW20	2.51 (1.95; 3.23)	0.514 (0.436; 0.592)	0.220 (0.206; 0.234)	0.564 (0.547; 0.581)
AAW10	4.61 (3.77; 5.64)	0.485 (0.426; 0.544)	0.164 (0.145; 0.185)	0.562 (0.531; 0.592)
AAW15	1.98 (1.53; 2.55)	0.567 (0.483; 0.651)	0.197 (0.170; 0.229)	0.546 (0.510; 0.582)
AAW20	2.05 (1.77; 2.38)	0.512 (0.467; 0.556)	0.115 (0.0986; 0.134)	0.631 (0.589; 0.674)
F600	4.05 (3.50; 4.69)	0.462 (0.422; 0.502)	0.150 (0.142; 0.159)	0.486 (0.475; 0.498)
G219	2.63 (2.08; 3.32)	0.484 (0.426; 0.543)	0.127 (0.112; 0.143)	0.540 (0.515; 0.564)
Picazine	0.099 (0.081; 0.121)	0.616 (0.563; 0.668)	0.00193 (0.00150, 0.00248)	0.841 (0.797, 0.884)

* Units of K: $(mg/g)(L/\mu g)^{1/n}$

4.8. Figures

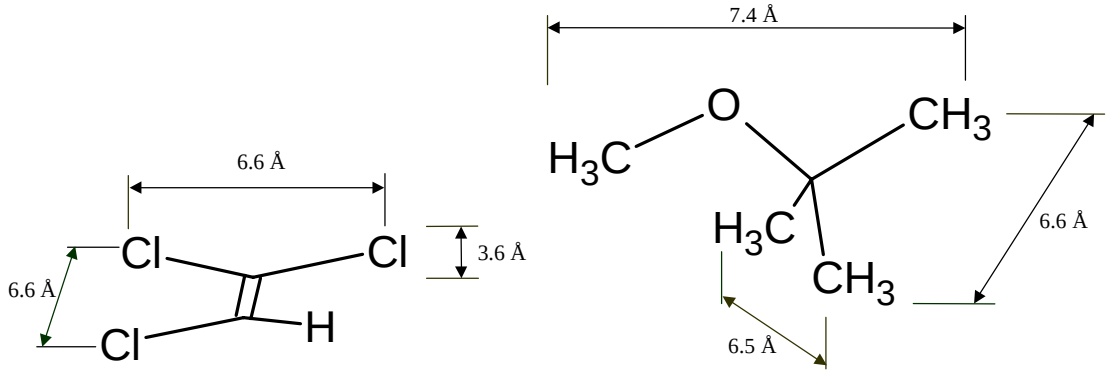

Figure 4.1. Molecular structures and dimensions for trichloroethene and methyl tertiary-butyl ether
Molecular dimensions were calculated from the Cambridge Structural Database [Cambridge Structure Database] and the van der Waals radii for methyl groups and chlorine (2.0 and 1.8 Å, respectively [Pauling 1960]).

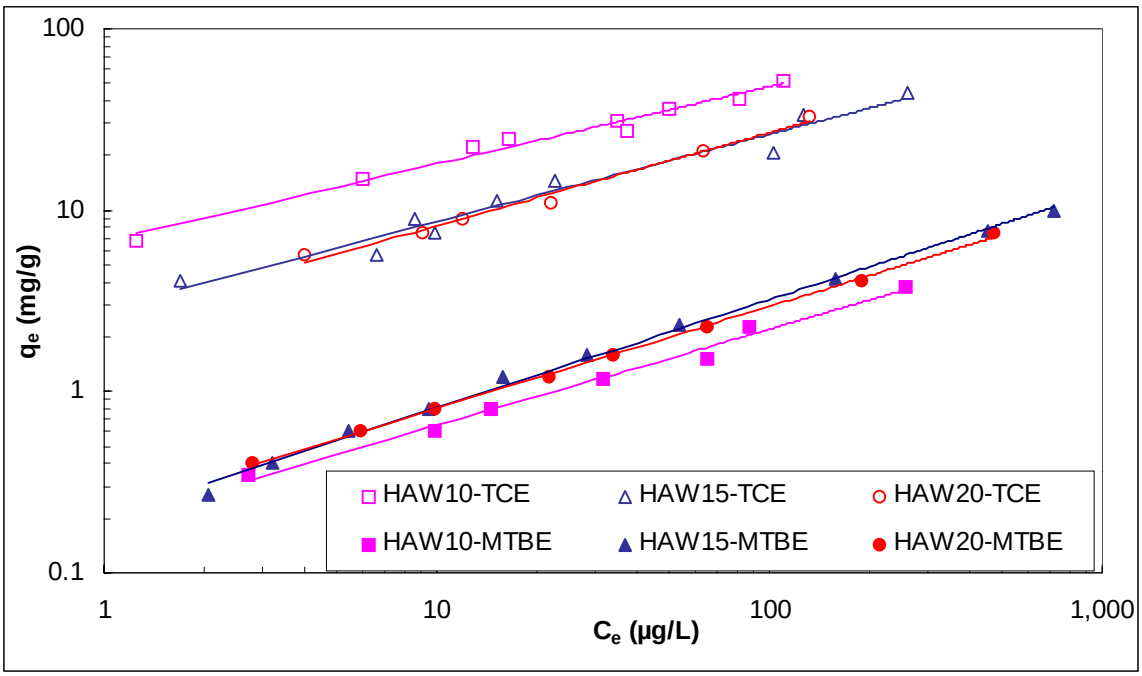

Figure 4.2. TCE and MTBE isotherms on hydrogen-treated ACFs

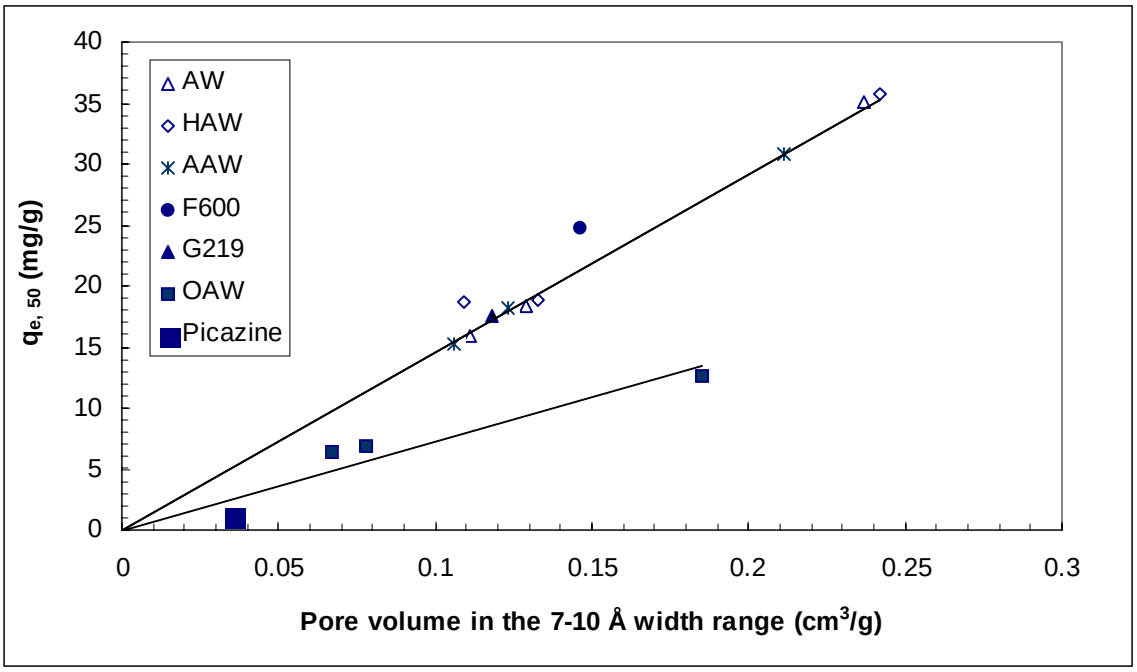

Figure 4.3. Effect of pore volume on TCE adsorption

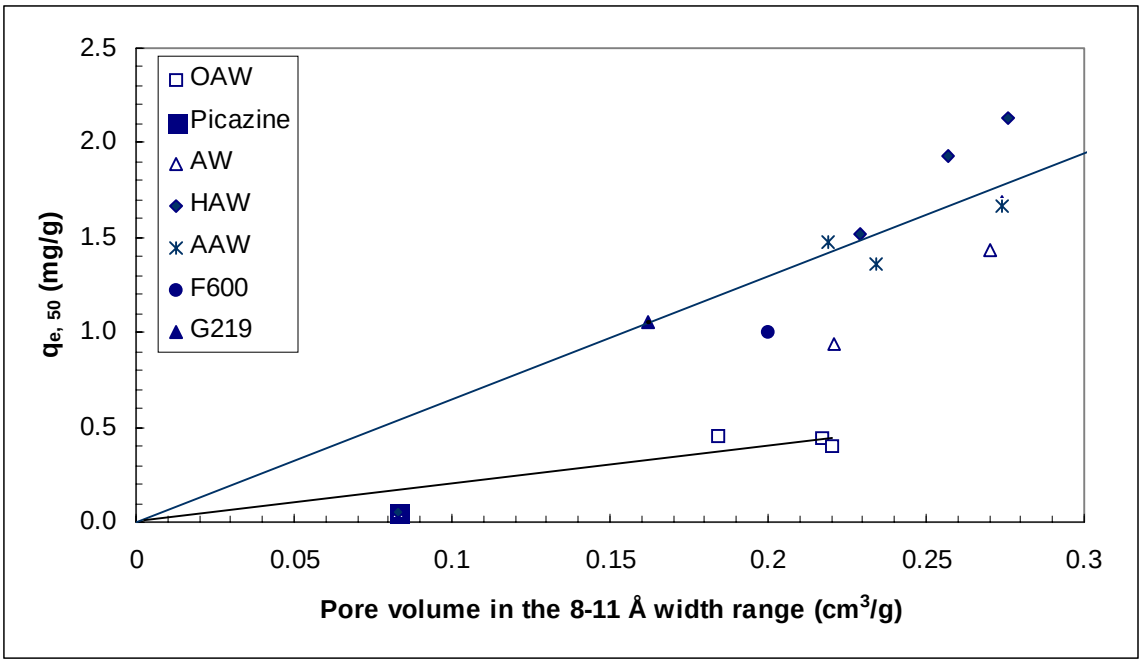

Figure 4.4. Effect of pore volume on MTBE adsorption

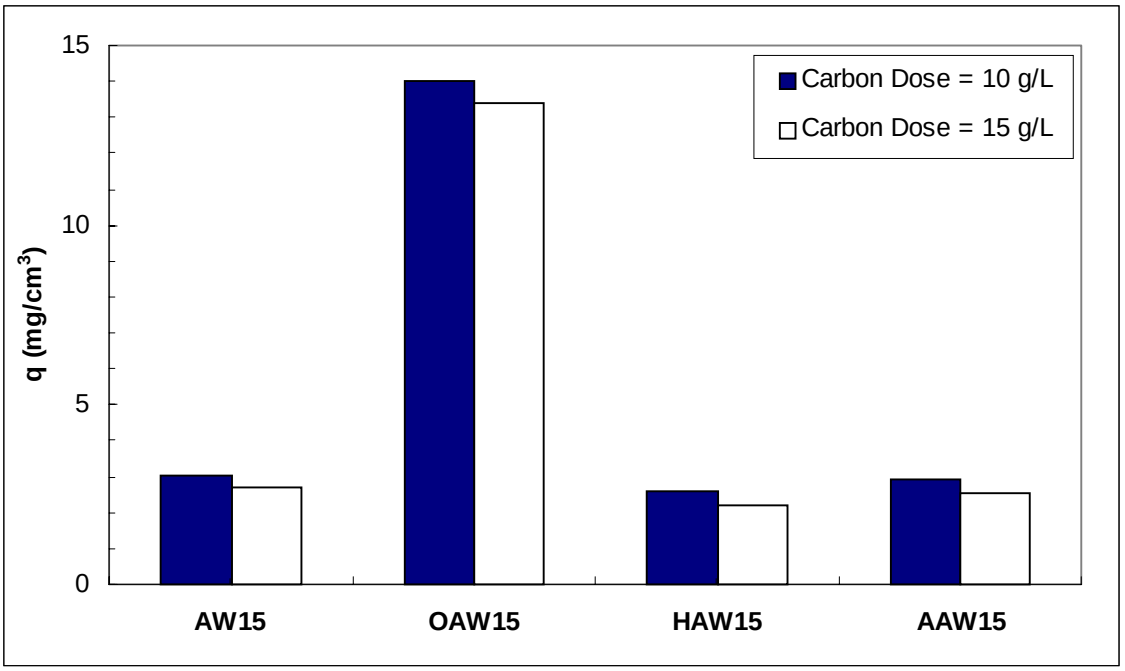

Figure 4.5. Effect of chemical treatments on MTBE adsorption from cyclohexane. Solid-phase MTBE concentrations were normalized by the pore volume in the 8-11 Å width range.

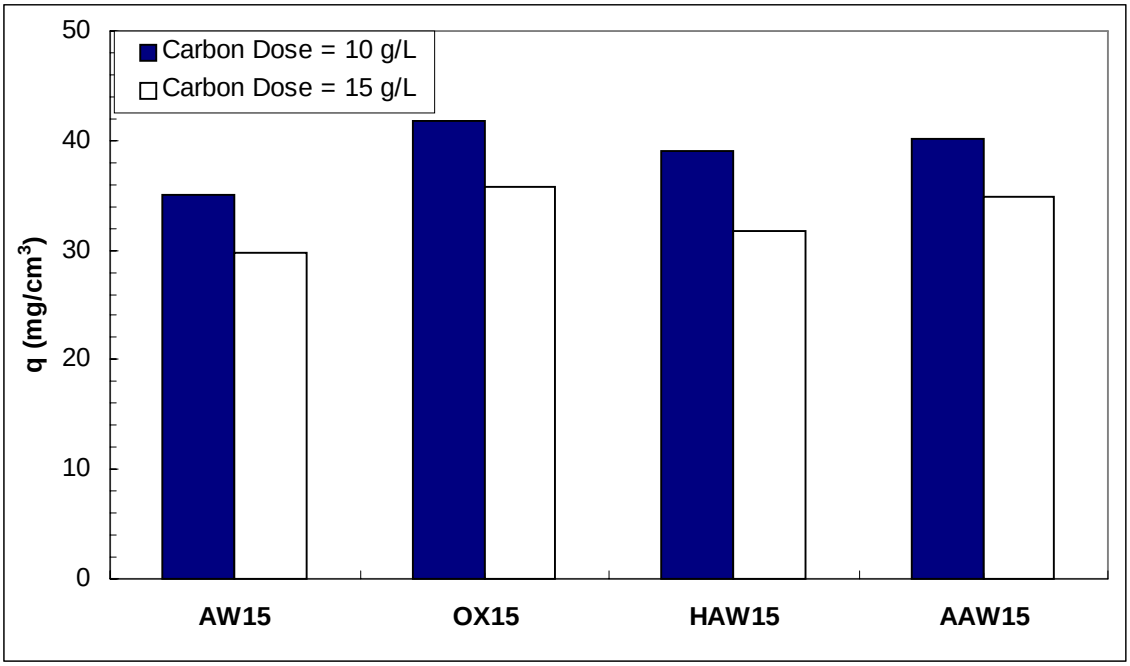

Figure 4.6. Effect of chemical treatments on TCE adsorption from cyclohexane. Solid-phase TCE concentrations were normalized by the pore volume in the 7-10 Å width range.

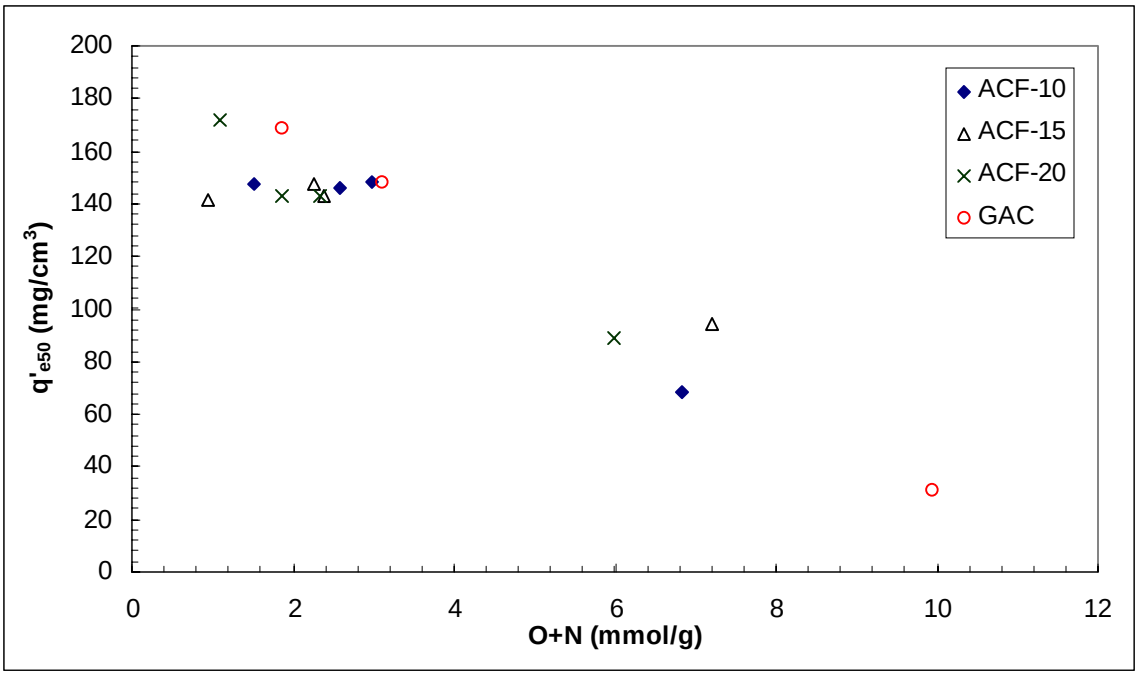

Figure 4.7. Effect of adsorbent hydrophobicity on TCE adsorption capacity

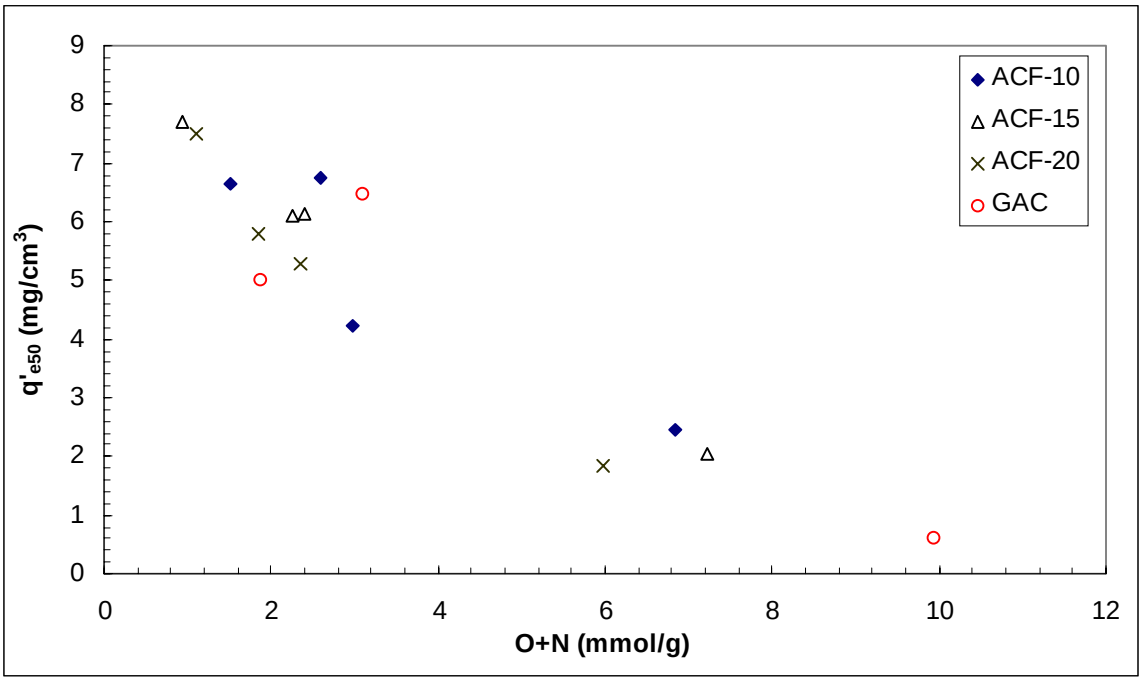

Figure 4.8. Effect of adsorbent hydrophobicity on MTBE adsorption capacity

Chapter 5. Effects of Activated Carbon Surface Chemistry and Pore Structure on the Adsorption of MTBE and TCE from Natural Water

5.1. Objectives

The objectives were (1) to systematically evaluate the effects of activated carbon pore structure and surface chemistry on the adsorption of MTBE and TCE in the presence of natural organic matter (NOM), and (2) to develop simple descriptors of activated carbon characteristics that facilitate the selection of suitable adsorbents for the removal of organic contaminants from natural water.

5.2. Background

It has been widely observed that the adsorption capacity of activated carbons for organic micropollutants is lowered in the presence of NOM [Najm et al. 1991a, Qi et al. 1994, Narbaitz and Benedek 1994, Chen et al. 1997, Newcombe et al. 1997, Knappe et al. 1998, Pelekani and Snoeyink 1999, Ebie et al. 2001]. The concentration of NOM in drinking water is about 3 to 6 orders of magnitude larger than the concentration of most micropollutants, and the degree of competition is dependent on the initial concentration of the micropollutant [Najm et al. 1991a, Narbaitz and Benedek 1994, Knappe et al. 1998, Pelekani and Snoeyink 1999]. The nature of the NOM (e.g. chemical composition, adsorbability) also affects the extent of competition [Bernazeau et al. 1996, Müller et al. 1996].

5.2.1. Effects of Activated Carbon Pore Structure

Newcombe et al. [1997] studied the adsorption of 2-methylisoborneol (MIB) in the presence of NOM. Experiments with NOM fractions showed that the smallest size fraction (MW < 500) resulted in a greater reduction in MIB adsorption than larger size fractions, indicating that NOM molecules in a size range similar to that of the target compound directly compete with the target compound for adsorption sites. This observation is consistent with the findings of other researchers who determined that smaller NOM molecules are adsorbed preferentially on activated carbons because a large percentage of internal surface area of activated carbon is located in the micropore region that cannot be accessed by larger NOM molecules [Summers and Roberts 1988b, Kilduff et al. 1996].

Pelekani and Snoeyink [1999] examined the effect of pore size on the adsorption of atrazine from natural water using a series of ACFs with different activation levels. From these experiments, the two main mechanisms in competitive adsorption were determined to be pore blockage and direct competition, and the dominating mechanism was dependent on the ACF pore size distribution. If pores were large enough to admit the micropollutant but not large enough to admit NOM, then pore blockage was the dominant competition mechanism. However, if pores were large enough to admit both NOM and the micropollutant, then direct competition became the dominant competition mechanism. Furthermore, the data showed that pore blockage by NOM as a result of size exclusion more severely reduced the micropollutant capacity than direct competition between NOM and atrazine for adsorption sites. Pelekani and Snoeyink [1999] therefore suggested that adsorbents with a broader pore size distribution in the micropore range

reduce pore blockage effects and thus the negative impact of NOM on micropollutant adsorption. In a study looking at the adsorption of four different micropollutants from natural water by three activated carbons, Ebie et al. [2001] also concluded that the extent of competition was lessened when the pore size distribution was broadened and there was a larger volume percentage of pores greater than 30 Å.

To better understand the role of pore size distribution on competitive adsorption, Pelekani and Snoeyink [2000] performed a series of experiments that examined the adsorption of atrazine in the presence of methylene blue (MB), a dye with a molecular size similar to that of atrazine. Again, ACFs were used to elucidate pore size effects. Because the adsorbates were similar in size, direct competition was observed. By increasing the pore volume and shifting the pore size distribution from the primary micropores to the secondary micropores, the effect of competition on atrazine adsorption was lessened because more adsorption sites were available in the pore size region accessible to both atrazine and MB. Adsorption capacities for atrazine and MB correlated best with pore volumes in the 7.5-10 and 7.5-20 Å range, respectively. Furthermore, atrazine could more easily displace MB in the secondary micropores because the adsorption potential was smaller. A similar study was performed by Pelekani and Snoeyink [2001] in which MB was replaced with congo red (CR), a dye that is larger in size than atrazine. For an ACF that contained principally primary micropores, both pore blockage and pore constriction occurred, the former lowering the atrazine adsorption capacity and the latter slowing the kinetics of adsorption. Once again, by increasing the pore volume and by shifting the micropore size distribution towards the secondary micropores, the effect of NOM competition was lessened. As the pore volume shifted to

smaller end of the secondary micropore region, the CR competition mechanism was primarily one of pore constriction that reduced adsorption kinetics but not adsorption capacity. In the presence of a significant secondary micropore volume, atrazine capacity reductions as a result of direct site competition between atrazine and CR started to become important while reductions in adsorption kinetics as a result of pore constriction were no longer observed. Pelekani and Snoeyink [2001] also proposed that further activation of ACFs yielded a branched pore structure, in which small micropores branch off from mesopores or larger micropores. In this case, both direct competition in mesopores and large micropores and pore blockage at the entrance of small micropores were observed.

5.2.2. Effects of Activated Carbon Surface Chemsitry

Although several studies have explored the effects of activated carbon pore structure on the adsorption of micropollutants in the presence of competing organic matter [Newcombe et al. 1997, Pelekani and Snoeyink 2000, Pelekani and Snoeyink 2001, Ebie et al. 2001], the effect of activated carbon surface chemistry on the adsorption of micropollutants in the presence of NOM remains largely unexplored to date.

5.3. Materials and Methods

Solvents

Micropollutant adsorption in the presence of NOM was evaluated with Sacramento-San Joaquin Delta Water (SJDW). Upon arrival, the water was preserved with 100 mg/L sodium azide. Prior to use in isotherm experiments, the water was vacuum

filtered through a 0.45-μm nylon membrane filter (Magna-R, MSI, Westboro, MA). The DOC of SJDW was 4.0 mg/L, the pH was 7.9, the total alkalinity was 53 mg/L as $CaCO_3$, and the total hardness was 72 mg/L as $CaCO_3$.

Isotherms

For TCE and MTBE isotherms in natural water, adsorbent doses between 2 and 5500 mg/L were utilized. Adsorbents were placed into brown glass bottles that were subsequently filled to the neck with SJDW. Micropullutant stock solution was added with a constant rate syringe (CR-700, Hamilton, Reno, NV) to yield an initial concentration of approximately 100 μg/L. Once the micropollutant was added, the bottle was topped off immediately with SJDW to create headspace-free conditions and capped using PTFE-faced silicon septa and open-top closures. A mixing time of 4 weeks in a rotary tumbler was sufficient to reach adsorption equilibrium, and micropollutant losses were not observed in blanks containing no carbon over that time period. Remaining liquid phase concentrations of TCE and MTBE were measured by GC as described in Chapter 4.

For NOM isotherms, adsorbent doses between 10 and 2000 mg/L were utilized. Adsorbents were transferred into 4 oz, 8 oz, or 16 oz amber glass bottles depending on the carbon dose. The bottles were subsequently filled with 100 mL (4 oz bottles), 200 mL (8 oz bottles), or 400 mL (16 oz bottles) of SJDW and capped. A mixing time of 2 weeks in a rotary tumbler was sufficient to reach adsorption equilibrium as determined by kinetic tests. Upon equilibration, samples were filtered through 0.22 μm nylon membrane filters (Magna-R, MSI, Westboro, MA). DOC levels were quantified using a TOC-5000A TOC analyzer (Shimadzu, Columbia, MD). All samples were acidified with 1 N HCl and

sparged with air for 4 minutes to measure non-purgeable organic carbon (NPOC). UV absorbance measurements were conducted on filtered samples prior to acidification using a UV/vis spectrophotometer (Unicam UV 1, Spectronic Unicam, Cambridge, United Kingdom). Samples were analyzed in a 1-cm quartz cell at a wavelength of 280 nm, a wavelength at which sodium azide did not interfere with UV absorbance measurements.

5.4. Results and Discussion

5.4.1. NOM Adsorption

Table 5.1 shows the Freundlich isotherm parameters for dose-normalized DOC and UV280 isotherms for ACFs and pulverized GACs. As summarized in Table 5.1, AW10 had a significantly lower DOC adsorption capacity than AW15 and AW20. Similar observations were made when quantifying NOM adsorption by UV absorbance at 280 nm. Given the narrow pores of AW10 (primarily 7-11 Å width), size exclusion effects can explain the small DOC adsorption on this ACF. In contrast, AW15 and AW20 exhibited larger DOC adsorption capacities, a result that is consistent with the presence of wider pores in these ACFs (primarily 9-13 Å width for both ACFs).

Figure 5.1 depicts dose-normalized DOC isotherms for the ACF10 members of the adsorbent matrix. The results in Figure 5.1 suggest that surface chemistry modifications had only a small effect on DOC adsorption isotherms. Slightly enhanced DOC adsorption on OAW10 may have been a result of a small increase in mesopore volume that resulted from the oxidation process. Figure 5.2 shows dose-normalized DOC isotherms for the ACF20 members of the adsorbent matrix. NOM adsorption capacities among the hydrophobic ACFs (i.e., AW, HAW, and AAW) were similar while a loss in

adsorption capacity was observed for OAW20 at low Ce/D values or low surface loading levels. This result suggests that the negative surface charge of OAW20 adversely affected the adsorption of negatively charged NOM. Furthermore, enhanced water adsorption on the more polar oxidized ACF may have reduced the pore volume available to NOM as a result of pore blockage or pore constriction. However, at higher Ce/D values or higher surface loading levels, the NOM adsorption capacity of OAW20 was similar to that of the other ACFs. It is likely that adsorbed NOM controlled the ACF surface charge at higher loading levels, which explains why adsorption capacities were independent of surface chemistry modifications at higher Ce/D values. Results for ACF15 were similar to those depicted for ACF20 in Figure 5.2.

When quantifying NOM adsorption by UV absorbance at 280 nm, which targets the adsorption of aromatic and unsaturated NOM components, Figure 5.3 illustrates that OAW10 exhibited a larger adsorption capacity than the remaining ACF10 members of the adsorbent matrix. As explained above, a small increase in mesopore volume that resulted from the oxidation step may explain this result. For the ACF20 members of the adsorbent matrix, Figure 5.4 illustrates that the adsorption of UV280-absorbing NOM components was not affected by ACF surface chemistry modifications.

The contrasting results between Figures 5.2 (DOC isotherms) and Figure 5.4 (UV280 isotherms) suggests that the negative surface charge on OAW20 only reduced the adsorption of aliphatic NOM components, i.e., NOM components that do not adsorb UV light.

Figure 5.5 depicts dose-normalized DOC isotherms for the three commercially available GACs. Furthermore, Table 5.1 shows the Freundlich K and 1/n values that resulted from the regression analyses. The results in Figure 5.5 and the Freundlich parameters in Table 5.1 indicate that G219 exhibited the largest NOM adsorption capacity while that of Picazine and F600 was similar. The latter result was somewhat surprising given that the mesopore volume of Picazine GAC was approximately 3 times larger than that of F600 while the micropore volumes were similar for both GACs. Therefore, both adsorbent surface chemistry and pore structure affected the adsorption of DOC by the tested GACs.

To separate surface chemistry and pore structure effects, DOC and UV280 adsorption capacities of the hydrophobic ACFs (i.e., AW, HAW, and AAW ACFs) were correlated with pore volumes in a given size range. Following a trial-and-error approach similar to that described by Ebie et al. (1995), the results showed that DOC and UV280 adsorption were controlled by pores in the 12-500 Å width range (Figures 5.6 and 5.7). The observation that DOC adsorption occurs in mesopores and large micropores is consistent with the results of prior studies that investigated the adsorption of aquatic NOM (e.g., Ebie et al. 1995, Newcombe et al. 1997). Figure 5.6 illustrates that oxidized ACFs exhibited slightly smaller DOC adsorption capacities than the remaining ACFs. However, the same was not true when comparing adsorption capacities of UV280-absorbing NOM components (Figure 5.7). When plotting NOM adsorption capacities of the pulverized GACs, both Figures 5.6 and 5.7 illustrate that the strongly acidic Picazine GAC exhibited an NOM adsorption capacity that falls slightly below the line that best described NOM adsorption on the hydrophobic ACFs. This result may be attributable to

greater electrostatic repulsion between negatively charged NOM molecules and the negatively charged GAC surface. In contrast, the basic F600 and G219 GACs exhibited NOM adsorption capacities that greatly exceeded those of the ACFs at a given pore volume. Given that the pHPZC of ammonia-treated ACFs fell between those of G219 and F600, this result was somewhat unexpected. Further studies would be needed to measure the surface charge of each adsorbent at the pH of SJDW. If both G219 and F600 exhibited a larger positive surface charge at the pH of SJDW than the ammonia-treated ACFs, the enhanced NOM adsorption capacity of G219 and F600 could be explained based on enhanced electrostatic attraction between the negatively charged NOM and the positively charged GAC surfaces.

5.4.2. TCE and MTBE Adsorption Isotherms in the Presence of NOM

Figure 5.8 compares the TCE isotherm for AW20 in ultrapure water to that in SJDW. Figure 5.8 shows that competition between NOM and TCE lowered the TCE adsorption capacity. At an equilibrium liquid-phase concentration of 10 µg/L, the equilibrium solid-phase concentration of TCE decreased from 6.1 mg/g in ultrapure water to 2.6 mg/g in the presence of NOM, a capacity decrease of about 58%. In the presence of NOM, TCE and MTBE adsorption capacities of the adsorbents tested in this study decreased by 15-70%.

Effects of Activated Carbon Pore Structure

To assess the effects of adsorbent pore structure on TCE adsorption from SJDW, Figure 5.9 compares TCE isotherms for the three acid-washed carbons in an alternative

format, where the percentage of TCE remaining in solution at equilibrium is plotted as a function of the applied ACF dosage. In the presence of competing NOM, micropollutant isotherms plotted in this format are not dependent on the initial micropollutant concentration, provided that the micropollutant is present at trace levels. The points in Figure 5.9 are the experimental data, and the lines through each data set represent the best fits of the ideal adsorbed solution theory (IAST) model.

According to Figure 5.9, AW10 exhibited the largest adsorption capacity for TCE in SJDW while AW20 exhibited the lowest. This trend is the same as that observed for single-solute TCE isotherm experiments. For all four surface chemistry modifications, ACF10 performed better than ACF15 and ACF20 for the removal of TCE from natural water, a result that concurred with the trends observed in ultrapure water

Figure 5.10 shows the effect of ACF pore structure on the removal of MTBE from SJDW for the acid-washed ACFs. For MTBE, AW10 performed worse than AW15 and AW20. Furthermore, the IAST model could not describe the adsorption behavior of AW10 especially at intermediate adsorbent doses. Because the IAST model is only capable of modeling direct site competition, it is likely that NOM adsorption on AW10 caused pore blockage and/or pore constriction that prevented MTBE from accessing a portion of the pore structure over the tested 4-week equilibration time. One possible explanation is that NOM adsorbed at the openings of the pores thus narrowing the pore entrances. Because MTBE approximates the shape of a tetrahedron, it would be more difficult for an MTBE molecule to enter this constricted pore entrance than for a TCE molecule, which has a flat configuration. The ability of the IAST to describe the MTBE adsorption data on AW10 at the largest carbon doses suggests that the competition

mechanism shifted from pore constriction/blockage at high NOM loadings to direct site competition at lower NOM loadings. Similarly, the IAST was incapable of predicting the adsorption behavior of HAW10 and AAW10. However, the IAST was able to describe MTBE adsorption on OAW10. Because the acidic OAW10 carried a negative surface charge at the pH of SJDW, repulsive electrostatic forces likely decreased NOM adsorption at the pore entrances. In contrast, the remaining ACFs exhibited less negative or positive surface charges at the pH of SJDW according to their pHpzc data. Consequently, electrostatic forces would have favored NOM adsorption on the latter ACFs.

To assess in which pore sizes TCE and MTBE adsorb preferentially in the presence of NOM, adsorption capacities at an equilibrium liquid-phase concentration of 10 µg/L (qe_{10}) were correlated with ACF pore volumes in a given size range for each surface chemistry modification. Following a trial-and-error approach similar to that described by Ebie et al. (1995), the results showed that TCE adsorption was controlled by pores in the 7-9 Å pore width range while MTBE adsorption was controlled by pores in the 8-11 Å pore width range. For TCE, Figure 5.11 illustrates that the available pore volume in the 7-9 Å pore width range primarily controlled TCE adsorption on the more hydrophobic ACFs (AW, HAW, AAW) although TCE adsorption capacities of hydrogen-treated ACFs were consistently larger than those of acid-washed and ammonia-treated ACFs. Single-solute TCE adsorption capacities correlated best with the volume of pores in the 7-10 Å pore width range. The most likely explanation for this change is that NOM out-competed TCE in pores with pore widths in the 9-10 Å range or that TCE adsorbed relatively uninhibited in pores in the 7-9 Å pore width range. Figure 5.11 also shows that

the correlation established by the more hydrophobic ACFs predicted the adsorption capacity of the relatively hydrophobic F600 and G219 GACs reasonably well. For the oxidized ACFs, a separate correlation indicated that surface chemistry effects in addition to the availability of a suitable pore volume controlled TCE adsorption for ACFs with larger oxygen contents (~10%). The correlation established by the oxidized ACFs appropriately predicted the adsorption capacity of Picazine GAC with an oxygen content of about 16%.

As shown in Figure 5.12, a plot of MTBE adsorption capacity versus micropore volume in the 8-11 Å pore width range showed a trend similar to that for TCE, i.e., one correlation described MTBE adsorption on the more hydrophobic ACFs while a separate correlation described MTBE adsorption on oxidized ACFs. MTBE adsorption from ultra-pure water and natural water were controlled by pores in the same width range. This result suggests that MTBE had to compete with NOM over the entire pore size range that controls MTBE adsorption.

Two hydrophobic adsorbents that deviated from the trend established by the hydrophobic ACFs were AW10 and AAW10, a result that was likely attributable to pore blockage effects. Given that MTBE adsorption occurred primarily in pores with pore widths in the 8-11 Å range and given that the dominant pore sizes of ACF10 were in the 7-11 Å width range, it appears reasonable that even a small quantity of adsorbed NOM caused pore blockage or constrictions in pore size that precluded MTBE access to adsorption sites. MTBE isotherms in SJDW were also poorly described by the IAST, a result that further suggests that strongly adsorbing NOM components caused pore blockage or constrictions at pore entrances. As a result of pore blockage, MTBE

adsorption capacities (q_{e10}) of AW10 and AAW10 in SJDW were 69 and 64% smaller, respectively, than the single-solute MTBE adsorption capacities. These capacity reductions were the most severe among the studied adsorbents and suggest that pore blockage is especially detrimental to the adsorption of micropollutants from natural water, a result that concurs with the findings of Pelekani and Snoeyink [1999]. Pore blockage/constriction effects were not observed for MTBE adsorption from SJDW on ACF15 and ACF20, adsorbents whose dominant pore sizes were in the 9 to 13 Å width range. Therefore, these results suggest that the adverse effects of pore blockage by NOM can be avoided if the micropore size distribution extends to pore widths that are approximately twice the kinetic diameter of the adsorbate molecule.

Effects of Activated Carbon Surface Chemistry

Figure 5.13 illustrates the effect of surface chemistry on TCE adsorption for ACF20. TCE adsorption capacities increased with increasing adsorbent hydrophobicity, and similar results were observed for ACFs 10 and 15. These results confirm the trends described for single-solute systems and illustrate that hydrophobic adsorbents retain their advantage over more polar adsorbents in the presence of NOM.

The effects of surface chemistry on the adsorption of MTBE by ACF20 are shown in Figure 5.14. As was observed for TCE, the more hydrophobic carbons (AW20, HAW20, and AAW20) adsorbed MTBE more effectively than the more hydrophilic carbon (OAW20). Surface chemistry modifications of ACF15 yielded trends similar to those observed for ACF20 in Figure 5.14. However, surface chemistry modifications of ACF10 yielded a different trend for MTBE adsorption from SJDW. Figure 5.15

illustrates that OAW10 performed similarly or better than AW10. As explained earlier, a likely explanation for this result is that pore blockage/restriction occurred on AW10 but not on OAW10 as a result of repulsive electrostatic forces between the negatively charged surface of OAW10 and negatively charged NOM. Figure 5.15 also illustrated that HAW10 exhibited a larger adsorption MTBE adsorption capacity in SJDW than OAW10 once the mechanism of competition shifted from pore blockage/constriction to direct competition on HAW10.

To determine the effects of adsorbent surface chemistry on micropollutant adsorption from SJDW, TCE and MTBE adsorption capacities were plotted as a function of the adsorbent polarity. The polarity of each adsorbent was represented by the sum of its oxygen and nitrogen contents (mmol/g). To eliminate pore structure effects, TCE and MTBE adsorption capacities (q_{e10}) were normalized by the pore volume in the appropriate range of pore widths (i.e., 7-9 Å for TCE, 8-11 Å for MTBE). Consequently, normalized TCE and MTBE adsorption capacities (q'_{e10}) were expressed in units of mg micropollutant/cm^3 pore volume. Figure 5.16 shows that the normalized TCE adsorption capacity decreased with increasing adsorbent polarity, and a similar trend was observed for MTBE in Figure 5.17.

These results illustrate that hydrophobic adsorbents, i.e., adsorbents with a low heteroatom content, are more effective for the removal of both relatively hydrophobic and relatively hydrophilic pollutants from natural water. Furthermore, Figures 5.16 and 5.17 illustrate that the trends established by the ACF matrix appropriately described the performance of the commercially available GACs. Overall, the results in Figures 5.16 and 5.17 suggest that micropollutant adsorption is most effective on adsorbents that are

hydrophobic [(O+N) < 2 to 3 mmol/g] and exhibit a large volume of pores with a diameter that corresponds to approximately 1.5 times the kinetic diameter of the adsorbate. Furthermore, MTBE adsorption data from SJDW suggests that the detrimental effects of pore blockage as a result of NOM adsorption can be avoided if the micropore size distribution extends to pore widths that correspond to approximately twice the kinetic diameter of the adsorbate.

5.5. Conclusions

From the relationships observed between the adsorbent characteristics and the micropollutant adsorption isotherm data in natural water, the following conclusions were drawn:

(1) For carbons with similar surface chemistry, the pore volume of micropores with widths corresponding to about 1.5 times the kinetic diameter of the target pollutant controlled the adsorption capacity. However, if the dominant pore size range and the range of pore sizes in which the micropollutant adsorbs have similar upper bounds, pore blockage or restriction can occur as a result of NOM adsorption. Consequently, adsorption capacities decreased greatly as was observed for MTBE adsorption from SJDW on AW10 and AAW10. To prevent pore blockage, the dominant micropore range should be extended to pore widths that are approximately twice the kinetic diameter of the target adsorbate.

(2) Adsorbent polarity, as expressed by the sum of the oxygen and nitrogen contents (mmol/g), can serve as a useful activated carbon selection criterion. As the polarity of a carbon increases, or the molar concentration of O+N increases, the adsorption capacity decreases. Based on the results of this study, effective adsorbents should have an O+N content of less than 2-3 mmol/g.

(3) Attempts to minimize the adverse effects of NOM adsorption by selecting carbons with a negative surface charge (i.e. oxidized ACFs) were unsuccessful because the carbons contained a larger concentration of polar functional groups. The detrimental effects of enhanced water adsorption on these carbons outweighed any benefits that were derived from minimizing NOM adsorption through repulsive electrostatic forces.

5.6. References

Bernazeau F, Mandra V, Charles P, Anselme C, Bersillon J. Pesticides removal of activated carbon: competitive adsorption with natural organic matter. Water Supply 1996; 14(2): 43-48.

Chen G, Dussert W, Suffet H. Evaluation of granular activated carbons for removal of methylisoborneol to below odor threshold concentration in drinking water. Water Research 1997; 31(5): 1155-1163.

Chin, YP, Aiken G., O'Loughlin E. Molecular weight, polydispersity, and spectroscopic properties of aquatic humic substances. Environmental Science and Technology 1994; 28(11): 1853-1858.

Ebie K, Li F, Azuma Y, Yuasa A, Hagishita T. Pore distribution effect of activated carbon in adsorbing organic micropollutants from natural water. Water Research 2001; 35(1): 167-179.

Ebie K, Li F, Hagishita, T. Effect of pore size distribution of activated carbon on the adsorption of humic substances and trace organic compounds. Water Supply 1995; 13(3/4): 65-70

Karanfil T, Kitis M, Kilduff JE, Wigton A. Role of granular activated carbon surface chemistry on the adsorption of organic compounds. 2. Natural Organic Matter. Environmental Science and Technology. 1999; 33(18): 3225-3233.

Kasaoka S, Sakata Y, Tanaka E, Naitoh R. Design of molecular-sieve carbon. Studies on the adsorption of various dyes in the liquid phase. International Chemical Engineering 1989b; 29(4): 734-742.

Kasaoka S, Sakata Y, Tanaka E, Naitoh R. Preparation of activated fibrous carbon from phenolic fabric and its molecular-sieve properties. International Chemical Engineering 1989a; 29(1): 101-114.

Kilduff JE and Wigton A. Sorption of TCE by humic-preloaded activated carbon: Incorporating size-exclusion and pore blockage phenomena in a competitive adsorption model. Environmental Science and Technology 1999; 33(2): 250-256.

Kilduff JE, Karanfil T, Chin Y, Weber WJ. Adsorption of natural organic polyelectrolytes by activated carbon: A size exclusion chromatography study. Environmental Science and Technology 1996; 30: 1336-1343.

Kilduff JE. Polyelectrolyte adsorption by activated carbon and the effects of preloading on trichloroethylene adsorption. Ph.D. Dissertation. The University of Michigan: Ann Arbor, MI. 1995.

Knappe D, Matsui Y, Snoeyink VL. Predicting the Capacity of Powdered Activated Carbon for Trace Organic Compounds in Natural Waters. Environmental Science and Technology 1998; 32(11): 1694-1698.

Najm IN, Snoeyink VL, Lykins BW, Adams JQ. Using powdered activated carbon: A critical review. Journal of the American Water Works Association 1991b; 83(1): 65-76.

Najm, IN, Snoeyink VL, Richard Y. Effect of initial concentration of a SOC in natural water on its adsorption by activated carbon. Journal of the American Water Works Association 1991a; 83(8): 57-63.

Narbaitz RM and Benedek A. Adsorption of 1,1,2-trichloroethane from river water. Journal of Environmental Engineering 1994; 120(6): 1400-1415.

Newcombe G, Drikas M, Hayes R. Influence of characterized natural organic matter on activated carbon adsorption: II. Effect on pore volume distribution and adsorption of 2-methylisoborneol. Water Research 1997; 31(5): 1065-1073.

Pauling L. The nature of the chemical bond, and the structure of molecules and crystals: an introduction to modern structural chemistry; 3rd edition. Ithaca NY: Cornell University Press. 1960.

Pelekani C, Newcombe G, Snoeyink VL, Hepplewhite C, Assemi S, Beckett R. Characterization of natural organic matter using high performance size exclusion chromatography. Environmental Science & Technology 1999b; 33(16): 2807-2813.

Pelekani C, Snoeyink VL. A kinetic and equilibrium study of competitive adsorption between atrazine and Congo red dye on activated carbon: the importance of pore size distribution. Carbon 2001; 39: 25-37.

Pelekani C, Snoeyink VL. Competitive adsorption between atrazine and methylene blue on activated carbon: the importance of pore size distribution. Carbon 2000; 38: 1423-1436.

Pelekani C, Snoeyink VL. Competitive adsorption in natural water: role of activated carbon pore size. Water Research 1999a; 33(5): 1209-1219.

Qi S, Adham SS, Snoeyink VL, Lykins BW. Prediction and verification of atrazine adsorption by PAC. Journal of Environmental Engineering 1994; 120(1): 202-218.

Summers RS and Roberts PV. Activated carbon adsorption of humic substances II. Size exclusion and electrostatic interactions. Journal of Colloid and Interface Science 1988; 122(2): 382-39

5.7. Tables

Table 5.1. Freundlich isotherm parameters for dose-normalized DOC and UV_{280} isotherms for ACFs and pulverized GACs

Carbon	Dose-Normalized DOC Isotherms		Dose-Normalized UV_{280} Isotherms	
	$K\ (mg/g)^{1-1/n}$	1/n	$K\ (L\ g^{-1}\ cm^{-1})^{1-1/n}$	1/n
AW10	0.269	0.735	.201	.897
AW15	2.65	0.423	.452	.492
AW20	3.33	0.419	.544	.540
OAW10	.469	.678	.402	.674
OAW15	1.21	.710	.750	.666
OAW20	1.09	.708	.578	.567
HAW10	.370	.570	.196	.782
HAW15	2.89	.477	.595	.479
HAW20	3.52	.406	.476	.489
AAW10	.268	.695	.149	.762
AAW15	3.58	.442	.500	.469
AAW20	2.69	.429	.566	.511
F600	3.60	.523	.842	.470
G219	7.16	.415	.916	.439
Picazine	2.74	.609	.981	.636

5.8. Figures

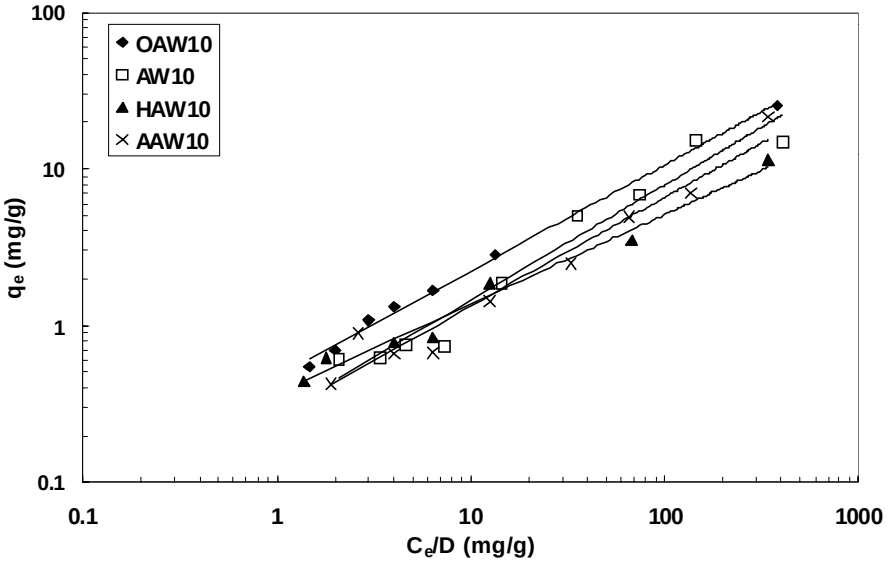

Figure 5.1. Effect of surface chemistry modifications on dose-normalized DOC isotherms for ACF10

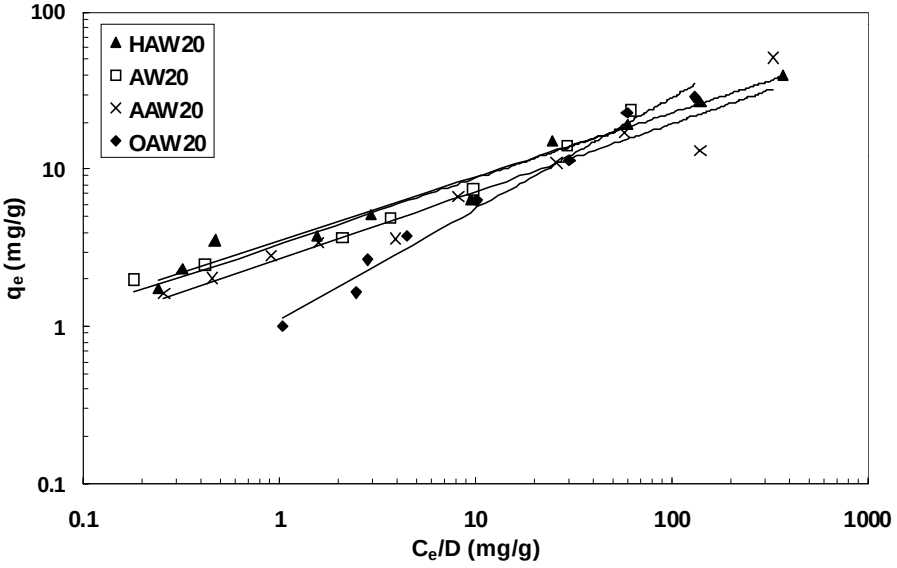

Figure 5.2. Effect of surface chemistry modifications on dose-normalized DOC isotherms for ACF20

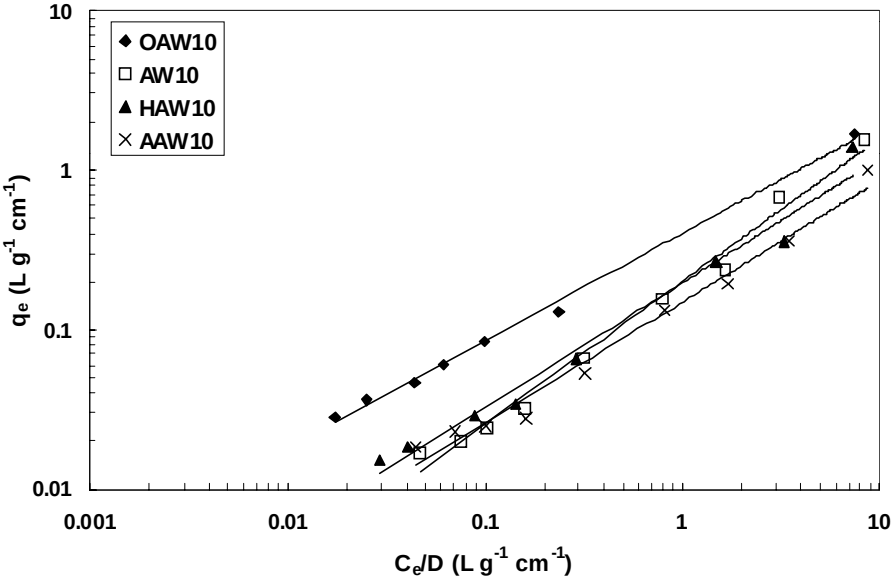

Figure 5.3. Effect of surface chemistry modifications on dose-normalized isotherms of UV_{280}-absorbing NOM components for ACF10

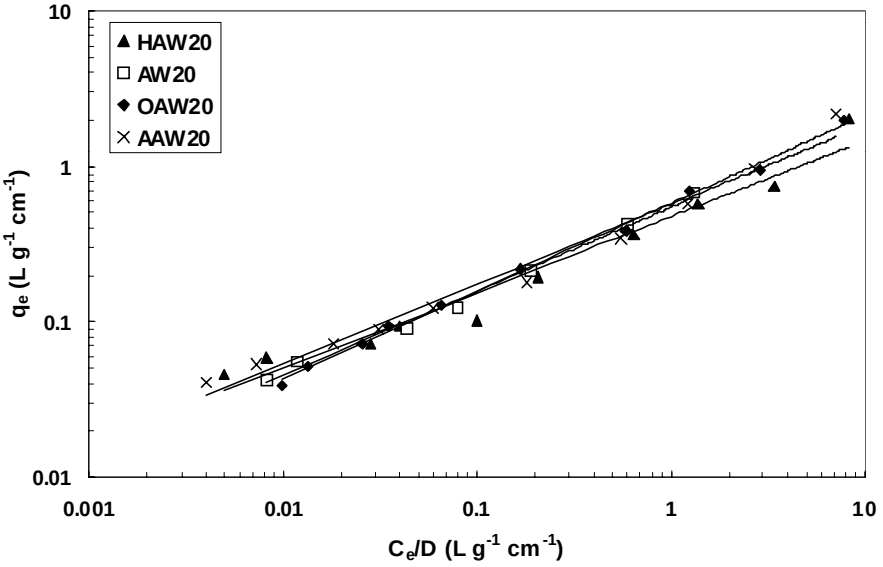

Figure 5.4. Effect of surface chemistry modifications on dose-normalized isotherms of UV_{280}-absorbing NOM components for ACF20

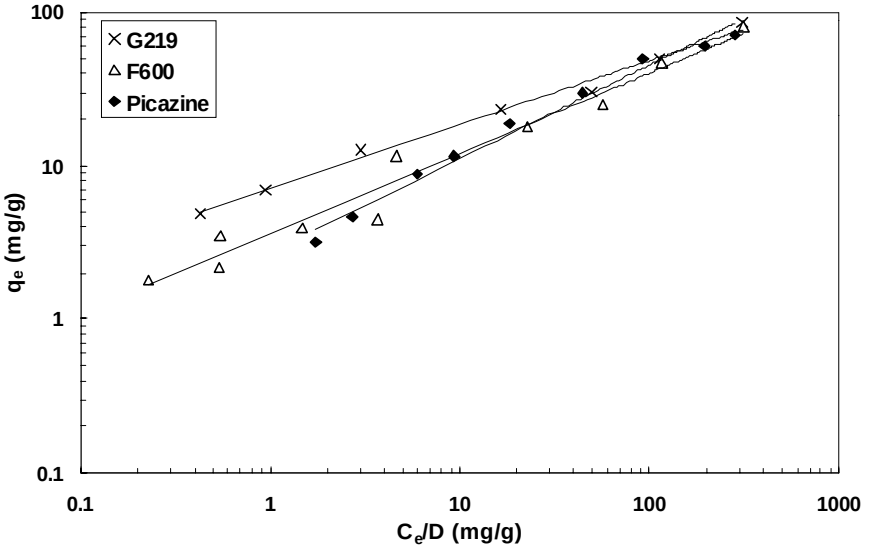

Figure 5.5. Dose-normalized DOC isotherms on pulverized GACs

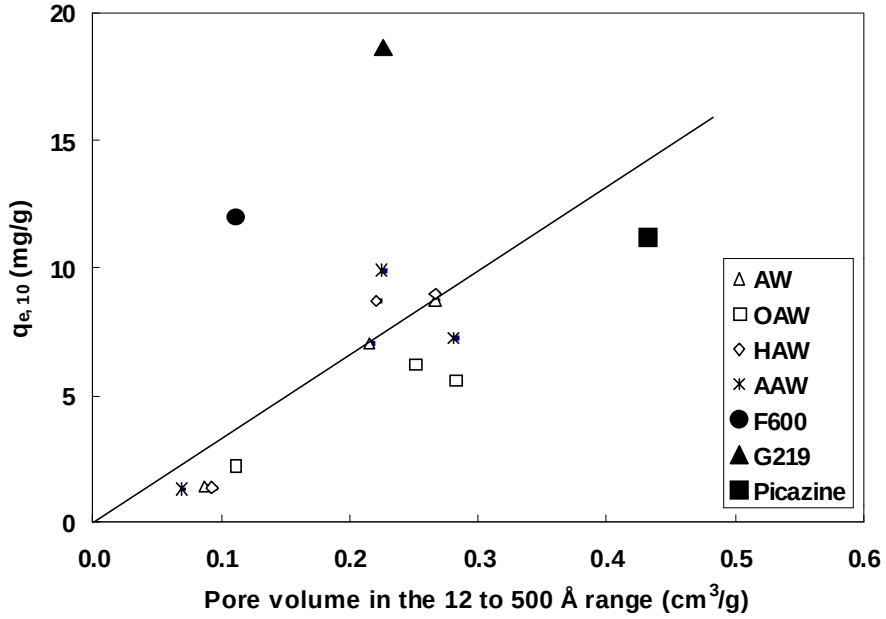

Figure 5.6. Correlation between the DOC adsorption capacity at C_e/D = 10 mg/g and pore volume in the 12-500 Å width range

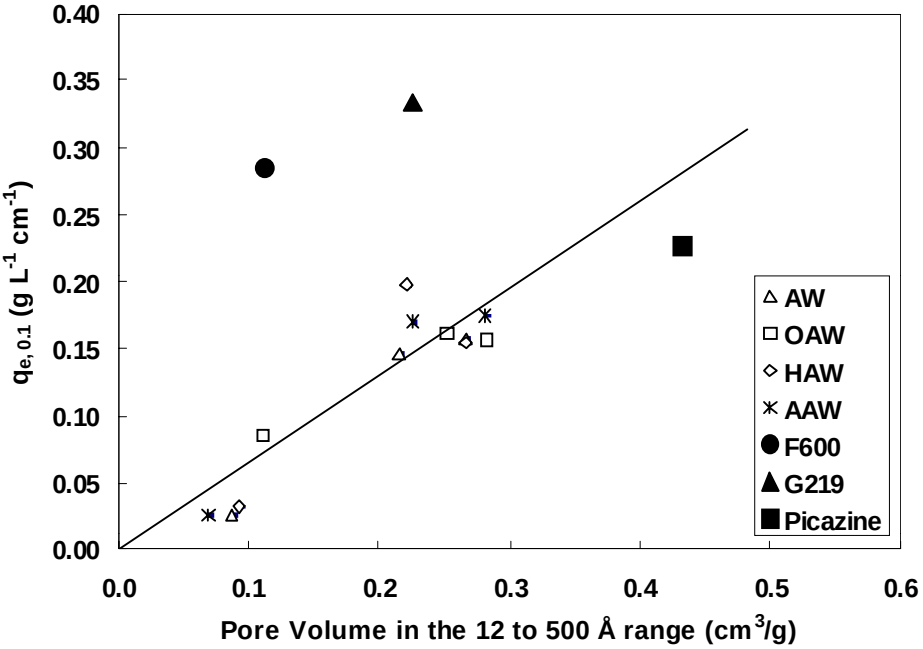

Figure 5.7. Correlation between the adsorption capacity of UV_{280}-absorbing NOM components at C_e/D = 0.1 g L^{-1} cm^{-1} and pore volume in the 12-500 Å width range

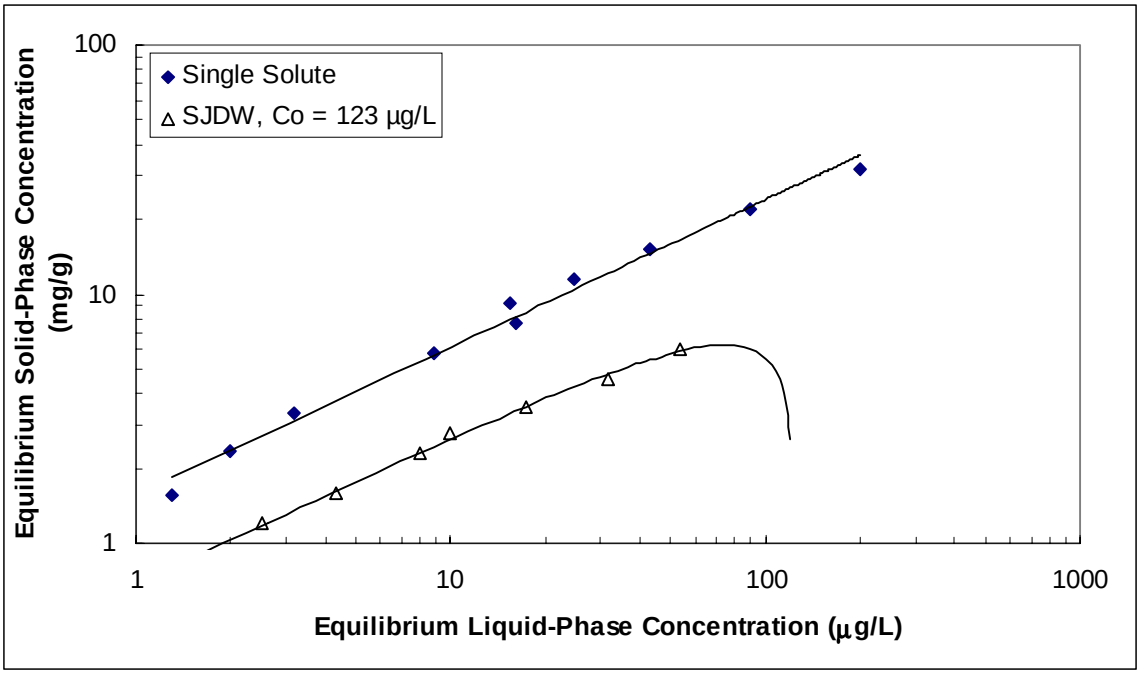

Figure 5.8. Effect of NOM on TCE adsorption by AW20
(Solid line through single solute data represents Freundlich isotherm fit. Solid line through SJDW data represents IAST model fit)

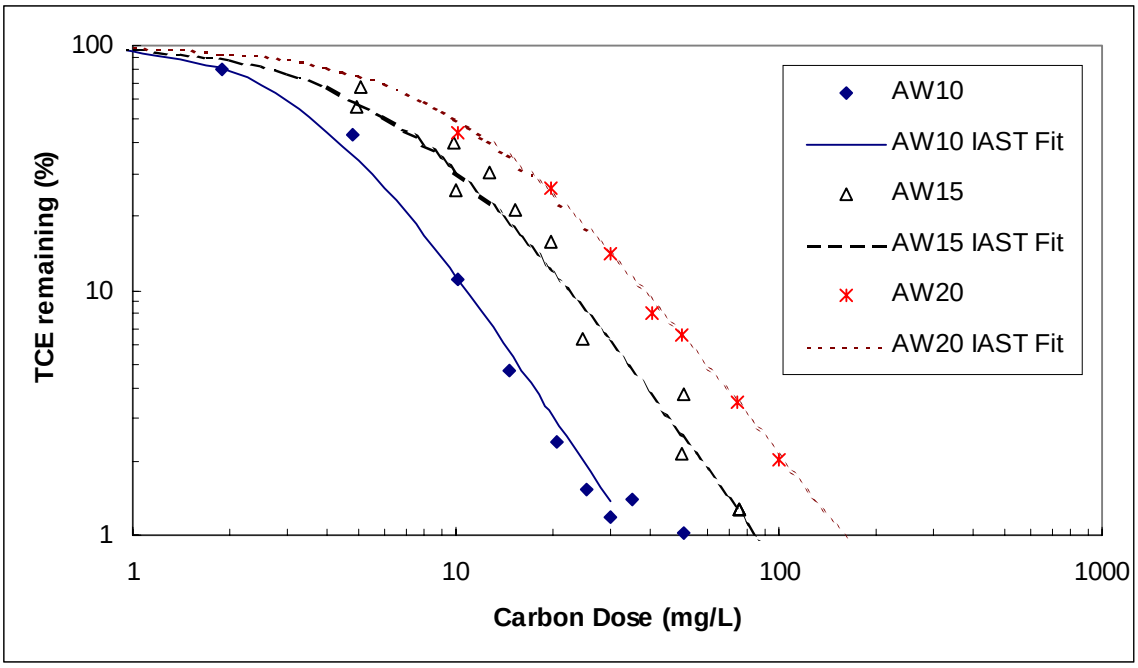

Figure 5.9. Effect of ACF pore structure on TCE adsorption from SJDW (acid-washed ACFs)

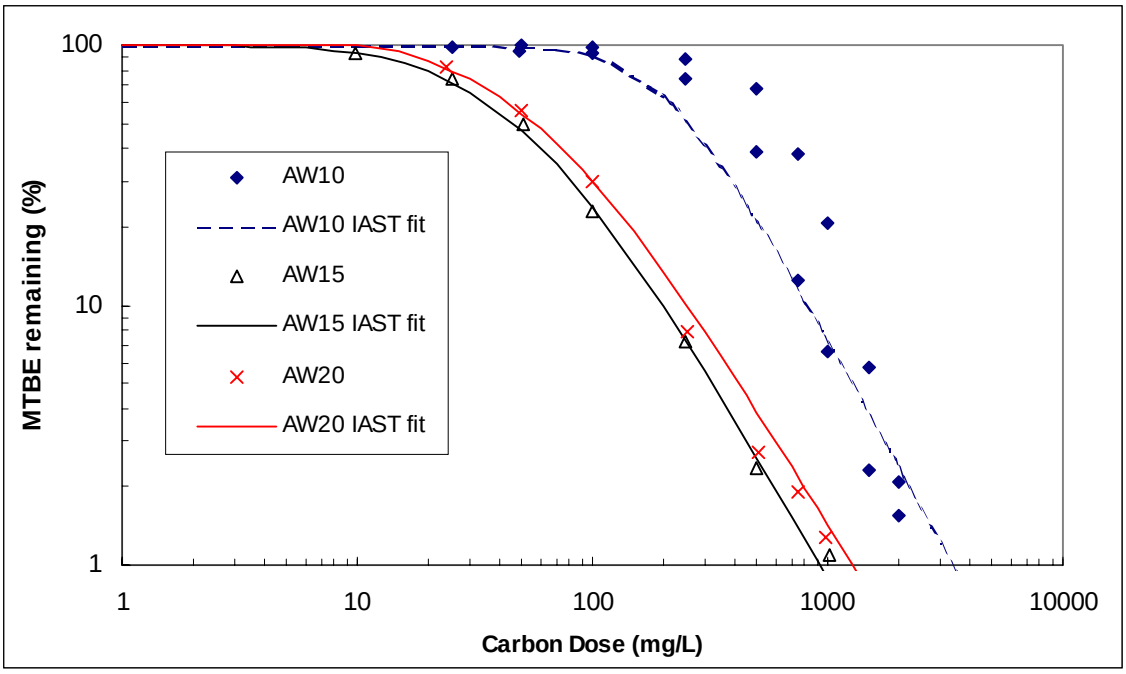

Figure 5.10. Effect of ACF pore structure on MTBE adsorption from SJDW (acid-washed ACFs)

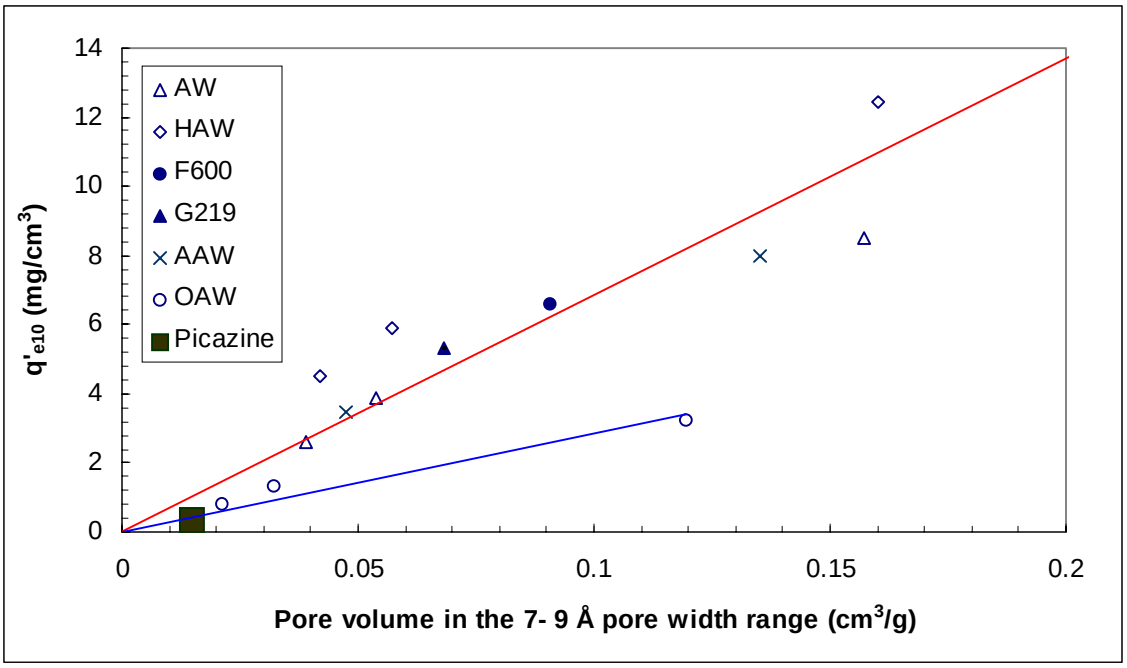

Figure 5.11. Effect of pore volume on TCE adsorption from SJDW

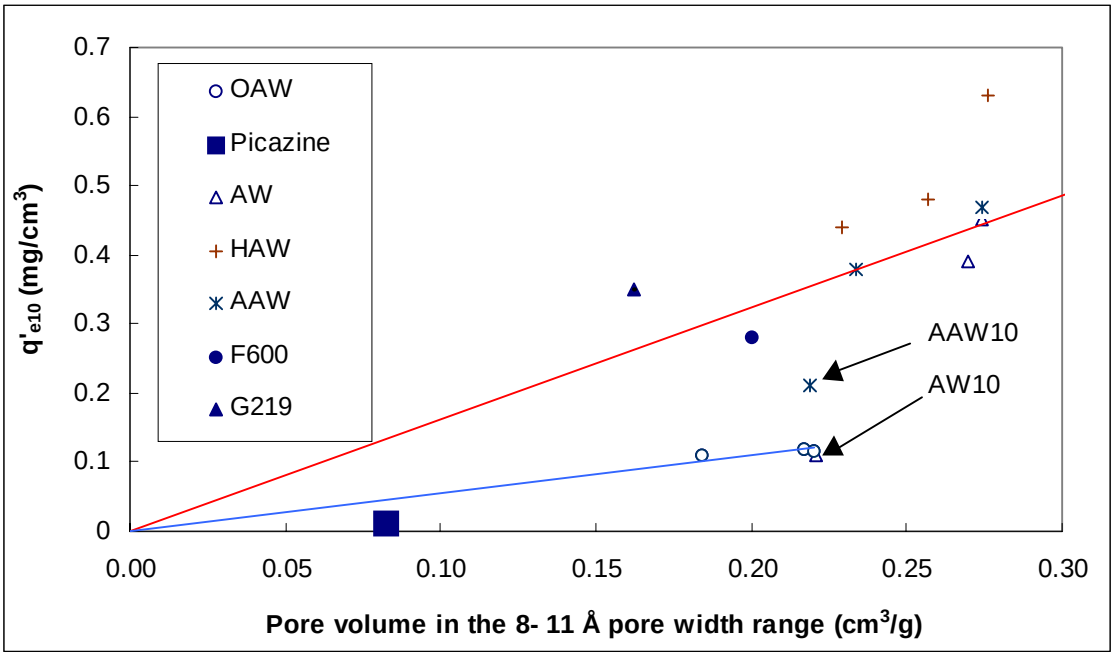

Figure 5.12. Effect of pore volume on MTBE adsorption from SJDW

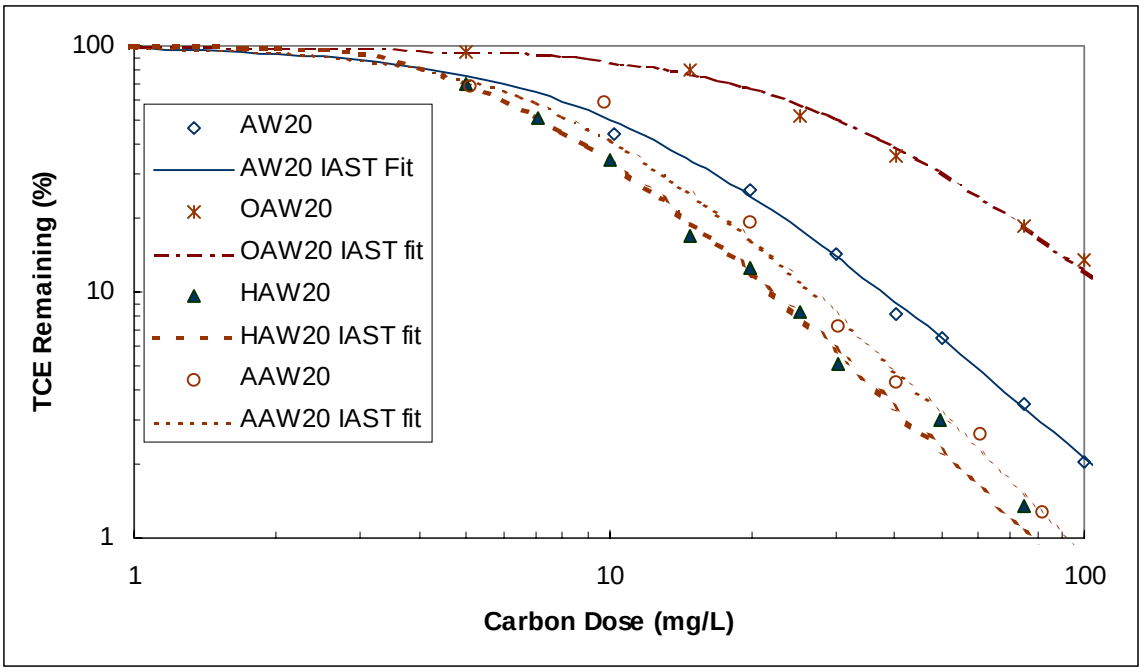

Figure 5.13. Effect of ACF surface chemistry modifications on TCE adsorption from SJDW (ACF20s)

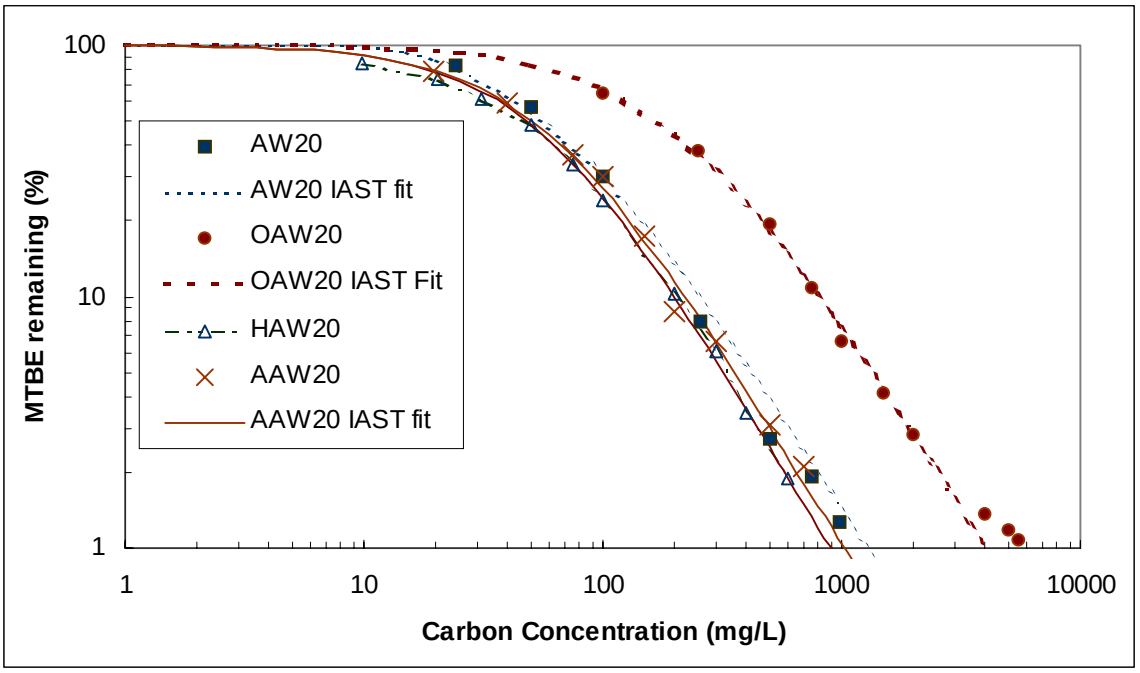

Figure 5.14. Effect of ACF surface chemistry modifications on MTBE adsorption from SJDW (ACF20s)

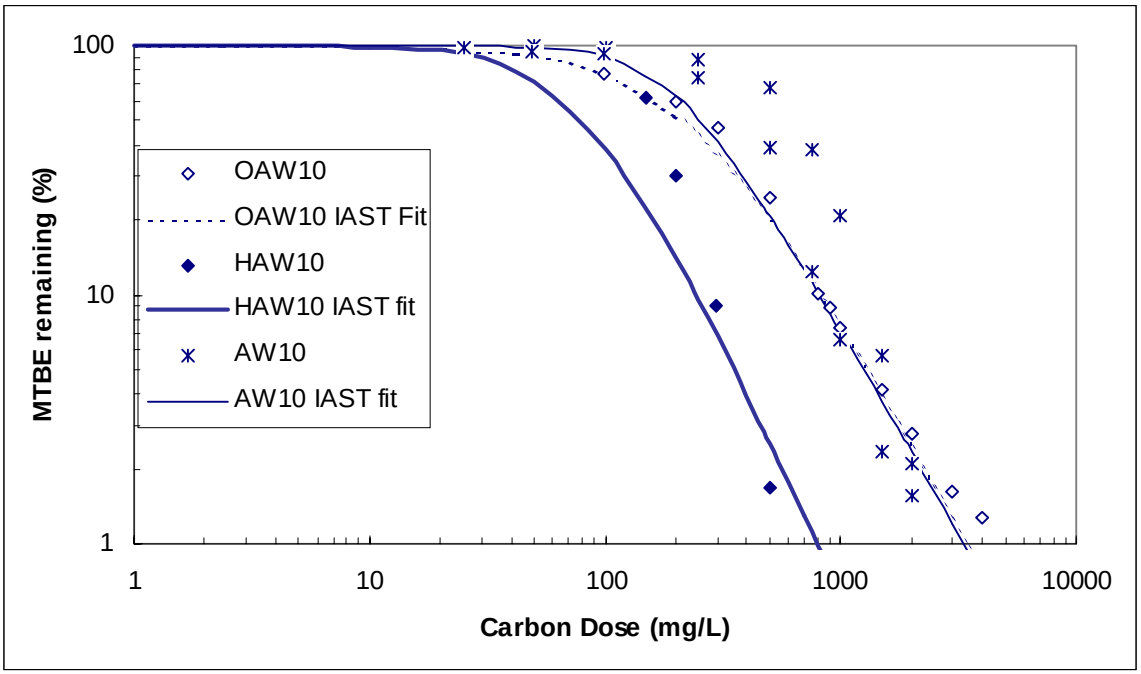

Figure 5.15. Effect of ACF surface chemistry modifications on MTBE adsorption from SJDW (HAW10 and AW10 vs. OAW10)

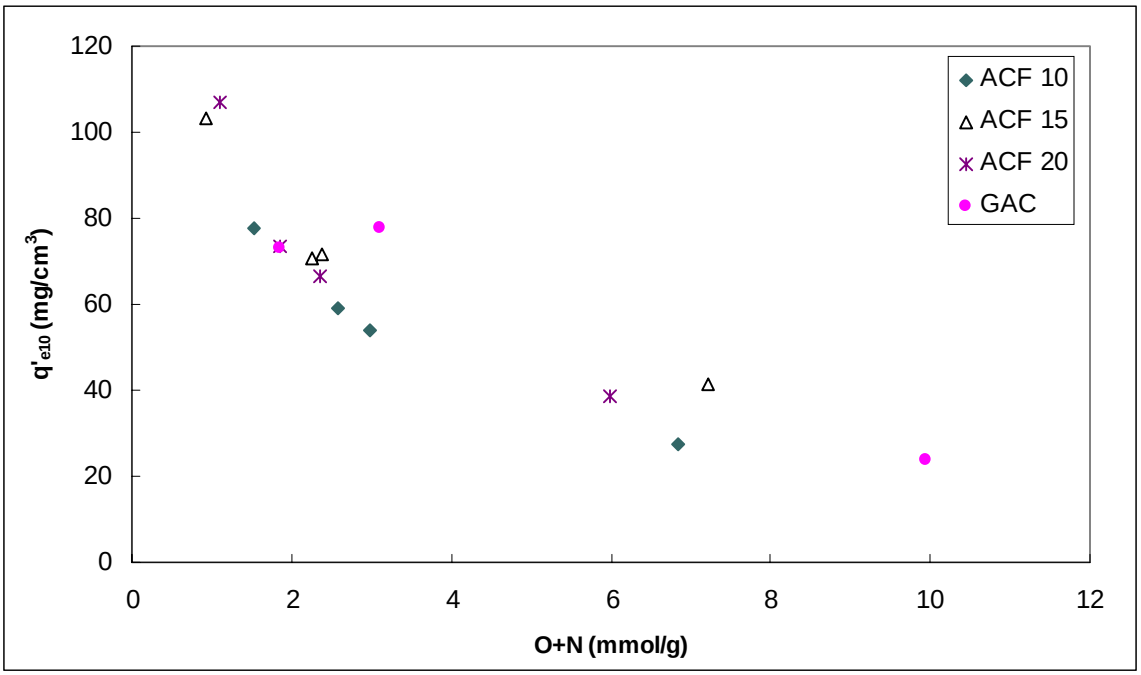

Figure 5.16. Effect of adsorbent hydrophobicity on TCE adsorption capacity in the presence of NOM ($C_{0,\,TCE}$ = 100 µg/L)

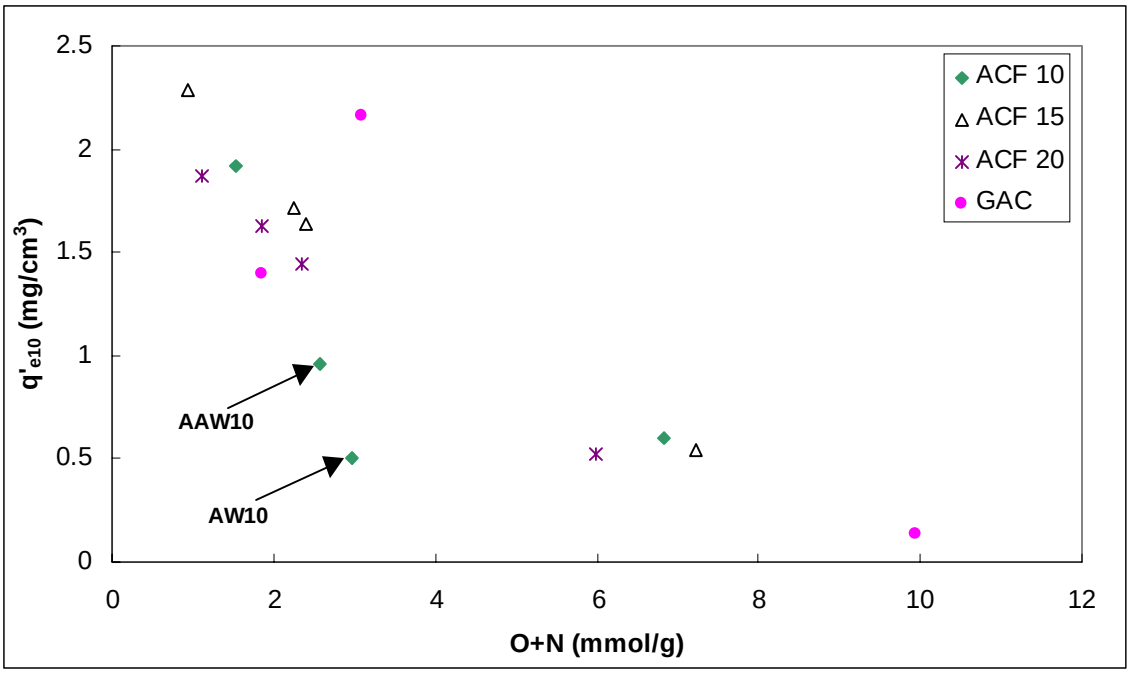

Figure 5.17. Effect of adsorbent hydrophobicity on MTBE adsorption capacity in the presence of NOM ($C_{0,\,MTBE}$ = 100 µg/L)

Chapter 6. Prediction of Activated Carbon Adsorption Capacities from Aqueous Solution Using a Polanyi Potential Theory Model

6.1. Objectives

The objectives were (1) to describe the previously presented single-solute adsorption data through a generalized adsorption model based on the Polanyi Potential Theory (PPT), (2) to correlate water adsorption coalescing factors with adsorbent polarities, and (3) to verify model predictions for two adsorbates and three activated carbons that were not used for the model calibration.

6.2. Background

Proper design of an activated carbon adsorber requires that the adsorption capacity of an activated carbon for a target organic compound is known. However, relatively few adsorption isotherms are available for the 70 000 organics currently in use and the wide array of activated carbons that are marketed by numerous manufacturers. Therefore, it is desirable to predict adsorption capacities using an isotherm model with parameters based on the physical and chemical properties of adsorbents and adsorbates. The Polanyi Potential Theory (PPT) provides a framework for such predictions, and it has been successfully applied to describe the adsorption of gases, vapors and aqueous adsorbates on activated carbons [Manes 1998, Grant and Manes 1964, Wohleber and Manes 1971, Crittenden et al. 1999]. Numerous studies that employed the PPT focused on the determination of the most appropriate adsorbate characteristic to estimate affinity coefficients (or coalescing factors) that unite the adsorption equilibria of different

adsorbates on a given adsorbent into a single characteristic curve [Manes 1998, Crittenden et al. 1999, Lee et al. 1984, Speth 1986]. However, no study to date quantitatively incorporated the effects of activated carbon surface chemistry on water adsorption. As a result, it is impossible to use data obtained for one activated carbon to predict the adsorption isotherms of trace organic compounds in aqueous solution for other activated carbons with different surface chemistries.

The PPT has been widely applied to describe physical adsorption on heterogeneous adsorbents such as activated carbons. All prior physical adsorption theories were based on the assumption that one or multiple adsorption layers form on an adsorbent surface. In contrast, Polanyi proposed that adsorption is characterized by pore filling within the adsorption space, which, for microporous adsorbents such as activated carbon, is largely located in the micropores. Polanyi further proposed that the adsorbed substance is present in a form of a pure liquid or solid depending on the state of the pure compound at the adsorption temperature. In the PPT, the adsorption potential, ε, is defined as the work required to move an adsorbate molecule from its position in the adsorption space to an infinite distance from the surface. An important concept in the PPT is the *characteristic curve* which states that the (V) of an adsorbate adsorbed on a given adsorbent is a function of the adsorption potential

$$V = f(\varepsilon) \tag{1}$$

For the adsorption of gases and vapors, the value of the adsorption potential is defined as [Dubinin 1960]

$$\varepsilon_l = RT/\ln(P_s/P) \tag{2}$$

where ε_l is the gas-phase adsorption potential; R is the ideal gas constant; T is the adsorption temperature; and P_s and P are the saturation and equilibrium pressures of the solute at temperature T, respectively. For the adsorption of aqueous organic compounds that are partially miscible in water, the adsorption potential is defined as [Manes, 1998]

$$\varepsilon_{lw} = RT/\ln(c_s/c) \quad (3)$$

where ε_{lw} is the aqueous-phase adsorption potential; and c_s and c are the saturation and equilibrium concentrations of the solute at temperature T, respectively. For aqueous-phase adsorption, the adsorption space is initially filled with water, and an adsorbate condensing or precipitating from aqueous solution has to displace this water. As a result, the adsorption energy of an aqueous organic compound is reduced by that required to displace an equal volume of water. Consequently, the aqueous-phase adsorption potential of an organic compound (ε_{lw}) is related to adsorption potential of the pure vapor (ε_l) by [Manes 1998]

$$RT \ln(c_s/c) = \varepsilon_{lw} = \varepsilon_l - V_m (\varepsilon_w / V_w) \quad (4)$$

where ε_l and ε_w are the adsorption potentials for the adsorbate and water as pure vapors, respectively, and V_m and V_w are molar volumes of the adsorbate and water, respectively. Dividing by V_m gives

$$(RT/V_m) \ln(c_s/c) = \varepsilon_{lw}/V_m = \varepsilon_l/V_m - \varepsilon_w/V_w \quad (5)$$

or in a more compact form

$$A_{lw} = A_l - A_w \quad (6)$$

where $A_{lw} = \varepsilon_{lw}/V_m$, $A_l = \varepsilon_l/V_m$ and $A_w = \varepsilon_w/V_w$. To correlate adsorption isotherms of different compounds on a given adsorbent, Manes and coworkers introduced a reference curve called the *hydrocarbon standard curve*, which was determined by the adsorption of

normal paraffin hydrocarbons such as methane, propane and on a given adsorbent butane [Manes 1998, Grant and Manes 1964, Grant et al. 1962]. The abscissa value for a target adsorbate was then scaled to that of the hydrocarbon standard curve as follows:

$$A_{lw}/A_h = A_l/A_h - A_w/A_h \quad (7)$$

or

$$\gamma_{lw} = \gamma_l - \gamma_w \quad (8)$$

where A_h is the abscissa value of the hydrocarbon standard curve ($\gamma_{lw} = A_{lw}/A_h$, $\gamma_{lw} = A_l/A_h$, $\gamma_w = A_w/A_h$). γ is often called the *coalescing factor*. Equations (7) and (8) provide a useful link between aqueous- and gas-phase adsorption. Once the hydrocarbon standard curve of a given carbon is determined, the aqueous-phase adsorption capacity of any adsorbate can be predicted on this carbon if γ_l and γ_w values are known.

To determine γ_l, correlations developed for the affinity coefficient β_l can be used. γ_l is related to β_l by

$$\gamma_l = \beta_l V_{m,\,ref}/V_m. \quad (9)$$

where $V_{m,\,ref}$ is the molar volume of the reference compound at the adsorption temperature. Prior studies showed that β_l of an adsorbate can be predicted from the physicochemical properties of a given adsorbate based on the assumption β_l is adsorbate-dependent but adsorbent-independent [Prakash et al. 1994]. These physicochemical properties include molar volume (V_m), polarizability (P_e), parachor (Ω), and the molecular connectivity index [Prakash et al. 1994, Nirmalakhandan and Speece 1993, Qi et al. 2000, Wood 2001]. By correlating more than one hundred experimental affinity coefficients from different data sources with molar volume, polarizability and parachor, Wood [2001] recently concluded that (1) polarizability can be more easily calculated and

has a more fundamental theoretical relation to adsorption potential, (2) parachor is the parameter that produced the smallest standard deviation, and (3) unlike molar volume, polarizability and parachor are temperature-, pressure-, and density-invariant properties, which is desirable for describing characteristic curves that are also assumed to be temperature invariant.

γ_w can be estimated directly by deriving the water adsorption affinity coefficient β_w from water adsorption isotherms at different pressures [Wood 2001] or from calorimetric measurements [Barton et al. 1994, Stoeckli and Lavanchy 2000]. In addition, γ_w can be calculated indirectly for a given activated carbon if the hydrocarbon standard curve and aqueous-phase adsorption isotherm data are known. In that case, $\gamma_w = \gamma_l - \gamma_{lw}$. Using the hydrocarbon standard curve and aqueous-phase adsorption isotherm data for five aliphatic hydrocarbons, Wohleber and Manes [1971] obtained an average γ_w of 0.28 for a BPL activated carbon. Equation (8) could therefore be rewritten as

$$\gamma_{lw} = \gamma_l - 0.28 \qquad (10)$$

Arbuckle [1981] applied equation (10) to predict the adsorption of 9 alcohols and 13 additional compounds (aldehydes, alkyl acetates, ketones and one ether). Adsorption isotherms were predicted from the PPT with some success for some compounds but not for others. Two possible sources for error were (1) the γ_w value for F400 is different from that for BPL, and (2) at the tested concentrations, the polar compounds evaluated by Arbuckle [1981] exhibited specific interactions with polar functional groups on the activated carbon surface (equilibrium liquid-phase concentration for the tested compounds ranged from about 0.3 to 3 mmol/L).

It needs to be noted that the applicability of equation (10) is limited to carbons with surface chemistries that are similar to that of the BPL sample tested by Wohleber and Manes [1971]. Resent results indicated that the amount of water adsorbed increased with an increasing concentration of the surface oxides [Tamon and Okazaki 1996, Phillips et al. 2000, Wood 2001]. Wood [2001] summarized water adsorption affinity coefficient (β_w) values based on the water adsorption isotherms on about 30 activated carbons. β_w values (referenced to benzene) were derived from the Dubinin-Astakhov (DA) equation, and the results showed that β_w differed from one carbon to another if the two carbons had different surface properties. For example, the β_w values of a series of Calgon BPL activated carbons that were oxidized to different degrees varied from 0.34-0.58 at low water pressure and from 0.11-0.19 at higher water pressures. Therefore, it is not appropriate to take γ_w as a constant value in studying activated carbons with different surface chemistry.

In the Polanyi model, van der Waals forces are assumed to be the dominant force responsible for adsorption. However, an affinity coefficient considering only van der Waals forces may not be applicable in the cases where dipole-dipole, induced-dipole, and hydrogen-bonding donor-acceptor interactions exist. Using the PPT, Crittenden et al. [1999] recently developed a normalizing factor which incorporated the LSER (linear solvation energy relationship) parameters: intrinsic molar volume, polarity/polarizability parameter, hydrogen-bonding acceptor parameter and hydrogen-bonding donor parameter. These parameters represent adsorption interactions between: (1) the organic adsorbate and the adsorbent, (2) water and the adsorbent, (3) adsorbed organic adsorbates, (4) the organic compound and water molecules, and (5) water molecules. The

correlation was developed using 56 organic compounds (halogenated aliphatics, aromatics and halogenated aromatics, polyfunctional organics and sulfonated aromatics) and 8 adsorbents (activated carbons and synthetic polymeric adsorbents). Normalizing factors derived from the Polanyi-LSER approach showed an improved prediction than those derived from molar volume. In addition, the results indicated the importance of water-adsorbent interactions. However, the limitations of this Polanyi-LSER approach are (1) the correlation involved many fitting parameters, (2) fitting parameters were adsorbent-specific, and (3) no quantitative correlation between the fitting parameters and adsorbent properties was obtained. As a result, it is difficult to use data obtained for one activated carbon to predict the performance of other activated carbons with different surface properties. In contrast, the Polanyi–Manes approach is easy to apply. For a given adsorbate/adsorbent system, this approach simply requires the determination of the hydrocarbon standard curve for an adsorbent and some physicochemical adsorbate properties such as molar volume, polarizability, or parachor. Based on adsorption data collected with the activated carbon fiber (ACF) matrix in Chapter 4, we propose that adsorbent surface chemistry primarily influences the interaction of water with polar functional groups on the adsorbent surface while the adsorption of trace organic contaminants is controlled by nonspecific interactions with the carbon basal plane. Therefore, if the dependence of water adsorption on adsorbent polarity (a function of adsorbent surface chemistry) can be described, the PPT should be a valid tool to model the adsorption of trace organic compounds from aqueous solution.

6.3. Materials and Methods

Adsorbent Characterization

In addition to previous adsorbent characterizations (Chapter 3), CO_2 adsorption isotherm data were collected at 273 K for each adsorbent (Autosorb-1-MP, Quantachrome Corporation, Boynton Beach, FL) over a relative pressure range from 10^{-6} to 10^{-2}. Prior to measurement, the samples were outgassed overnight at 473K.

Micropollutant adsorption isotherms from aqueous solution

Single solute trichloroethene (TCE) and methyl tertiary butyl ether (MTBE) adsorption isotherm data were obtained for each adsorbent as described previously. In addition, single solute *cis*-1,2-dichloroethene (DCE) and tetrachloroethene (PCE) isotherm experiments were also completed to evaluate the predictive capacities of the procedure developed in this chapter.

Calculation of characteristic curves

To develop a characteristic curve from adsorption isotherm data, values of the adsorbate molar volume (V_m) or density (ρ_m) in the adsorbed state (condensed state) were needed. For adsorbates that exist as liquids at the temperature, at which an adsorption experiment is conducted, the molar volume in the adsorbed state corresponds to the bulk molar volume at that temperature. The density of CO_2 in the adsorbed state has been a matter of debate and in this study, a density of 1.023 g/ cm^3 was employed [Cazorla-Amoros 1998]. The density of N_2 was 0.808 g/cm^3, the value at its normal boiling point. The saturation pressures and calculated molar volumes of N_2 and CO_2 are summarized in

Table 6.1. Following the notation of Manes [1998], the abscissa (A) of a characteristic curve was in the format of $A = \varepsilon/V_m$, where ε is defined in equations (2) and (3) for gaseous and aqueous adsorbates, respectively. The ordinate V represents the volume of condensed (liquid) adsorbate at a given A normalized by adsorbent mass.

6.4. Results and Discussion

6.4.1. Adsorbent Characterization

Figure 6.1 shows representative N_2 and CO_2 adsorption characteristic curves on for ACFs and GAC Picazine, respectively. For comparison, the characteristic curves were plotted in the Dubinin-Radushkevich format of ln(V) vs $(A/\gamma)^2$, where γ values for N_2 and CO_2 are listed in Table 6.1. As indicated by Figure 6.1, there is a good continuation between N_2 and CO_2 adsorption on ACFs as depicted by AW10 and AW15, which is similar to the observation of Cazorla-Amoros et al. [1998]. It should be noticed that on each GAC (illustrated by Picazine in Figure 6.1), an evident deviation of the N_2 adsorption data was observed when $(A/\gamma)^2 > 0.035$ $(KJ/cm^3)^2$, which can be attributed to diffusional limitations for N_2 adsorption at very low temperature [Cazorla-Amoros et al. 1996]. The different slopes in three characteristic curves are related to the pore size distributions of the adsorbents. A steeper slope observed in Picazine represents a wider PSD, which is consistent with the results in Chapter 3.

Figure 6.2 depicts the characteristic curves of N_2 and CO_2 on surface modified ACF20s. The N_2 and CO_2 adsorption curves on AW20, OAW20, HAW20 and AAW20 superimposed on each other, and the same was also observed for ACF15s and ACF10s (not shown). Figure 6.2 indicated that N_2 and CO_2 adsorption isotherms do not change

with the oxygen content of the adsorbent (range for ACF20s: 0.77 mmol/g to 6.0 mmol/g). Recently, Lopez-Ramon et al. [2000] also showed that the adsorption of CO_2 was not affected by the oxygen content of activated carbons despite an increase in the surface oxygen concentration from 0.8 to 7 mmol/g. Although the current results as well as those of Lopez-Ramon et al. [2000] do not directly prove the absence of specific interactions between CO_2 and oxygen-containing functional groups on carbon surface, the results suggest that CO_2 adsorption is not affected by the oxygen content of activated carbons.

6.4.2. Modeling Approach

Following Manes' method, the approach followed in this study was (1) to determine the standard hydrocarbon curve for each adsorbent from N_2 and CO_2 adsorption isotherms; (2) to derive the coalescing factor γ_{lw} from aqueous-phase micropollutant adsorption isotherms; (3) to estimate the coalescing factor γ_l for each micropollutant from its parachor and molar volume; and (4) to derive the coalescing factor for water adsorption, γ_w, from equation (11). The resulting γ_w values for different adsorbents were then correlated with a measure of adsorbent polarity.

$$\gamma_w = \gamma_l - \gamma_{lw} \tag{11}$$

Determination of hydrocarbon standard curves

As indicated by Grant and Manes [1964], the adsorption characteristic curve of nitrogen and argon correlated well with the hydrocarbon curve (the standard curve) of a given carbon. Figures 6.1 and 6.2 also showed that nitrogen and carbon dioxide

adsorption data on a given carbon fit a single characteristic curve. Furthermore, N_2 and CO_2 adsorption was not sensitive to the presence of surface oxygen complexes. Therefore, CO_2 and N_2 represent suitable compounds for constructing the hydrocarbon standard curve of a given adsorbent. To construct the hydrocarbon standard curve, the N_2 and CO_2 adsorption data need to be scaled, however, to represent the adsorption of a suitable reference hydrocarbon. In Manes' approach, heptane was used as the reference compound. The use of heptane was for convenience, as suggested by Manes and Hofer [1969], because quantities such as the molar volume, refractive index, polarizability and parachor are more reliably obtained for hydrocarbons that are a liquid at the temperature of interest than for those that are gases. In addition to heptane, hexane or pentane can also be used as reference compounds [Holland et al. 2001]. Benzene, recommended by Dubinin [1960], is another common reference adsorbate, because the chemical structure of activated carbon is mainly composed of benzene-like rings. Although benzene has been widely used as a reference for studying the microporosity of activated carbon, its use in studying activated carbons with a variety of surface functional groups is questionable because specific interactions are possible between the delocalized π-electrons of the carbon surface and benzene. These specific interactions can be minimized if alkanes are selected as reference compounds [Lu et al. 1991].

Following Manes' approach, heptane was used in this study as the reference adsorbate. The heptane characteristic curve for each adsorbent was obtained by dividing the abscissa values of N_2 and CO_2 characteristic curves by the corresponding γ_l values listed in Table 6.1. The heptane characteristic curve derived from N_2 and CO_2 adsorption data is depicted in Figure 6.3. The regression analysis showed that the heptane

characteristic curve is in the format of $\log(V) = a(A)^3+b(A)^2+c(A)+d$, which agrees with the results obtained from hydrocarbon adsorption on activated carbons [Manes, 1998]. The derived heptane characteristic curve of each carbon was used as the standard hydrocarbon curve in subsequent calculations.

Determination of γ_{lw}

After the standard curve for a given activated carbon was developed, single-solute MTBE and TCE adsorption isotherm data for that carbon were plotted on the same graph, as illustrated in Figure 6.3. $\gamma_{lw,MTBE}$ and $\gamma_{lw,TCE}$ in Figure 6.3 are coalescing factors that collapse the characteristic curves of MTBE and TCE onto the hydrocarbon standard curve. The γ_{lw} values for MTBE and TCE on each carbon were determined from a regression analysis by minimizing the sum of the squares of the difference between the scaled abscissa values and the hydrocarbon standard curve abscissa values at each experimental V.

Determination of γ_w

Once γ_{lw} was obtained, the corresponding γ_w value for each carbon was determined from equation (11). The values for $\gamma_{l,\ TCE/heptane}$ and $\gamma_{l,\ MTBE/heptane}$ were estimated from parachor as shown in Table 6.2. Table 6.3 summarizes γ_w values that were obtained indirectly from aqueous-phase TCE and MTBE adsorption isotherms. Theoretically, γ_w values derived from TCE isotherm data should be consistent with those derived from MTBE isotherm data. For most adsorbents, the γ_w values estimated from TCE isotherm data closely matched γ_w values estimated from MTBE isotherm data. It

should be noted that γ_w values were less consistent when γ_l was estimated from other methods such as polarizability and molecular connectivity index. Therefore, γ_l was estimated from molecular parachor in this study. For subsequent calculations, γ_w was taken as the average of $\gamma_{w,TCE}$ and $\gamma_{w,MTBE}$ on a given carbon. Table 6.3 shows that γ_w varied from 0.39 on HAW20 to 0.60 on Picazine. For comparison, γ_w values were converted to β_w using benzene as the reference compound. β_w (benzene) values were in the range of 0.070 to 0.11. Wood [2001] showed that range of β_w (benzene) values obtained at high relative humidities (>50%) is in the range of 0.041-0.19, a range that includes the β_w values obtained in this study.

As indicated in Tables 2.4 and 6.3, γ_w values increase with increasing adsorbent oxygen content. Water adsorption is initiated by hydrogen bonding of water molecules onto specific adsorption sites on activated carbon [e. g. Salame and Bandosz 1999]. These adsorption sites represent oxygen-containing functional groups that are located at the edges of the micro-crystallite building blocks of activated carbon. However, water adsorption may also occur on other heteroatoms, such as nitrogen or inorganic species in ash. Therefore, the adsorbent polarity can be expressed in a variety of formats, such as mmol O/g carbon, mmol O/g carbon [daf] (daf represents dry ash-free activated carbon), mmol (O+N)/g carbon, etc. The results below showed that the polarity expressed as mmol O/g carbon [daf] resulted in the best prediction of micropollutant adsorption from the aqueous-phase. Figure 6.4 shows the correlation developed between γ_w and adsorbent polarity. Adsorbent polarity, correlated well with $\gamma_{w,}$ explaining over 95% of the variance in the data:

$$\gamma_w = 0.0193*P+0.3895 \qquad (r^2 = 0.950) \qquad (12)$$

where P is the adsorbent polarity expressed as mmol O/g carbon [daf].

Equation (12) yields an extrapolated γ_w value of 0.39 (β_w (C_6H_6) =0.0711) when oxygen content is zero, which is reasonably close to the reported β_w (C_6H_6) value of 0.063 derived by Dubinin-Astakhov (DA) equation from activated carbons with very small amounts of surface oxygen [Lodewyckx and Vansant 1999].

A variety of oxygen containing functional groups such as phenolic, lactonic, carboxylic, hydroxyl and carbonyl groups can be present on the carbon surface. The results in Figure 6.4 and equation (12) show that changes in γ_w correlate with the total oxygen content of the ash-free adsorbent, which indicated that the water/adsorbent interaction is roughly independent of the type of surface oxygen groups. Although no direct correlation between γ_w (or β_w) and surface functional groups has been developed to date, several studies [Barton 1994, Stoeckli and Lavanchy 2000] have established a correlation between ΔH (H_2O) (enthalpies of immersion in water) and the total oxygen content of activated carbons. Barton et al. [1994] showed ΔH (H_2O) was linearly correlated with the total concentration of surface oxides (mmol [O]/g Carbon), which were measured by temperature programmed desorption (TPD). Furthermore, they indicted that there is a 1:1 relationship between the total concentration of surface oxides and the number of primary and secondary adsorption sites on the carbon surface. This 1:1 relationship implied that the interactions between water and oxygen containing functional groups is essentially independent of the chemical groups (phenolic, carboxylic, carbonyl, etc.) in which the oxygen atom is incorporated. Based on the ΔH (H_2O) values of 15 activated carbons oxidized to different degrees, Stoeckli and Lavanchy [2000] recently indicated that the ΔH $(H_2O)_{spec}$ (enthalpy of immersion due to specific interactions) is a

function of [O] + [HCl], where [O] is the sum of surface oxygen (mmol/g Carbon, measured by TPD) and [HCl] represents the concentrations of basic sites on carbon surface. According to Stoeckli and Lavanchy [2000], basic sites were introduced into the correlation because they can be titrated so they are also likely capable of interacting with water. However, as indicated by Stoeckli and Lavanchy [2000], the bulk of the specific interactions was still due to interactions with oxygen atoms. The results of these studies support why only one variable (adsorbent polarity as expressed by the total oxygen content per gram of adsorbent [daf]) was needed to describe the variability in γ_w among the tested adsorbents. Equation (12) therefore provides a practical approach to estimate coalescing (or affinity coefficients) factors for water adsorption on activated carbons.

As indicated in Table 6.3 and equation (12), the higher the adsorbent oxygen content, the larger the value of γ_w. The general accepted mechanism of water vapor adsorption includes the following steps: (1) water adsorption on specific adsorption sites; (2) each adsorbed water molecule is then a secondary adsorption center, which is also capable of forming hydrogen bonds with other water molecules and results in the creation of water clusters; and (3) pore filling occurs until all pores are filled [Salame and Bandosz 1999]. Water clusters, which formed through the enhanced water adsorption on polar surface functional groups, can block micropollutant access to adsorption sites. This explains why a hydrophobic adsorbent with less polar surface groups is desirable for the removal of both hydrophobic and hydrophilic adsorbates from water (Chapters 4 and 5).

6.4.3. Model Validation

Based on the developed relationship between the coalescing factor for water adsorption, γ_w, and adsorbent polarity, the value of γ_w for an activated carbon can be predicted from equation (12) if the oxygen and ash contents of the adsorbent have been experimentally determined. After the estimation of γ_l for a target adsorbate from its molecular parachor, the aqueous phase coalescing factor γ_{lw} of a micropollutant can be estimated from equation (8). The isotherm of the target micropollutant can then be predicted by scaling the abscissa values of the hydrocarbon standard curve. This method represents a practical approach to predict the adsorption of trace organic compounds from aqueous solution.

To test the validity of the developed approach, the adsorption of MTBE and TCE on two relatively hydrophobic GACs, G219 and F600, and a relatively hydrophilic ACF, OAW15, were predicted. The experimental and predicted isotherms are compared in Figures 6.5 to 6.7. For clarity, the figures were plotted in the traditional isotherm format with C/C_s as the abscissa and the equilibrium solid-phase concentration (q_e) as the ordinate. For OAW15 and G219, the experimental data closely matched the model prediction (Figures 6.5 and 6.6). For F600, the predicted TCE isotherm agreed well with the experimental data, while the model overpredicted the MTBE adsorption capacity by a factor of 2 at the large liquid phase concentration (Figure 6.7).

Furthermore, the model was tested to predict the adsorption capacities of *cis*-1, 2-dichloroethene (*cis*-DCE) and tetrachloroethene (PCE), two adsorbates that were not used for calibrating the model. The γ_l values (calculated from their parachors) of *cis*-DCE and

PCE are listed in Table 6.2. The experimental and predicted isotherms on GAC F600 and G219 are presented in Figures 6.8 and 6.9, respectively. Because of the uncertainty in the documented DCE solubility, the experimental isotherm data of DCE were normalized using a typical solubility value (3500 mg/L) as well as the highest and lowest reported solubility values (Table 6.2). Predicted PCE adsorption capacities agreed well with the experimentally determined values on the two commercial GACs. For DCE, a discrepancy between experimental data and predicted adsorption capacities was observed if a typical C_s (3500 mg/L) was used to normalize the experimental DCE isotherm data (at $C/C_s = 5*10^{-5}$, predicted adsorption capacities for both F600 and G219 were about 35% lower than experimentally determined adsorption capacities). However, the predicted isotherm fell within the bounds of the experimental isotherm when upper (7700mg/L) and lower (800mg/L) estimates of the aqueous DCE solubility [Mackay et al. 1992] were used to normalize experimentally determined equilibrium liquid-phase concentrations.

The results presented in Figures 6.5 to 6.9 illustrated that the PPT is useful for predicting the aqueous phase adsorption capacities of trace organic contaminants on different adsorbents once the dependence of γ_w on adsorbent polarity was known. Over the past decades, several quantitative structural activity relationship (QSAR) models (i.e. correlations involving Linear Solvation Energy Relationships, Octanol-Water Partition Coefficients and Molecular Connectivity Indexes) have been developed to predict the adsorption of organic chemicals on activated carbon [Blum et al. 1994, Brasquet and Lecloirec 1999 a and b]. QSAR correlations are capable of effectively predicting a single adsorption capacity descriptor, such as the Freundlich isotherm constant K, or the slope of the isotherm at the lowest concentration tested ($(X/C)_{min}$). In contrast, the PPT permits

the prediction of an entire isotherm instead of a single point. Hence, the PPT, in conjunction with the developed correlation between γ_w and adsorbent polarity, represents a more powerful predictive tool.

6.4.4. Sensitivity Analysis

To determine the sensitivity of the PPT to uncertainty related to the estimates of γ_w and $\gamma_{l,}$ a sensitivity analysis was conducted. Figure 6.10 shows that MTBE and TCE adsorption capacities on OAW15 differed greatly from the experimental data when the predicted γ_w values increased or decreased by 10%. For example, when γ_w increased by 10%, the predicted TCE adsorption capacity decreased by 50.7% and the predicted MTBE adsorption capacity decreased by 67.0%. When γ_w decreased by 10%, the predicted TCE adsorption capacity increased by 80.0% and the predicted MTBE adsorption capacity increased by 139.4% (all comparisons were made at $C/C_s = 10^{-5}$). A similar sensitivity to γ_w was observed for a more hydrophobic adsorbent (G219). The sensitivity of trace micropollutant adsorption capacities to γ_w implies that it is not appropriate to treat the coalescing factor for water adsorption as a constant when adsorbents with different surface chemistry are compared, as was done in prior studies [Arbuckle 1980, Aytekin 1991]. The results confirmed the necessity to incorporate the adsorbent surface chemistry effects into the Polanyi-Manes approach, when predictions for adsorbents with different surface chemistries are desired.

Similarly, the sensitivity of the model to γ_l was tested, and results for OAW15 are summarized in Figure 6.11. When γ_l values varied by 10% from the values estimated from parachor, the predicted isotherms shifted dramatically from the baseline predictions

and the experimental curves. When γ_l increased by 10%, the predicted TCE adsorption capacity increased by 222.0% and the predicted MTBE adsorption capacity increased by 416.5%. When γ_l decreased by 10%, the predicted TCE adsorption capacity decreased by 79.4% and the predicted MTBE adsorption capacity decreased by 88.4%. (All comparisons were made at $C/C_s = 10^{-5}$). These results indicate that the prediction of aqueous-phase adsorption capacities by the PPT is very sensitive to changes in both γ_w and γ_l. Therefore, proper estimation of γ_w and γ_l are essential when the PPT is used to predict the adsorption of trace organic compounds from aqueous solution on activated carbons with a range of surface chemistries.

6.5. Conclusions

To estimate the adsorption capacities of micropollutants from water, a prediction procedure based on the Polanyi Potential Theory was developed and validated. The following conclusions were drawn:

(1) As a conventional characterization method for activated carbon porosity, N_2 adsorption isotherm data at 77K and CO_2 adsorption isotherm data at 273K can not only provide information about the pore volume and pore size distribution of a given adsorbent, but they can also serve as a basis for developing a hydrocarbon standard curve for a given adsorbent.

(2) The coalescing factor for water (γ_w) increases with the adsorbent polarity as expressed by the oxygen content per unit mass of dry, ash-free carbon. This result is consistent with the observation that enhanced water adsorption at oxygen-containing functional groups on activated carbon surfaces. For the first time, a simple, one variable

(adsorbent polarity) correlation was developed to predict γ_w for a range of adsorbents with different oxygen contents.

(3) Coalescing factors for organic adsorbates γ_l can be predicted from adsorbate molar volume and parachor.

(4) The prediction of aqueous-phase adsorption capacities by the Polanyi Potential Theory is very sensitive to changes in both γ_w and γ_l. The prediction of aqueous-phase adsorption capacities therefore depends on the proper estimation of both γ_l and γ_w.

(5) The developed model can appropriately predict the aqueous-phase adsorption of both relatively polar and non-polar adsorbates on both relatively hydrophobic and hydrophilic activated carbons.

6.6. References

Abe, I and Hirashima, T. The Relationship Between Activated Carbon Adsorption and Water Quality Indexes. Water Research 1985; 19: 1191-1193.

Arbuckle, WB. Estimating Equilibrium Adsorption of organic Compounds on Activated Carbon from Aqueous Solution. Environmental Science and Technology 1980; 15(7): 812-819.

Aytekin C. Application of the Polanyi Adsorption Potential-Theory to Adsorption Phenolic-Compounds from Water Solution onto Activated Carbon. Spectroscopy Letters 1991; 24 (5): 653-664.

Barton SS, Evans MJB and Macdonald JAF. Adsorption of Water Vapor on Nonporous Carbon. Langmuir 1994; 10: 4250-4252.

Blum DJW, Suffet IH and Duguet JP Quantitative Structure-Activity Relationship Using Molecular Connectivity for the Activated Carbon Adsorption of Organic Chemicals in Water. Water Research 1994; 28(3): 687-699

Brasquet C and Lecloirec P Effects of Activated Carbon Cloth Surface on Organic Adsorption in Aqueous Solutions. Use of Statistical Methods to Describe Mechanisms. Langmuir 1999; 15(18): 5906-5912

Brune BJ, Payne, GF and Chaubal MV, Linear Solvation Energy Relationships to Explain Interactions Responsible for Solute Adsorption onto a Polar Polymeric Sorbent. Langmuir 1997; 13(21): 5766-5769.

Burg P, Fydrych P, Abraham MH, Matt M and Gruber R. The Characterization of an Active Carbon in term of Selectivity towards Volatile Organic Compounds Using an LSER Approach. Fuel 2000; 79(9):1041-1045.

Cazorla-Amoros D, Alcaniz- Monge J, and Linares-Solano, A. Characterization of Activated Carbon Fibers by CO_2 Adsorption. Langmuir 1998; 12: 2820-2824

Cazorla-Amoros D, Alcaniz- Monge J, Casa-Lillo MA, Linares-Solano, A. CO_2 as an Asorptive to Characterize Carbon Molecular Sieves and Activated Carbons. Langmuir 1998; 14: 4589-4596.

Crittenden JC, Sanongraj S, Bulloch J, Hand DW, Rogers TN, Speth TF and Ulmer Markus. Correlation of Aqueous-phase Adsorption Isotherms. Environmental Science and Technology 1999; 33(17): 2926.

Dubinin MM. The Potential Theory of Adsorption of Gases and Vapors for Adsorbents with Energetically Nonuniform Surface. Chem. Revs., 1960, 60(235): 235-241.

Grant RJ and Manes M. Correlation of Some Gas Adsorption Data Extending to Low Pressures and Supercritical Temperatures. I&EC Fundamentals 1964; 3(3): 221-224.

Grant RJ, Manes M and Smith SB. Adsorption of Normal Paraffins and Sulfur Compounds on Activated Carbon. A. I. Ch. E. Journal 1962; 8(3): 403-406.

Holland, CE, Muhtaseb, SA and Titter JA. Adsorption of C1-C7 Normal Alkanes on BAX Activated Carbon Ind. Eng. Chem. Research 2001, 40: 338-346.

Kuennen RW, Dyke KV, Crittenden JC and Hand DW. Predicting the Multicomponent Removal of Surrogate Compounds by a Fixed-bed Adsorber. Journal American Water Works Association 1989; 81(12): 46-58.

Lee TV, Huang JC, Rothstein D and Madey, R. Correlation of Adsorption Isotherms of Hydrocarbon Gases on Activated Carbon. Carbon 1984, 22(6): 493-499.

Lodewyckx P and Vansant EF Water isotherms of activated carbons with small amounts of surface oxygen. Carbon, 1999; 37: 1647-1649.

Lopez-Ramon MV, Stoeckli F, Moreno-Castilla C and Carrasco-Martin F. Specific and Nonspecific Interactions between Methanol and Ethanol and Active Carbons. Langmuir 2000; 16: 5967-5972.

Lu X, Jaroniec M and Madey R. Use of Adsorption Isotherm of Light Normal Alkanes for Characterizing Microporous Activated Carbons. Langmuir 1991; 7: 173-177.

Mackay D, Shiu WY and Ma CK. Illustrated Handbook of Physical-Chemical Properties and Environmental Fate for Organic Chemicals. Volume 3, Boca Raton, Lewis Publishers, 1992

Manes M. Activated Carbon Adsorption Fundamentals in “Encyclopedia of Environmental Analysis and Remediation”. 1998; Editor: Meyers, RA. John Wiley & Sons Inc. NY.

Manes M, Hofer LJE. Application of Polanyi Adsorption Potential Theory to Adsorption from Solution on Activated Carbon Journal of Physical Chemistry 1969; 73 (3): 584.

Nirmalakhandan NN and Speece RE Prediction of Activated Carbon Adsorption Capacities for Organic Vapors Using Quantitative Structure Activity Relationship. Environ. Sci. Technol. 1993; 27: 1512-1516.

Phillips J, Kelly D, Radovic L and Xie F. Micrcalorimetric Study of the Influence of Surface Chemistry on the Adsorption of Water by High Surface Area Carbons Journal of Physical Chemistry 2000; 104 (34): 8170-8176.

Prakash J, Nirmalakhandan NN and Speece RE Prediction of Activated Carbon Adsorption Isotherms for Organic. Environ. Sci. Technol. 1994; 28: 1403-1409.

Qi S, Hay KJ, Rood, MR and Cal MP. Carbon Fiber Adsorption Using Quantitative Structure Activity Relationship. Journal of Environmental Engineering 2000; 9: 865-868.

Salame II and Bandosz TJ. Experimental study of water adsorption on activated carbons. Langmuir 1999; 15 (2): 587-593.

Speth, TF. Prediction Equilibrium for Single Solute and Multicomponent Aqueous-Phase Adsorption onto Activated Carbon. Ms. Thesis, 1986; Michigan Technological University.

Stoeckli F and Lavanchy A. The adsorption of Water by Activated Carbons, in Relation to Their Chemical and Structural Properties. Carbon 2000; 38: 475-494.

Tamon H and Okazaki M. Influence of Acidic Surface Oxides of Activated Carbon on Gas Adsorption Characteristics. Carbon 1996; 34(6): 741-746.

Wohleber DA and Manes M Application of the Polanyi Adsorption Potential Theory to Adsorption from Solution on Activated Carbon. Journal of Physical Chemistry 1971; 75(1): 61-64.

Wood GO. Affinity coefficients of the Polanyi/Dubinin Adsorption Isotherm Equations , A Review with Complications and Correlations. Carbon 2001; 39: 343-356.

6.7. Tables

Table 6.1. Gaseous Adsorbate Properties

Adsorbate	P_s [a] (atm)	V_m [b] (cm^3/mol)	$\beta_{adsorbate/benzene}$ [c]	$\gamma_{l,\ adsorbate/heptane}$ [d]
N_2	1	34.65	0.33	0.940
CO_2	34.28 [e]	43.01	0.40	0.918
Heptane	N/A	144.18	1.46	1.000

[a] P_s: saturation pressure at adsorption temperature (77 K for N_2, 273 K for CO_2)
[b] V_m: molar volume in adsorbed state, calculated from ρ = 0.808 g/cm^3 for N_2 at 77 K and ρ = 1.023 g/cm^3 for CO_2 at 273 K [Cazorla-Amoros et al. 1998]; calculated with ChemSketch v. 4.55 for heptane at 298 K
[c] $\beta_{adsorbate/benzene}$: affinity coefficients [Dubinin 1960, Lopez-Ramon et al. 2000]
[d] calculated: $\gamma_l = (\beta_{adsorbate/benzene}/\beta_{heptane/benzene})*(V_{m,\ heptane}/V_{m,\ adsorbate})$
[e] calculated from Clausius-Clapeyron equation
N/A: not applied

Table 6.2. Liquid Adsorbate Properties

Adsorbate	C_s [a] (mg/L)	V_m [b] (cm^3/mol)	Ω [c]	$\gamma_{l,\ adsorbate/heptane}$ [d]
heptane	N/A	144.2	310.6	1.000
MTBE	51,000 [e]	117.5	245.8	0.971
PCE	150	100.3	245.0	1.1336
TCE	1,100	89.1	210.4	1.096
cis-1,2-DCE	3,500 [f]	77.9	175.8	1.0463

[a] C_s: aqueous solubility at adsorption temperature, from Mackay et al. [1992]
[b] V_m: molar volume in adsorbed state, calculated from ChemSketch v. 4.55 (at 298K)
[c] Ω: parachor calculated from ChemSketch v. 4.55
[d] calculated: $\gamma_l = (\Omega_{adsorbate}/\Omega_{heptane})*(V_{m,\ heptane}/V_{m,\ adsorbate})$
[e] range: 23186 to 54353 mg/L [Mackay et al. 1992]
[f] range: 800 to 7700 mg/L [Mackay et al. 1992]
N/A: not applied

Table 6.3. Calculated γ_{lw} and γ_w values for ACFs and GAC[a]

Carbon	$\gamma_{lw,\ adsorbate/heptane}$		$\gamma_{w/heptane}$			$\beta_{w/benzene}$
	Adsorbate = MTBE	Adsorbate = TCE	From $\gamma_{lw,\ MTBE}$	From $\gamma_{lw,\ TCE}$	Average	
AW10	0.4907	0.6896	0.4801	0.4061	0.4431	0.0809
AW15	0.5502	0.6733	0.4206	0.4224	0.4215	0.0770
AW20	0.5503	0.6686	0.4205	0.4271	0.4238	0.0774
OAW10	0.4413	0.5774	0.5295	0.5183	0.5239	0.0957
OAW20	0.4987	0.5994	0.4721	0.4963	0.4842	0.0884
HAW10	0.5058	0.7011	0.4650	0.3946	0.4298	0.0785
HAW15	0.5727	0.6836	0.3981	0.4121	0.4051	0.0740
HAW20	0.5863	0.6980	0.3845	0.3977	0.3911	0.0714
AAW10	0.5122	0.6778	0.4586	0.4179	0.4383	0.0800
AAW15	0.5654	0.6838	0.4054	0.4119	0.4087	0.0746
AAW20	0.5621	0.6760	0.4088	0.4197	0.4142	0.0757
Picazine	0.4196	0.4495	0.5512	0.6462	0.5987	0.1093

[a] ACF OAW15 and GACs F600 and G219 were reserved for prediction.

6.8. Figures

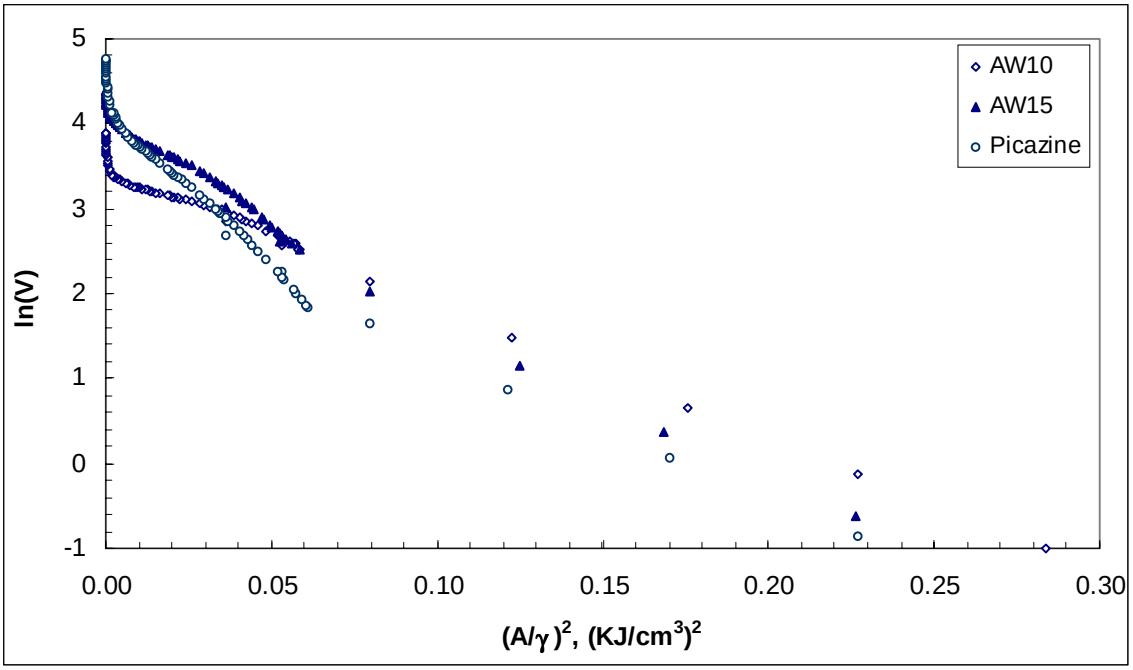

Figure 6.1. N_2 and CO_2 adsorption on ACFs and GACs

γ values are shown in Table 6.1.
Units of V are cm^3 [liquid]/100g

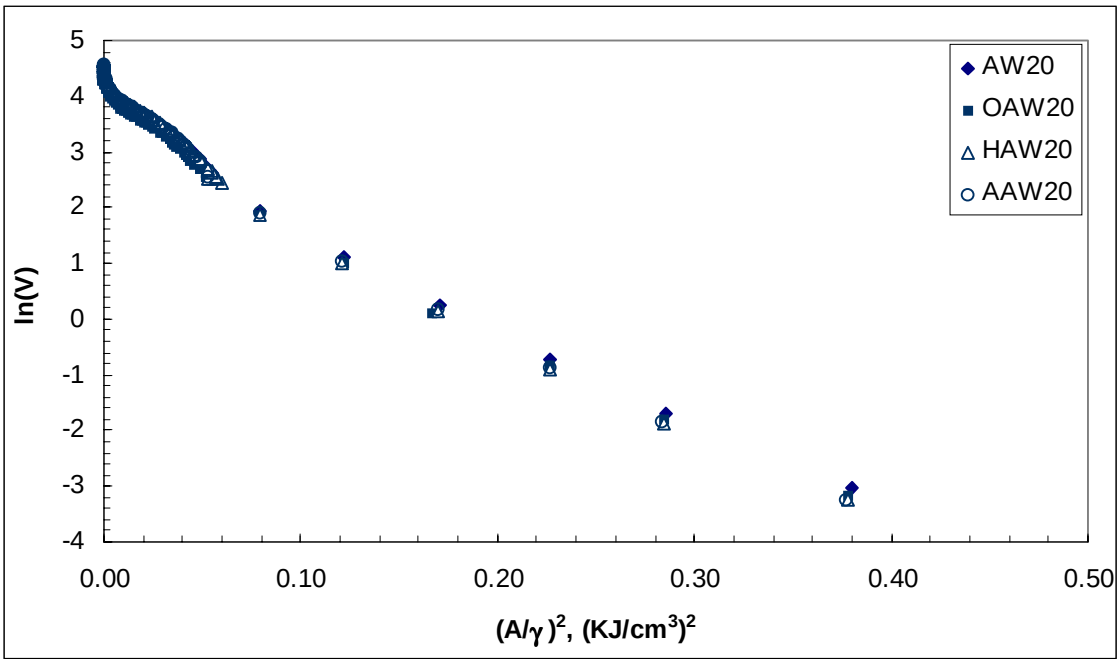

Figure 6.2. N_2 and CO_2 adsorption on ACF20s

γ values are shown in Table 6.1.
Units of V are cm^3 [liquid]/100g

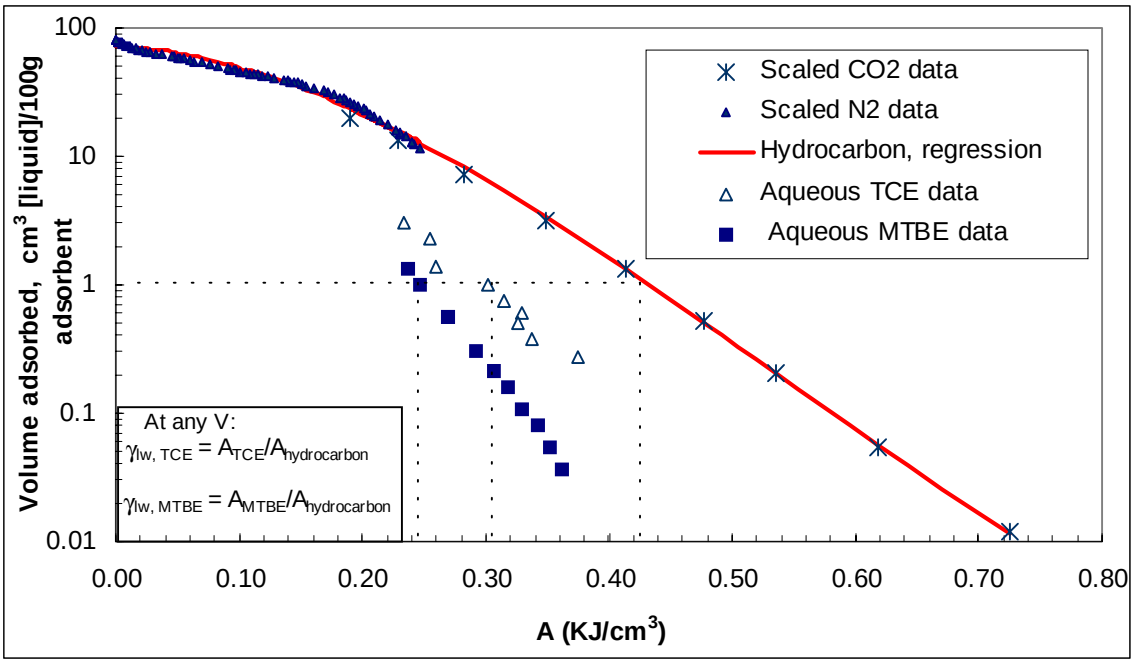

Figure 6.3. Determination of heptane adsorption characteristic curve and γ_{lw} on HAW15

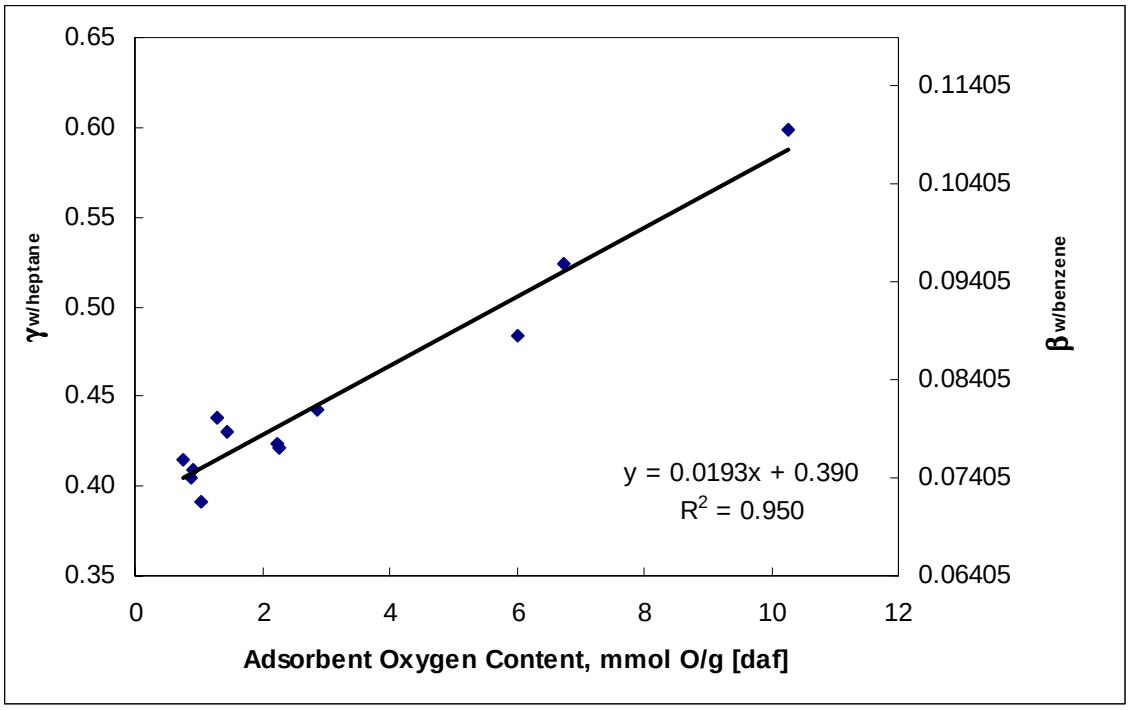

Figure 6.4. Correlation between adsorbent polarity and γ_w (β_w)

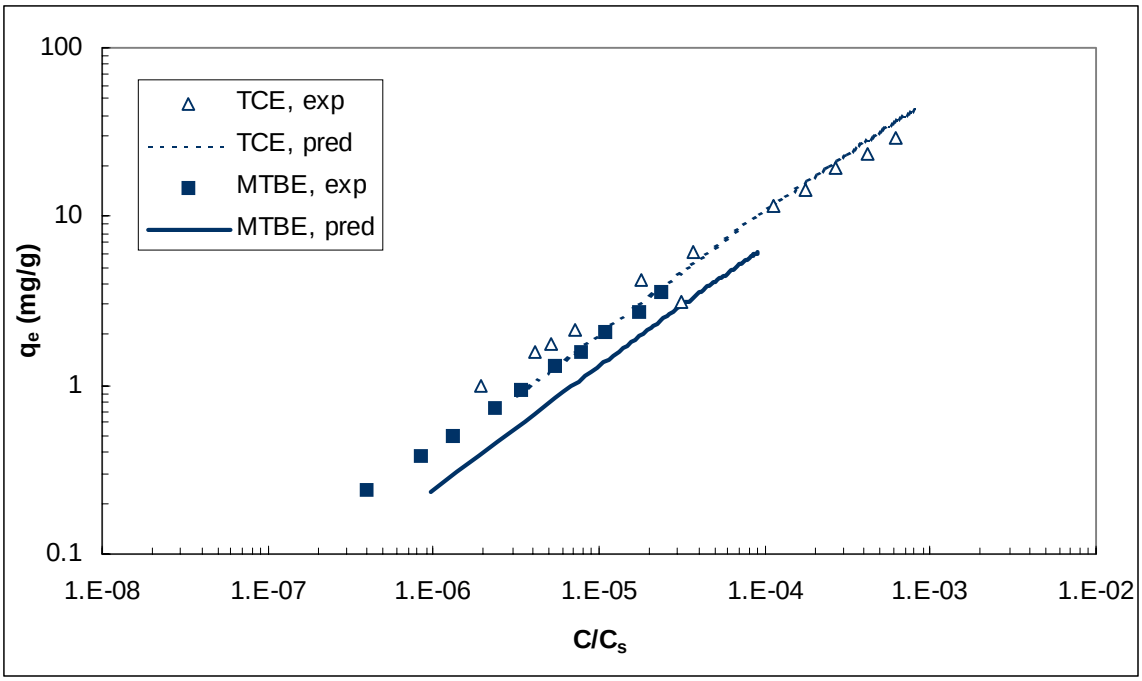

Figure 6.5. Prediction of MTBE and TCE adsorption in water on OAW15

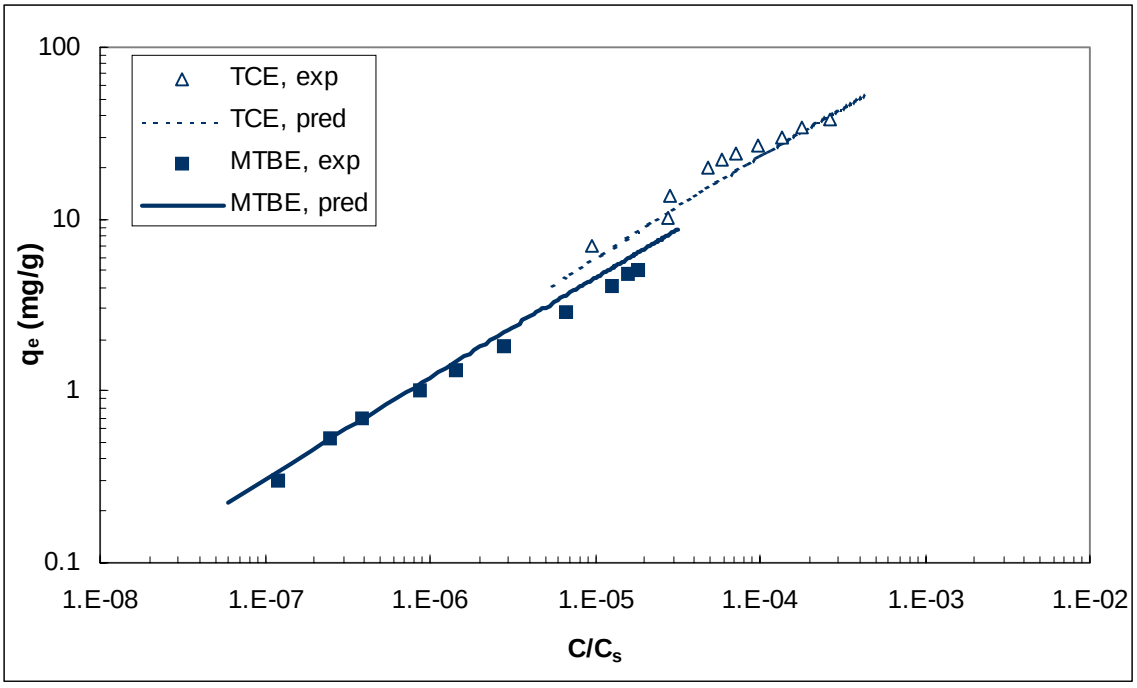

Figure 6.6. Prediction of MTBE and TCE adsorption in water on G219

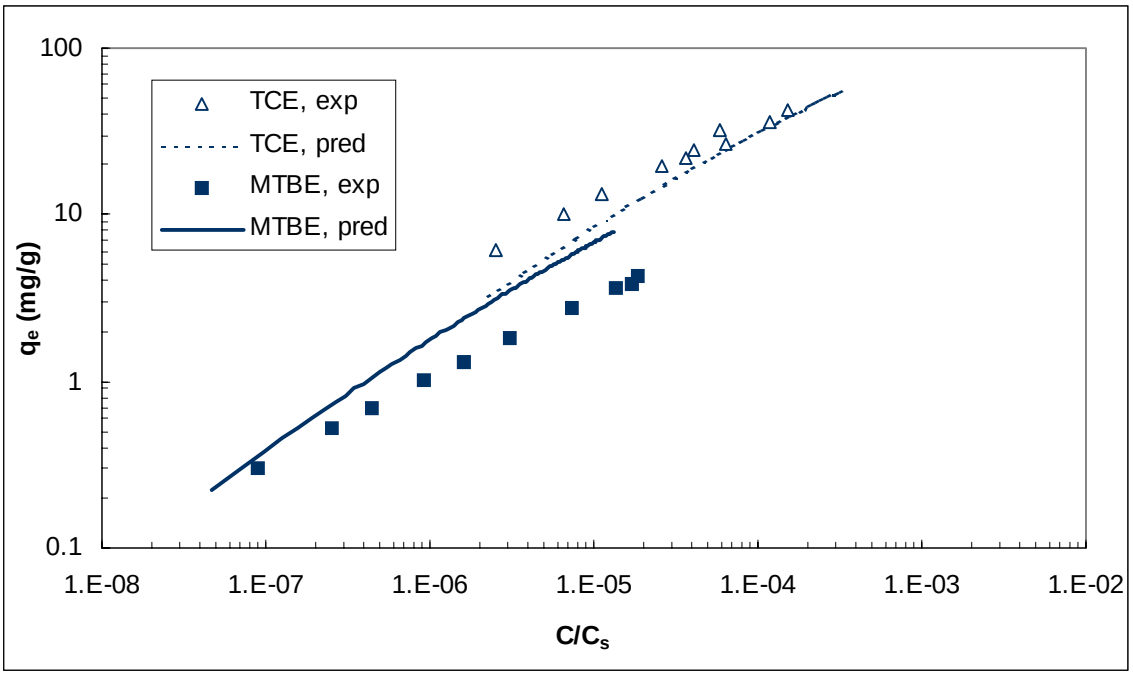

Figure 6.7. Prediction of MTBE and TCE adsorption in water on F600

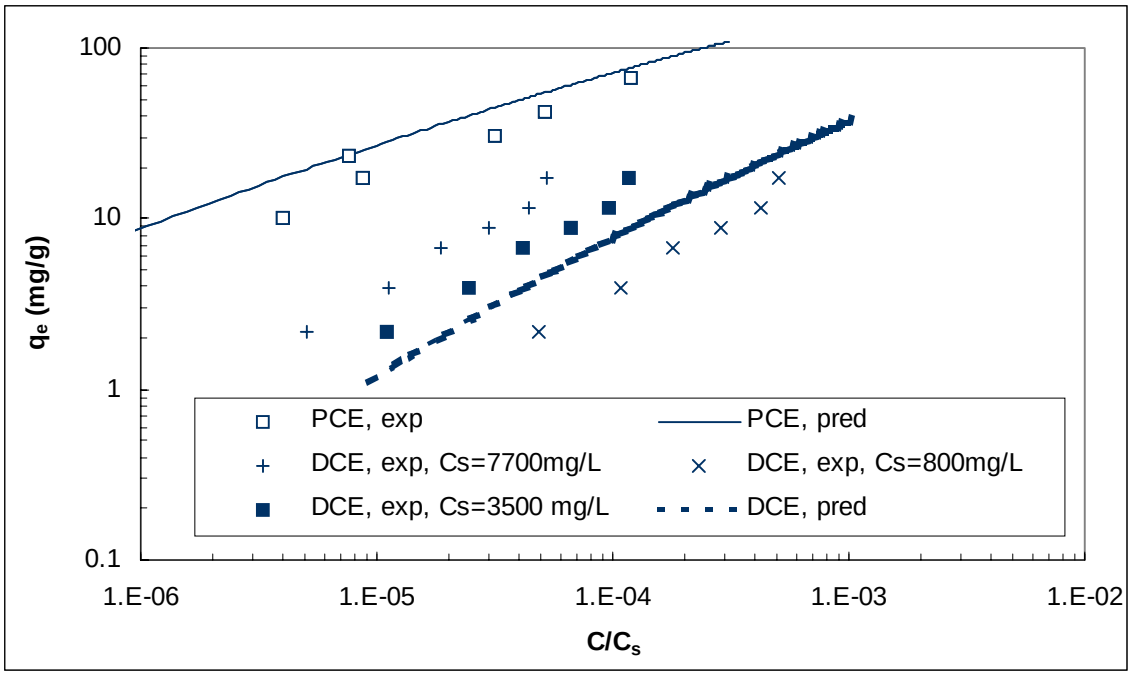

Figure 6.8. Prediction of 1,2-cis DCE and PCE adsorption in water on F600

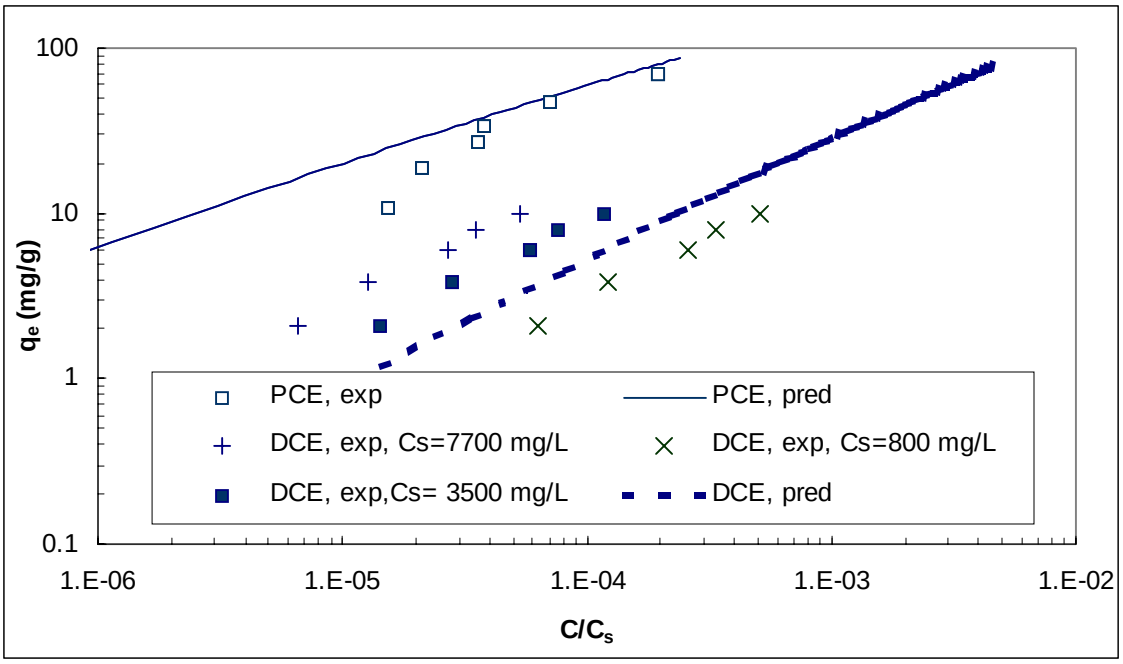

Figure 6.9. Prediction of 1,2-cis DCE and PCE adsorption in water on G219

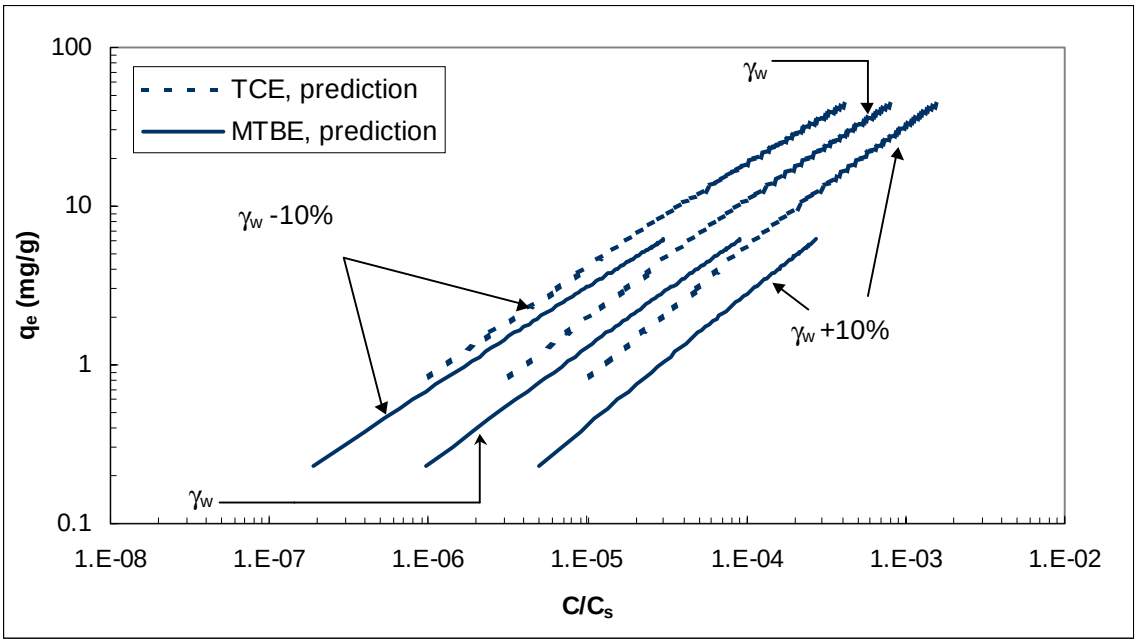

Figure 6.10. Sensitivity of PPT model predictions to γ_w (OAW15)

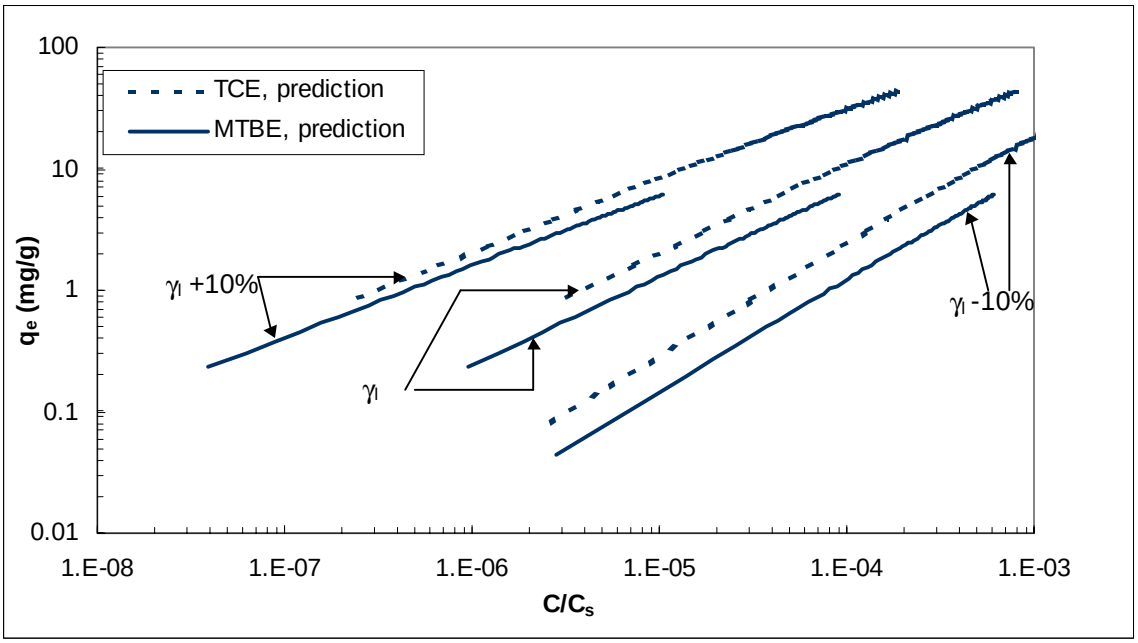

Figure 6.11. Sensitivity of PPT model predictions to γ_l (OAW15)

Chapter 7. Conclusions and Recommendations

Conclusions

A wide array of activated carbons are marketed by numerous manufacturers, and water treatment professionals face the challenge to select the most economical adsorbent for a given water quality problem. One objective of this research was, therefore, to develop activated carbon selection criteria that assure the effective removal of trace organic contaminants from drinking water sources. A second objective was to develop a procedure with which the aqueous-phase adsorption capacity of a given activated carbon for a given target micropollutant can be predicted from fundamental adsorbent and adsorbate properties and which therefore would eliminate the need for costly experimental studies.

The adsorbents used in this study were an activated carbon fiber (ACF) matrix and three commercially available GACs. The ACF matrix was prepared by surface chemical treatments (acid washing, oxidation, hydrogen-treatment, and ammonia-treatment) of as-received ACFs. The results from elemental analysis, mass titration and infrared spectroscopy indicated that a given chemical treatment yielded ACFs with similar heteroatom content and surface acidity/basicity, which permitted the study of pore structure effects on micropollutant adsorption with little interference from surface chemistry effects. Furthermore, density functional theory (DFT) results indicated that chemical modifications had no noticeable effects on pore size distributions, which allowed the evaluation of surface chemistry effects on micropollutant adsorption in the absence of pore size effects.

The relatively hydrophilic fuel oxygenate methyl tertiary-butyl ether (MTBE) and the relatively hydrophobic chlorinated solvent trichloroethene (TCE), two common drinking water contaminants, served as adsorbate probes. Isotherm experiments were performed in both ultrapure water and natural water (Sacramento-San Joaquin Delta water). The aqueous-phase adsorption capacities were correlated with adsorbent surface chemistry and pore structure. With respect to pore size, the correlations showed that relatively small changes in the micropore size distribution of an adsorbent (e.g. 7-11 Å widths in ACF 10 versus 9-13 Å widths in ACFs 15 and 20) can alter the effectiveness of an adsorbent for a given micropollutant. Similarly, small differences in the kinetic diameters among individual target adsorbates (e.g. 5.6 Å for TCE vs. 6.2 Å for MTBE) affect the choice of the most effective adsorbent. With respect to the hydrophobicity of activated carbons, the correlations showed that for carbons with similar pore size distributions, hydrophobic carbons, i.e., carbons with low oxygen and nitrogen contents, are most effective for the removal of both hydrophobic (e.g. TCE) and hydrophilic (e.g. MTBE) trace organics from natural water. This could be explained by the preferential adsorption of water on polar surface functional groups. Therefore, to optimize the activated carbon selection process, water treatment utilities need to consider (1) the size of the targeted pollutant, (2) the pore size distribution of the activated carbon, and (3) the hydrophobicity of the activated carbon. The results of this research also verified that iodine number and BET surface area, two commonly used selection criteria, did not correlate with MTBE and TCE adsorption capacities.

In summary, the results obtained in this study showed that an effective adsorbent for the removal of micropollutants from water requires

(1) a large volume of micropores with widths that are about 1.5 times larger than the kinetic diameter of the target adsorbate,

(2) a micropore size distribution that extends to widths that are approximately twice the kinetic diameter of the target adsorbate to prevent pore blockage by NOM, and

(3) a hydrophobic pore surface chemistry which, when expressed as the sum of the oxygen and nitrogen contents, should not exceed 2 to 3 mmol/g.

In addition, a prediction tool based on the Polanyi Potential Theory (PPT) was developed with which activated carbon adsorption capacities can be estimated from fundamental adsorbent and adsorbate properties. For the first time, a quantitative relationship between the coalescing factor for water (γ_w) and activated carbon polarity was established, and the results indicated that γ_w increased with adsorbent polarity. This trend is consistent with enhanced water adsorption on polar surface functional groups. A sensitivity analysis indicated that the prediction of the aqueous-phase adsorption isotherm for a given adsorbate/activated carbon pair depends on the proper estimation of the vapor phase adsorbate coalescing factor γ_l and the water adsorption coalescing factor $\gamma_{w.}$ The model developed in this study can be used to predict aqueous-phase adsorption isotherms for both relatively polar and non-polar organic liquids that are partially miscible in water on both relatively hydrophobic and hydrophilic activated carbons.

Overall, the PPT-based prediction tool requires the following information to estimate the aqueous-phase adsorption isotherm for a given adsorbate/adsorbent system:

(1) an N_2 adsorption isotherm at 77 K and a CO_2 adsorption isotherm at 273 K to develop the hydrocarbon standard curve for a given adsorbent,

(2) the oxygen and ash contents of the adsorbent, and

(3) the liquid molar volume and the molecular parachor of the target adsorbate.

Compared to the selection criteria presented above, the advantage of this prediction tool is that it is easy to apply and does not require the determination of pore size distributions.

Recommendations

While this research conclusively showed that the pore size distribution (PSD) of an activated carbon affects the adsorption of micropollutants from drinking water, it has to be realized that the determination of PSDs is still an inexact science. The density functional theory (DFT) allows the calculation of PSDs from gas adsorption isotherm data. However, inconsistent results, which are related to the different adsorbate gases and DFT kernels, are often obtained. A standard method for determining micropore size distributions, is therefore urgently needed before water treatment professionals can compare micropore size distributions from different sources in a reliable manner.

Furthermore, the results of this study showed that aqueous-phase adsorption capacities are strongly affected by adsorbent polarity. The oxygen content of an adsorbent can be obtained from elemental analysis or other methods (e.g., temperature-programmed desorption). However, these methods can not determine whether the oxygen is associated with the activated carbon surface, the bulk carbon, or ash, and reliable methods for the identification and quantification of surface oxygen groups in activated carbon micropores are still lacking. Therefore, the activated carbon selection criteria and the prediction tool established in this study are only applicable to low-ash adsorbents at this point. In terms of future research, the results of this study illustrate that improved

techniques for the determination of micropore size distributions and activated carbon surface chemistry need to be developed to improve the performance prediction of activated carbons from fundamental adsorbent properties.

.

Appendix

N_2 adsorption isotherms

AW10

P/Po	cc/gCarbon	P/Po	cc/gCarbon
5.07E-06	80.36181818	1.31E-02	170.7743802
5.40E-06	80.49719008	1.67E-02	173.3570248
5.71E-06	86.12975207	2.14E-02	176.0305785
6.14E-06	86.49669421	3.12E-02	179.2586777
7.02E-06	87.91570248	4.17E-02	181.8942149
7.71E-06	89.20165289	5.23E-02	184.2082645
9.16E-06	91.80661157	6.20E-02	186.3719008
1.03E-05	93.75371901	7.23E-02	188.253719
1.52E-05	100.3727273	8.25E-02	189.9421488
2.03E-05	105.4520661	9.25E-02	191.6280992
2.52E-05	109.2066116	1.02E-01	193.5917355
3.03E-05	112.3471074	1.50E-01	200.6545455
3.53E-05	114.8818182	2.01E-01	207.5859504
4.07E-05	117.2545455	2.50E-01	214.7429752
5.03E-05	120.5520661	3.01E-01	221.3719008
6.10E-05	123.3983471	3.51E-01	228.1
7.02E-05	125.4107438	4.03E-01	237.1214876
8.12E-05	127.4157025	4.51E-01	243.2958678
9.12E-05	128.9247934	5.01E-01	249.6363636
9.97E-05	130.0553719	5.51E-01	256.1289256
1.33E-04	133.2834711	6.01E-01	262.2859504
1.74E-04	136.1347107	6.51E-01	268.4743802
2.04E-04	137.761157	7.02E-01	278.4553719
3.02E-04	141.3975207	7.60E-01	285.6785124
4.10E-04	144.0677686	8.01E-01	290.8016529
5.12E-04	145.953719	8.51E-01	297.0694215
6.10E-04	147.4123967	9.01E-01	303.5446281
7.15E-04	148.7247934	9.46E-01	309.4090909
8.05E-04	149.6917355	9.68E-01	316.1380165
9.10E-04	150.6900826	9.74E-01	316.546281
1.01E-03	151.6297521	9.97E-01	319.861157
1.53E-03	154.846281		
2.02E-03	156.961157		
2.58E-03	158.8859504		
3.01E-03	160.0652893		
3.54E-03	161.3024793		
4.08E-03	162.4347107		
5.06E-03	164.0834711		
6.18E-03	165.6338843		
7.08E-03	166.6768595		
8.05E-03	167.7181818		
9.15E-03	168.7115702		

AW15

P/Po	cc/gCarbon	P/Po	cc/gCarbon
4.93E-06	80.29027778	7.18E-03	289.4537037
6.61E-06	87.24175926	8.14E-03	292.6546296
7.79E-06	91.21851852	9.23E-03	295.8592593
8.71E-06	94.46944444	1.14E-02	301.1231481
9.00E-06	95.53518519	1.46E-02	307.9537037
9.71E-06	98.02777778	2.12E-02	318.9324074
1.00E-05	98.84074074	3.10E-02	331.0425926
1.02E-05	99.35833333	4.17E-02	340.8268519
1.22E-05	105.0314815	4.98E-02	346.8361111
1.31E-05	107.3555556	5.97E-02	353.2777778
1.66E-05	115.2435185	7.03E-02	358.8342593
1.73E-05	116.7055556	8.08E-02	363.575
2.42E-05	129.0185185	9.10E-02	367.8351852
2.54E-05	130.7592593	1.01E-01	371.4055556
3.03E-05	137.1435185	1.47E-01	384.4185185
3.55E-05	143.0842593	2.03E-01	395.9898148
4.07E-05	148.0518519	2.50E-01	404.5666667
5.04E-05	155.6555556	3.00E-01	412.887037
6.05E-05	162.2203704	3.49E-01	422.0972222
7.07E-05	167.7861111	4.00E-01	430.2537037
8.06E-05	172.4444444	4.50E-01	437.7416667
9.16E-05	176.9601852	5.00E-01	445.2518519
1.00E-04	180.0231481	5.50E-01	452.4851852
1.32E-04	189.1712963	6.03E-01	462.787037
1.71E-04	197.4527778	6.51E-01	469.4740741
2.01E-04	202.5259259	7.00E-01	476.2888889
3.05E-04	214.5287037	7.51E-01	483.2407407
4.10E-04	222.4898148	8.03E-01	493.8240741
5.11E-04	228.1472222	8.51E-01	500.6269444
6.00E-04	232.1851852	9.00E-01	507.975
7.07E-04	236.1518519	9.50E-01	514.8055556
8.06E-04	239.2462963	9.64E-01	520.4555556
9.14E-04	242.1453704	9.77E-01	522.362963
1.02E-03	244.7537037	9.88E-01	523.6935185
1.53E-03	254.0518519	9.98E-01	518.5185185
2.03E-03	260.3351852		
2.54E-03	265.2564815		
3.01E-03	269.0824074		
3.56E-03	272.8712963		
4.07E-03	275.8703704		
5.08E-03	281.0472222		
6.16E-03	285.7018519		

AW20

P/Po	cc/gCarbon	P/Po	cc/gCarbon
7.32E-06	90.06885246	1.01E-02	323.707377
7.83E-06	93.16721311	1.56E-02	336.6434426
9.78E-06	99.89098361	2.07E-02	348.5295082
1.40E-05	110.8778689	3.00E-02	362.9
1.48E-05	113.0778689	4.06E-02	375.5754098
1.95E-05	122.657377	5.12E-02	385.9434426
2.01E-05	123.9081967	5.96E-02	392.6918033
2.43E-05	130.8598361	7.18E-02	401.25
2.49E-05	131.9672131	8.02E-02	406.1983607
2.93E-05	138.297541	9.01E-02	411.602459
3.49E-05	145.2909836	1.00E-01	416.4459016
3.97E-05	150.3713115	1.51E-01	434.2737705
4.02E-05	151.0254098	2.02E-01	447.4155738
5.01E-05	159.9065574	2.53E-01	458.995082
5.94E-05	166.7795082	3.03E-01	469.3663934
6.05E-05	167.6172131	3.53E-01	480.1885246
7.11E-05	174.1155738	4.00E-01	488.2713115
8.04E-05	179.05	4.49E-01	497.1909836
9.11E-05	183.957377	5.00E-01	505.8868852
1.01E-04	188.0401639	5.49E-01	516.0188525
1.31E-04	197.8934426	5.99E-01	524.3737705
1.70E-04	207.3581967	6.49E-01	532.4655738
2.03E-04	213.4368852	6.99E-01	541.0270492
3.01E-04	226.5598361	7.62E-01	553.6114754
4.08E-04	235.9754098	8.01E-01	559.6213115
5.02E-04	242.1188525	8.49E-01	567.5106557
6.04E-04	247.4229508	9.00E-01	575.6655738
7.05E-04	251.7852459	9.48E-01	586.2565574
8.03E-04	255.354918	9.67E-01	589.1122951
9.11E-04	258.7680328	9.73E-01	589.8951639
1.02E-03	262.2	9.96E-01	594.4468033
1.53E-03	272.6745902		
2.03E-03	279.9696721		
2.55E-03	285.8114754		
3.05E-03	290.4327869		
3.53E-03	294.1163934		
4.07E-03	297.897541		
5.10E-03	303.9590164		
6.12E-03	309.0098361		
7.13E-03	313.35		
8.09E-03	317.0655738		
9.19E-03	320.9040984		

OAW10

P/Po	cc/gCarbon	P/Po	cc/gCarbon
5.89E-06	64.92326733	1.30E-02	164.3613861
9.04E-06	75.24960396	1.67E-02	167.7237624
9.42E-06	75.37673267	2.15E-02	170.9792079
1.00E-05	76.83742574	3.12E-02	175.019802
1.38E-05	83.98168317	4.17E-02	178.2415842
1.41E-05	84.14485149	5.19E-02	180.9475248
1.49E-05	85.32564356	6.25E-02	183.2851485
1.90E-05	90.26287129	7.24E-02	185.4722772
1.99E-05	91.01069307	8.26E-02	187.3841584
2.40E-05	94.67811881	9.26E-02	189.3049505
2.57E-05	95.91217822	1.03E-01	190.9643564
3.09E-05	99.52970297	1.50E-01	199.6465347
3.60E-05	102.3841584	2.01E-01	208.0019802
4.10E-05	104.7128713	2.51E-01	216.2207921
5.10E-05	108.5475248	3.01E-01	224.0267327
6.16E-05	111.6207921	3.50E-01	233.3940594
7.19E-05	114.0069307	4.01E-01	241.7613861
8.18E-05	115.8049505	4.51E-01	249.1960396
9.29E-05	117.5435644	5.01E-01	255.8524752
1.02E-04	118.7217822	5.49E-01	266.0217822
1.31E-04	122.0861386	6.01E-01	274.6821782
1.73E-04	125.5594059	6.51E-01	283.3613861
2.06E-04	127.4861386	7.01E-01	292.0059406
3.15E-04	132.1752475	7.63E-01	306.2267327
4.03E-04	134.6613861	8.01E-01	312.380198
5.16E-04	137.0871287	8.50E-01	321.5960396
6.20E-04	138.8178218	9.00E-01	331.980198
7.10E-04	140.0485149	9.48E-01	345.290099
8.15E-04	141.2891089	9.68E-01	348.6762376
9.23E-04	142.3861386	9.74E-01	349.6623762
1.02E-03	143.1851485	9.95E-01	366.8782178
1.53E-03	146.8970297		
2.05E-03	149.4524752		
2.56E-03	151.3376238		
3.12E-03	153.0108911		
3.62E-03	154.1762376		
4.16E-03	155.3029703		
5.13E-03	157.1227723		
6.18E-03	158.7514851		
7.34E-03	159.9346535		
8.24E-03	160.8633663		
9.26E-03	161.8524752		

OAW15

P/Po	cc/gCarbon	P/Po	cc/gCarbon
6.93E-06	66.5732381	7.18E-03	244.8647619
7.98E-06	69.43333333	8.23E-03	248.1447619
8.85E-06	72.52171429	9.16E-03	250.8666667
9.86E-06	75.73752381	1.20E-02	255.7714286
1.02E-05	75.88619048	1.49E-02	262.6828571
1.24E-05	81.15542857	2.09E-02	274.4371429
1.29E-05	82.8592381	3.08E-02	287.1609524
1.32E-05	83.00057143	4.14E-02	297.8057143
1.64E-05	88.86752381	5.17E-02	306.5685714
1.71E-05	90.47219048	6.02E-02	312.767619
2.07E-05	95.31619048	6.97E-02	319.0609524
2.15E-05	96.11619048	8.01E-02	325.0295238
2.47E-05	99.99428571	9.01E-02	330.6561905
2.54E-05	100.8742857	1.01E-01	335.7619048
3.06E-05	106.1657143	1.46E-01	354.4219048
3.54E-05	110.6409524	2.01E-01	373.2238095
4.07E-05	114.8752381	2.52E-01	388.8704762
5.04E-05	121.3457143	3.03E-01	403.4542857
7.06E-05	131.7257143	3.52E-01	417.9819048
7.99E-05	135.5780952	4.03E-01	431.5161905
8.94E-05	138.9409524	4.53E-01	444.3628571
9.08E-05	139.4228571	5.02E-01	457.532381
1.00E-04	142.4371429	5.53E-01	470.812381
1.32E-04	150.3171429	6.03E-01	483.8580952
1.70E-04	157.4685714	6.51E-01	498.4352381
2.03E-04	162.3647619	7.02E-01	512.7685714
3.04E-04	172.9704762	7.52E-01	526.8152381
4.04E-04	180.0590476	8.02E-01	541.6371429
5.12E-04	185.8180952		
6.05E-04	189.7619048		
7.13E-04	193.5838095		
8.13E-04	196.5942857		
9.05E-04	199.0161905		
1.01E-03	201.8457143		
1.53E-03	210.8552381		
2.01E-03	216.6752381		
2.52E-03	221.4942857		
3.03E-03	225.4485714		
3.53E-03	228.787619		
4.08E-03	231.9114286		
5.04E-03	236.6371429		
6.18E-03	241.2942857		

OAW20

P/Po	cc/gCarbon	P/Po	cc/gCarbon
7.73E-06	77.25262136	1.01E-02	289.4106796
8.93E-06	80.78951456	1.58E-02	303.884466
9.98E-06	84.23757282	2.13E-02	314.0708738
1.46E-05	95.12757282	3.07E-02	327.7553398
1.52E-05	96.45475728	4.12E-02	340.5592233
2.00E-05	104.7708738	5.16E-02	350.6262136
2.50E-05	111.9961165	6.00E-02	357.515534
2.99E-05	118.1854369	6.96E-02	364.5407767
3.02E-05	118.3427184	7.97E-02	370.9854369
3.03E-05	118.4582524	8.98E-02	377.5223301
3.47E-05	123.4262136	1.00E-01	382.9669903
3.52E-05	123.9543689	1.51E-01	403.6601942
4.01E-05	128.7834951	2.02E-01	418.6475728
5.03E-05	136.7281553	2.53E-01	432.0456311
6.05E-05	143.576699	3.03E-01	443.8330097
7.06E-05	149.0786408	3.49E-01	453.1184466
8.05E-05	153.8805825	4.02E-01	468.1407767
9.94E-05	161.4834951	4.53E-01	478.792233
9.99E-05	161.484466	5.00E-01	487.7174757
9.99E-05	161.4932039	5.53E-01	498.7087379
1.31E-04	170.9330097	6.00E-01	507.6747573
1.74E-04	180.5242718	6.53E-01	518.5912621
2.02E-04	185.5893204	7.00E-01	527.9668932
3.03E-04	197.9718447	7.63E-01	540.1203883
4.05E-04	206.4223301	8.01E-01	546.1912621
5.04E-04	212.5504854	8.51E-01	562.9592233
6.07E-04	217.6058252	9.00E-01	571.276699
7.06E-04	221.6378641	9.46E-01	578.4067961
8.04E-04	224.9407767	9.67E-01	581.7038835
9.10E-04	228.0699029	9.73E-01	582.392233
1.02E-03	231.0048544	9.97E-01	586.0660194
1.54E-03	241.2699029		
2.01E-03	247.7533981		
2.52E-03	253.0854369		
3.04E-03	257.7		
3.55E-03	261.461165		
4.04E-03	264.5883495		
5.03E-03	270.1533981		
6.14E-03	275.3912621		
7.02E-03	279.1087379		
8.23E-03	283.4815534		
9.25E-03	286.8203883		

HAW10

P/Po	cc/gCarbon	P/Po	cc/gCarbon
2.90E-06	69.12685039	1.02E-02	184.0307087
4.32E-06	80.39055118	1.57E-02	187.6149606
5.86E-06	86.79606299	2.09E-02	190.9023622
6.53E-06	90.13937008	3.06E-02	194.5307087
7.37E-06	92.64488189	4.10E-02	197.4480315
9.86E-06	98.70708661	5.15E-02	199.911811
1.42E-05	105.5291339	6.20E-02	202.2889764
1.49E-05	106.4929134	7.21E-02	204.1440945
1.53E-05	106.9952756	8.20E-02	206.1456693
2.05E-05	112.923622	9.22E-02	207.9015748
2.57E-05	116.9992126	1.02E-01	209.7362205
3.05E-05	120.0551181	1.50E-01	217.1141732
3.58E-05	122.9708661	2.00E-01	224.3244094
4.09E-05	125.3322835	2.50E-01	231.303937
5.09E-05	129.088189	2.99E-01	239.1149606
6.14E-05	132.1874016	3.50E-01	246.1606299
7.18E-05	134.6322835	4.00E-01	253.0393701
8.17E-05	136.5724409	4.50E-01	259.4858268
9.04E-05	138.0511811	4.99E-01	266.711811
1.00E-04	139.5417323	5.50E-01	274.2606299
1.30E-04	142.911811	6.00E-01	280.9181102
1.73E-04	146.4102362	6.51E-01	287.3125984
2.00E-04	148.0677165	7.01E-01	293.7677165
3.14E-04	152.8779528	7.63E-01	303.8456693
4.07E-04	155.4299213	8.01E-01	308.876378
5.04E-04	157.4527559	8.51E-01	315.1811024
6.17E-04	159.3181102	9.01E-01	321.4590551
7.15E-04	160.6472441	9.48E-01	331.3559055
8.01E-04	161.6543307	9.68E-01	333.9165354
9.01E-04	162.6905512	9.74E-01	334.2629921
1.02E-03	163.8149606	9.96E-01	338.4913386
1.54E-03	167.4669291		
2.02E-03	169.7984252		
2.52E-03	171.7417323		
3.09E-03	173.5031496		
3.59E-03	174.8055118		
4.03E-03	175.796063		
5.09E-03	177.8496063		
6.21E-03	179.5826772		
7.08E-03	180.7614173		
8.13E-03	181.9740157		
9.20E-03	183.0889764		

HAW15

P/Po	cc/gCarbon	P/Po	cc/gCarbon
4.08E-06	74.23674797	1.01E-02	311.7560976
5.11E-06	81.47479675	1.56E-02	322.395122
5.49E-06	83.50325203	2.05E-02	332.9219512
5.72E-06	84.53577236	2.99E-02	345.4674797
7.31E-06	92.43739837	4.09E-02	356.4934959
8.66E-06	97.74390244	4.94E-02	363.1512195
9.15E-06	99.49918699	6.17E-02	371.3308943
1.03E-05	102.8943089	7.03E-02	375.9113821
1.52E-05	115.3577236	8.04E-02	380.5170732
2.03E-05	125.1902439	9.06E-02	384.8796748
2.52E-05	132.9788618	1.01E-01	388.4894309
3.02E-05	139.7081301	1.51E-01	402.099187
3.52E-05	145.5154472	2.02E-01	411.7399187
4.04E-05	150.8170732	2.50E-01	419.3609756
5.05E-05	159.3373984	3.00E-01	426.4365854
6.03E-05	166.1268293	3.49E-01	434.2252846
7.03E-05	171.9520325	4.00E-01	440.9211382
8.07E-05	177.098374	4.51E-01	447.1927642
9.05E-05	181.301626	5.01E-01	453.3846341
1.01E-04	185.300813	5.51E-01	459.3422764
1.30E-04	194.3130081	6.03E-01	468.1105691
1.71E-04	203.5674797	6.51E-01	473.495935
2.01E-04	208.7479675	7.01E-01	479.1406504
3.06E-04	221.6471545	7.60E-01	486.4690244
4.04E-04	229.7	8.03E-01	495.0235772
5.01E-04	235.6113821	8.51E-01	500.2813821
6.04E-04	240.6056911	9.01E-01	506.1219512
7.06E-04	244.6650407	9.46E-01	511.2658537
8.04E-04	247.9853659	9.69E-01	517.1276423
9.06E-04	250.9821138	9.74E-01	517.7341463
1.02E-03	254.2463415	9.97E-01	521.1129268
1.53E-03	264.1203252		
2.04E-03	270.9910569		
2.53E-03	276.0894309		
3.05E-03	280.6178862		
3.52E-03	284.1495935		
4.07E-03	287.7162602		
5.01E-03	292.9414634		
6.10E-03	298.0073171		
7.12E-03	302.0609756		
8.12E-03	305.6073171		
9.22E-03	309.1349593		

HAW20

P/Po	cc/gCarbon	P/Po	cc/gCarbon
4.28E-06	73.71113821	1.21E-02	335.5691057
5.22E-06	79.39422764	1.46E-02	343.4577236
5.91E-06	82.97154472	2.01E-02	357.9536585
6.10E-06	83.85447154	2.99E-02	373.8365854
7.20E-06	89.6601626	4.08E-02	387.301626
7.75E-06	91.87235772	5.15E-02	398.1650407
9.17E-06	96.83170732	5.96E-02	404.7284553
1.45E-05	112.0268293	7.21E-02	413.3138211
1.53E-05	113.7479675	8.06E-02	418.1495935
2.03E-05	123.796748	9.01E-02	423.7065041
2.53E-05	132.1235772	1.01E-01	428.5162602
3.05E-05	139.4804878	1.52E-01	444.9292683
3.55E-05	145.6707317	2.03E-01	455.5536585
4.05E-05	151.1691057	2.50E-01	463.3513008
5.06E-05	160.3577236	3.00E-01	470.5821138
6.06E-05	167.9512195	3.50E-01	477.098374
7.10E-05	174.5121951	4.01E-01	483.3569106
8.11E-05	180.1170732	4.54E-01	493.6407317
9.11E-05	184.9146341	5.01E-01	499.395122
1.00E-04	188.9065041	5.51E-01	505.3691057
1.30E-04	199.3162602	6.01E-01	511.3234959
1.72E-04	209.9813008	6.51E-01	516.9178049
2.02E-04	216.0439024	7.01E-01	522.5186992
3.05E-04	230.6747967	7.60E-01	528.795935
4.05E-04	240.1853659	8.02E-01	532.8690244
5.07E-04	247.3934959	8.51E-01	537.7828455
6.01E-04	252.7089431	9.02E-01	551.995935
7.12E-04	257.901626	9.47E-01	556.6202439
8.02E-04	261.4471545	9.68E-01	559.0764228
9.12E-04	265.2138211	9.74E-01	559.6357724
1.02E-03	268.7130081	9.97E-01	563.000813
1.51E-03	279.9943089		
2.03E-03	288.0349593		
2.54E-03	294.0788618		
3.03E-03	298.904878		
3.55E-03	303.303252		
4.05E-03	307.0130081		
5.04E-03	313.2552846		
6.09E-03	318.8471545		
7.13E-03	323.5674797		
8.20E-03	327.8845528		
9.19E-03	331.5065041		

AAW10

P/Po	cc/gCarbon	P/Po	cc/gCarbon
7.59E-06	83.19710145	1.26E-02	163.4224638
8.63E-06	85.31376812	1.67E-02	165.584058
9.13E-06	86.37608696	2.17E-02	167.6608696
1.00E-05	87.88985507	3.13E-02	170.6456522
1.40E-05	93.28043478	4.15E-02	173.0942029
1.52E-05	94.68913043	5.21E-02	175.157971
1.54E-05	94.79782609	6.23E-02	177.1528986
1.99E-05	99.21231884	7.25E-02	178.734058
2.03E-05	99.52318841	8.26E-02	180.2543478
2.43E-05	102.5384058	9.23E-02	182.0188406
2.55E-05	103.2905797	1.03E-01	183.576087
3.04E-05	106.184058	1.50E-01	189.7449275
3.54E-05	108.5536232	2.01E-01	195.4768116
4.10E-05	110.8746377	2.51E-01	201.3231884
5.16E-05	114.2405797	3.00E-01	207.8471014
6.11E-05	116.6202899	3.51E-01	213.6637681
7.17E-05	118.7724638	4.01E-01	219.407971
8.24E-05	120.5811594	4.50E-01	224.9318841
9.22E-05	121.9688406	5.01E-01	230.3043478
1.00E-04	123.0043478	5.53E-01	238.1326087
1.33E-04	126.1789855	6.00E-01	243.3413043
1.72E-04	128.8710145	6.51E-01	248.7181159
2.01E-04	130.4630435	7.01E-01	253.9
3.06E-04	134.3666667	7.63E-01	262.5868841
4.09E-04	136.8985507	8.02E-01	266.6673913
5.13E-04	138.8043478	8.50E-01	271.9898551
6.08E-04	140.2188406	9.01E-01	277.4398551
7.20E-04	141.5652174	9.47E-01	285.2710145
8.08E-04	142.4833333	9.67E-01	287.3746377
9.10E-04	143.4014493	9.73E-01	287.8376812
1.02E-03	144.4028986	9.97E-01	291.2231884
1.54E-03	147.5543478		
2.03E-03	149.6731884		
2.56E-03	151.4289855		
3.05E-03	152.7768116		
3.61E-03	154.0666667		
4.04E-03	154.9289855		
5.15E-03	156.8072464		
6.21E-03	158.2768116		
7.19E-03	159.4072464		
8.24E-03	160.4862319		
9.09E-03	161.2442029		

AAW15

P/Po	cc/gCarbon	P/Po	cc/gCarbon
5.79E-06	80.38216216	1.19E-02	295.381982
7.52E-06	86.91567568	1.47E-02	302.5252252
8.90E-06	92.47747748	2.06E-02	314.4504505
9.77E-06	95.44684685	3.05E-02	326.763964
1.01E-05	96.25315315	4.14E-02	336.8495495
1.38E-05	106.0333333	4.92E-02	343.0558559
1.50E-05	108.8936937	6.18E-02	351.0045045
2.00E-05	118.2198198	7.08E-02	355.4072072
2.04E-05	118.7918919	8.07E-02	359.8963964
2.44E-05	125.0378378	9.07E-02	364.4351351
2.52E-05	126.2900901	1.01E-01	367.9972973
3.53E-05	138.3792793	1.47E-01	380.3243243
3.98E-05	142.8351351	2.03E-01	391.1855856
4.05E-05	143.4072072	2.50E-01	399.3675676
5.06E-05	151.6792793	3.03E-01	410.6567568
6.09E-05	158.3891892	3.50E-01	417.9342342
7.06E-05	163.6567568	4.00E-01	425.2432432
8.08E-05	168.3972973	4.50E-01	432.5504505
9.16E-05	172.6945946	5.01E-01	439.2432432
9.99E-05	175.6666667	5.51E-01	446.0567568
1.31E-04	184.4864865	6.03E-01	457.2396396
1.70E-04	192.5378378	6.51E-01	463.5414414
2.00E-04	197.4945946	7.01E-01	470.0243243
3.02E-04	209.2297297	7.51E-01	476.4720721
4.07E-04	217.2477477	8.01E-01	482.6279279
5.09E-04	222.9297297	8.50E-01	489.4225225
6.12E-04	227.5243243	9.02E-01	501.918018
7.12E-04	231.2432432	9.50E-01	508.7306306
8.07E-04	234.2207207	9.67E-01	511.0072072
9.13E-04	237.1153153	9.78E-01	511.7297297
1.01E-03	239.8225225	9.97E-01	514.2918919
1.52E-03	248.9171171		
2.04E-03	255.4288288		
2.54E-03	260.3162162		
3.07E-03	264.5108108		
3.52E-03	267.590991		
4.05E-03	270.7774775		
5.10E-03	276.0900901		
6.16E-03	280.5927928		
7.14E-03	284.2144144		
8.17E-03	287.6315315		
9.12E-03	290.4414414		

AAW20

P/Po	cc/gCarbon	P/Po	cc/gCarbon
9.05E-06	92.66756757	1.20E-02	330.6864865
1.43E-05	107.2684685	1.45E-02	338.4171171
1.51E-05	109.2783784	2.01E-02	353.0288288
1.93E-05	117.8702703	2.99E-02	369.118018
2.01E-05	119.6945946	4.08E-02	382.8369369
2.51E-05	129.4603604	5.15E-02	393.6900901
3.01E-05	136.9432432	5.99E-02	400.7459459
3.45E-05	142.6918919	6.96E-02	407.7531532
3.52E-05	143.681982	7.98E-02	414.4963964
4.01E-05	149.1351351	9.04E-02	420.3108108
4.04E-05	149.2657658	1.01E-01	425.3693694
4.95E-05	157.645045	1.51E-01	444.7045946
5.04E-05	158.3936937	2.03E-01	458.0846847
6.01E-05	165.5891892	2.54E-01	470.2333333
7.00E-05	171.8252252	3.03E-01	482.2774775
8.00E-05	177.2576577	3.50E-01	491.5288288
8.95E-05	181.8036036	4.00E-01	500.9567568
9.96E-05	186.0612613	4.50E-01	510.054955
9.99E-05	186.0684685	5.00E-01	519.3342342
9.99E-05	186.0765766	5.53E-01	531.0901802
1.31E-04	196.8432432	6.00E-01	539.2008108
1.71E-04	206.7720721	6.51E-01	547.8089189
2.00E-04	212.3963964	7.00E-01	556.1361261
3.01E-04	226.4837838	7.60E-01	566.5585586
4.09E-04	236.4981982	8.03E-01	577.1612613
5.03E-04	243.0234234	8.51E-01	585.3486486
6.04E-04	248.5756757	9.00E-01	593.3054955
7.05E-04	253.1198198	9.46E-01	600.836036
8.03E-04	256.8720721	9.68E-01	604.5936937
9.11E-04	260.445045	9.70E-01	608.581982
1.02E-03	263.5972973	9.97E-01	614.063964
1.53E-03	274.9045045		
2.03E-03	282.5423423		
2.53E-03	288.5261261		
3.02E-03	293.236036		
3.52E-03	297.4279279		
4.02E-03	301.0936937		
5.02E-03	307.3864865		
6.13E-03	313.1954955		
7.16E-03	317.8873874		
8.15E-03	321.8369369		
9.24E-03	325.8459459		

F600

P/Po	cc/gCarbon	P/Po	cc/gCarbon
2.50E-06	52.87834862	1.26E-02	173.2385321
2.88E-06	56.1153211	1.61E-02	177.0816514
3.24E-06	57.45055046	2.07E-02	181.2715596
4.63E-06	63.1753211	3.02E-02	186.4541284
6.53E-06	69.51899083	4.05E-02	190.8119266
7.92E-06	72.61449541	5.13E-02	194.6321101
9.34E-06	75.70807339	6.17E-02	197.6834862
1.03E-05	77.63394495	7.17E-02	200.2293578
1.53E-05	85.16477064	8.18E-02	202.8504587
2.03E-05	90.02385321	9.20E-02	205.0174312
2.54E-05	94.21100917	1.02E-01	207.346789
3.04E-05	97.74862385	1.50E-01	216.0027523
3.56E-05	100.8256881	2.00E-01	224.2073394
4.06E-05	103.3917431	2.50E-01	232.1908257
5.08E-05	107.5422018	3.00E-01	240.1073394
6.11E-05	110.9247706	3.53E-01	249.3651376
7.15E-05	113.6559633	4.01E-01	256.6669725
8.94E-05	117.5211009	4.51E-01	263.9036697
9.04E-05	117.7798165	5.00E-01	271.2027523
1.00E-04	119.4394495	5.53E-01	281.0137615
1.30E-04	123.2449541	6.00E-01	288.1926606
1.72E-04	127.1761468	6.51E-01	295.4201835
2.01E-04	129.2293578	7.01E-01	302.7357798
3.12E-04	134.5761468	7.60E-01	311.5119266
4.03E-04	137.5697248	8.03E-01	321.3238532
5.00E-04	139.9568807	8.50E-01	329.3394495
6.15E-04	142.1834862	9.04E-01	339.9541284
7.12E-04	143.766055	9.46E-01	349.9963303
8.18E-04	145.2045872	9.69E-01	360.8614679
9.06E-04	146.2201835	9.73E-01	362.1779817
1.02E-03	147.5275229	9.95E-01	373.8266055
1.53E-03	151.6779817		
2.05E-03	154.6862385		
2.58E-03	157.0137615		
3.08E-03	158.8440367		
3.54E-03	160.3220183		
4.07E-03	161.7954128		
5.02E-03	164.0642202		
6.09E-03	166.2091743		
7.26E-03	168.1853211		
8.10E-03	169.4779817		
9.13E-03	170.8633028		

G219

P/Po	cc/gCarbon	P/Po	cc/gCarbon
2.86E-06	43.01439655	1.23E-02	248.112069
3.52E-06	46.81637931	1.53E-02	254.7448276
4.11E-06	49.2187931	1.94E-02	262.5086207
4.91E-06	56.63224138	3.12E-02	276.6008621
6.64E-06	66.4012069	3.95E-02	283.9534483
7.67E-06	69.70405172	4.98E-02	291.6818966
9.10E-06	73.55862069	6.00E-02	298.4836207
1.02E-05	76.7825	7.06E-02	304.1827586
1.52E-05	88.14396552	8.07E-02	309.3077586
2.02E-05	96.82586207	9.12E-02	313.7603448
2.51E-05	103.5155172	1.01E-01	317.8732759
3.02E-05	109.4698276	1.53E-01	334.4965517
3.52E-05	114.2327586	2.03E-01	346.512931
4.02E-05	118.6508621	2.54E-01	358.175
5.02E-05	125.6405172	3.00E-01	367.0103448
6.02E-05	131.4301724	3.50E-01	376.0500862
7.01E-05	136.2594828	4.00E-01	384.6137931
8.04E-05	140.4931034	4.49E-01	393.7112069
9.03E-05	144.0327586	5.00E-01	402.5293103
9.95E-05	146.9724138	5.51E-01	411.1198276
1.30E-04	154.5043103	6.01E-01	419.2413793
1.69E-04	161.7413793	6.50E-01	426.3827586
2.00E-04	165.9724138	7.04E-01	436.9982759
3.02E-04	175.9887931	7.60E-01	445.4991379
4.04E-04	182.5387931	8.02E-01	452.0077586
5.05E-04	187.3586207	8.52E-01	463.9594828
6.06E-04	191.1422414	9.01E-01	472.2008621
7.09E-04	194.2689655	9.45E-01	480.4577586
8.09E-04	196.8344828	9.66E-01	484.7060345
9.00E-04	198.9137931	9.73E-01	485.3784483
1.02E-03	201.4034483	9.95E-01	502.5189655
1.52E-03	208.9086207		
2.02E-03	214.1741379		
2.53E-03	218.2525862		
3.04E-03	221.662069		
3.55E-03	224.5905172		
4.04E-03	227.0172414		
5.06E-03	231.4448276		
6.17E-03	235.4241379		
7.15E-03	238.5318966		
8.10E-03	241.2086207		
9.18E-03	244.0008621		

Picazine

P/Po	cc/gCarbon	P/Po	cc/gCarbon
3.94E-06	40.92544776	1.17E-02	286.1835821
4.15E-06	41.78	1.55E-02	299.5604478
4.65E-06	44.09544776	2.04E-02	312.55
5.58E-06	47.97522388	2.97E-02	329.8791791
6.10E-06	49.52873134	4.04E-02	345.4753731
8.46E-06	56.47037313	5.08E-02	358.288806
9.05E-06	57.98559701	6.11E-02	369.7947761
1.02E-05	61.53835821	7.16E-02	379.9537313
1.52E-05	71.47858209	8.15E-02	389.1962687
2.02E-05	78.95671642	9.21E-02	397.9723881
2.52E-05	84.94552239	9.98E-02	403.9701493
3.02E-05	90.21044776	1.52E-01	439.3895522
3.51E-05	94.57761194	2.00E-01	464.969403
4.03E-05	98.72835821	2.51E-01	488.6671642
5.02E-05	105.5477612	3.02E-01	509.0395522
6.03E-05	111.4776119	3.50E-01	528.9208209
7.01E-05	116.3634328	4.02E-01	547.4910448
8.78E-05	123.8141791	4.52E-01	564.5940299
9.03E-05	124.8059701	5.02E-01	581.558209
9.96E-05	128.0634328	5.52E-01	598.2500746
1.29E-04	136.8097015	5.99E-01	617.4947761
1.70E-04	146.0141791	6.52E-01	635.6448507
1.99E-04	151.5559701	7.02E-01	653.1775373
3.01E-04	165.5231343	7.61E-01	674.2558955
4.02E-04	175.4708955	8.02E-01	689.1397761
5.04E-04	183.2261194	8.53E-01	711.0731343
6.02E-04	189.2014925	9.03E-01	726.1612687
7.03E-04	194.4873134	9.48E-01	736.7328358
8.02E-04	198.9246269	9.67E-01	740.5164925
9.07E-04	203.0820896	9.73E-01	741.6469403
1.02E-03	207.3223881	9.96E-01	758.5821642
1.53E-03	220.7858209		
2.02E-03	230.1395522		
2.54E-03	237.6731343		
3.05E-03	243.6940299		
3.53E-03	248.6432836		
4.05E-03	253.119403		
5.06E-03	260.6350746		
6.09E-03	266.9514925		
7.11E-03	272.4		
8.14E-03	277.1253731		
9.11E-03	281.2350746		

CO_2 adsorption isotherms

AW10

P/Po	cc/gCarbon
2.98E-06	0.065116279
1.87E-05	0.495681063
7.89E-05	1.923421927
2.08E-04	4.561362126
5.60E-04	10.06232558
1.84E-03	22.63960133
5.88E-03	44.08372093
1.46E-02	68.50863787
2.90E-02	89.02491694

OAW10

P/Po	cc/gCarbon
2.53E-06	0.073868852
1.79E-05	0.553147541
7.78E-05	2.111180328
2.07E-04	4.807245902
5.61E-04	10.11619672
1.83E-03	22.2432459
5.87E-03	42.47245902
1.47E-02	65.9442623
2.91E-02	86.07245902

HAW10

P/Po	cc/gCarbon
3.03E-06	0.069965986
1.87E-05	0.484387755
7.64E-05	1.817346939
2.09E-04	4.440680272
5.69E-04	9.898401361
1.85E-03	22.37710884
5.89E-03	44.0329932
1.46E-02	69.06394558
2.90E-02	91.37414966

AAW10

P/Po	cc/gCarbon
2.31E-06	0.046689895
1.82E-05	0.491020408
7.62E-05	1.831598639
2.10E-04	4.411428571
5.66E-04	9.730952381
1.84E-03	21.96401361
5.89E-03	43.5670068
1.46E-02	69.12210884
2.90E-02	91.72210884

AW15

P/Po	cc/gCarbon
2.89E-06	0.07443299
1.84E-05	0.303402062
7.81E-05	1.105618557
2.11E-04	2.801649485
6.48E-04	7.514793814
1.73E-03	16.37613402
5.95E-03	39.05778351
1.46E-02	70.51443299
2.91E-02	106.5850515

OAW15

P/Po	cc/gCarbon
2.72E-06	0.061768707
1.80E-05	0.297891156
7.58E-05	1.103945578
2.08E-04	2.741938776
6.14E-04	6.803401361
1.88E-03	15.82176871
5.92E-03	34.75884354
1.47E-02	63.50986395
2.91E-02	95.25

HAW15

P/Po	cc/gCarbon
2.83E-06	0.061889251
1.82E-05	0.281368078
7.62E-05	1.059153094
2.08E-04	2.707850163
6.06E-04	6.936123779
1.87E-03	16.74218241
5.88E-03	37.92703583
1.47E-02	69.75114007
2.91E-02	104.7456026

AAW15

P/Po	cc/gCarbon
3.58E-06	4.46E-02
1.88E-05	2.34E-01
7.76E-05	9.34E-01
2.10E-04	2.46E+00
6.14E-04	6.58E+00
1.88E-03	1.59E+01
5.91E-03	3.63E+01
1.45E-02	6.68E+01
2.91E-02	1.02E+02

AW20

P/Po	cc/gCarbon
3.34E-06	0.052810219
1.86E-05	0.248211679
7.68E-05	0.956532847
2.10E-04	2.485656934
6.24E-04	6.561605839
1.89E-03	15.70226277
5.91E-03	36.14390511
1.47E-02	67.47846715
2.91E-02	103.3510949

OAW20

P/Po	cc/gCarbon
3.90E-06	0.042527473
1.92E-05	0.218681319
7.83E-05	0.867435897
2.10E-04	2.302014652
6.73E-04	5.691391941
1.89E-03	14.03065934
5.91E-03	33.23659341
1.47E-02	62.71428571
2.91E-02	96.2992674

HAW20

P/Po	cc/gCarbon
3.68E-06	0.043272727
1.91E-05	0.206581818
7.80E-05	0.804072727
2.11E-04	2.132036364
6.36E-04	5.891636364
1.90E-03	14.27167273
5.94E-03	33.67509091
1.46E-02	63.81963636
2.91E-02	100.2596364

AAW20

P/Po	cc/gCarbon
4.05E-06	0.038254545
1.93E-05	0.202436364
7.87E-05	0.815963636
2.10E-04	2.197090909
6.32E-04	6.110872727
1.89E-03	14.97978182
5.92E-03	35.08789091
1.46E-02	65.86690909
2.91E-02	102.8509091

F600

P/Po	cc/gCarbon
3.40E-06	0.050880682
1.78E-05	0.290113636
7.82E-05	1.198778409
2.10E-04	2.698664773
6.13E-04	6.426136364
1.88E-03	14.83079545
5.94E-03	30.35795455
1.47E-02	50.02642045
2.90E-02	69.48153409

G219

P/Po	cc/gCarbon
2.38E-06	0.06410828
1.72E-05	0.421687898
7.70E-05	1.387070064
2.12E-04	3.088089172
6.11E-04	6.863726115
1.89E-03	14.70378981
5.93E-03	30.69433121
1.46E-02	53.46687898
2.89E-02	78.45

Picazine

P/Po	cc/gCarbon
3.52E-06	0.04622291
1.84E-05	0.241486068
7.70E-05	0.90876161
2.08E-04	2.225541796
6.25E-04	5.528947368
1.90E-03	12.42068111
5.95E-03	27.15959752
1.46E-02	49.39752322
2.91E-02	75.75077399